Understanding the role of transcription in organisation of the bacterial chromosome

Jonathan Leslie Stephen Norris

Thesis submitted in partial fulfilment of the requirements of the regulation for the degree of Doctor of Philosophy

Newcastle University

Faculty of Medical Sciences

Newcastle University Biosciences Institute

September 2024

Abstract

Bacterial chromosomes are organised by various proteins, types of supercoiling and other cellular processes. One such process, transcription, massively impacts the chromosomal structure from the local level up to overall organisation of the nucleoid. Uniquely to bacterial transcription, the process can be physically coupled with translation since they occur in the same cellular compartment. The processes and associated proteins can, thus, happen simultaneously and physically interact. This coupling can have further impact of the overall structure of the nucleoid. While transcription-translation coupling is well documented in *E. coli*, some work suggests that it does not happen in other bacteria, including the Gram-positive model bacterium *Bacillus subtilis*.

To study transcription-dependent chromosome organisation at a single cell level in *B. subtilis*, I fluorescently labelled DNA in the vicinity of the promoter of an inducible gene coding for a transmembrane protein and followed the localisation of the gene locus using fluorescence microscopy. We found that, upon induction, the gene migrates from a central position in the cell towards the membrane, and back towards the nucleoid when induction is removed. This movement was further confirmed by monitoring the fluorescently labelled locus in vertically immobilised cells (Vertical Cell Imaging by Nanostructured Immobilisation), which provides a better optical viewing angle for the observed process. Inhibiting either transcription and translation, via antibiotics and mutations in respective initiation regions, abolished the movement of fluorescently labelled locus towards the cell periphery. This loss of gene movement indicates the involvement of both transcription and translation in the process. Our results are fully consistent with transertion; a postulated process in which transmembrane proteins are inserted in the membrane co-translationally and co-transcriptionally thereby pulling the gene locus from the nucleoid core to the periphery of the cell and provide the first direct experimental evidence for transertion in Gram-positive bacteria. Furthermore, these findings demonstrate that translation and transcription can indeed be coupled in *B. subtilis,* alongside translocation, at least for genes encoding for membrane proteins.

Acknowledgements

Firstly, I would like to thank my supervisor Nikolay Zenkin for his support, mentorship, and patience during my PhD. Additionally, I would like to thank Henrik Strahl for his unending support given to me over the past four years which have helped me tremendously. I'd like to acknowledge the work by George Merces, Calum Jukes and James Grimshaw on the macro described in chapter 2.3.5/6. Jamie I would also like to thank for his friendship and unending support. I thank Kevin Whitley for allowing me to borrow micropillar wafers for VerCINI work.

I would also like to thank the members, both past and present, of the NZYY lab. In particular to Soren Neilsen, whose continuous support in the lab has kept it running through thick and thin. I'm not sure how anyone could manage without you. I would like to specially mention Maria Puiu, Shiney George-Matthews, Pavel Brazda and Nick Bailey, all of whom have been dear friends and shoulders to lean on throughout my time in Newcastle.

To the members of my second adoptive lab in the Strahl group, I thank you all. Your kindness, humour and acceptance of me has made me feel like I belonged, at a time where I felt most estranged. Specifically, I thank Maddie Humphreys, Jess Buttress, Maria D S and Laura Dobby, though I must mention Alisa, Olivia, Taylor, Matthieu and Rachel. Thanks to all that are a part of the CBCB family: from Tom, Fran and Julie and the unending job of suppling the building, to members on all floors of the building. Special thanks to Heath Murray, Seamus Holden and again Kevin Whitley for their mentorship from progression panels. (I didn't forget you either Fred).

I am privileged enough to be so loved by so many in life. I'd like to thank all my friends who've stayed with me during this project and allowed to me to keep my sanity. I'd like to thank the burrow+3: Joe, Myles, Marcus, Alex, Dina, Connor, Guy and Sam; my friends from Leicester: Lacey, Dean, Leanne, Nafeesa, Sarah, Jo, Femi, Chogg, Freddie, Oli and Sean; R+L=J: Rosie and Lucy (and Oli); and the Newcastle kingdom: Alex Longcake, Alex Faulkner and Loz.

To my family, I could never repay the love and faith you have in me. I love you all. Rest in peace to our beloved pets Bailey and Fluffy who passed away whilst I was writing this thesis. Finally, for once, I'd like to thank myself. Despite all the self-doubt and anxiety, I'm still going and thriving and enjoying life.

Table of Contents

..... i
Abstract iii
Acknowledgements iv
Table of Contents v
Table of Tables vii
Table of Figures viii
List of abbreviations x
Chapter 1: Introduction ..... **Error! Bookmark not defined.**
Chapter 2: Materials and Methods 26
2.1 Component lists 26
2.1.1 Bacterial strains 26
2.1.2 Plasmids 29
2.1.3 Oligonucleotides 30
2.1.4 Medias and buffers 42
2.1.5 Antibiotics 43
2.2 Cloning 43
2.2.1 Plasmid construction 43
2.2.2 Strain growth conditions 44
2.2.3 Genomic DNA extraction 44
2.2.4 Plasmid DNA extraction 45
2.2.5 Polymerase Chain Reaction 45
2.2.6 Restriction Enzyme Digest 45
2.2.7 Agarose Gel Electrophoresis 45
2.2.8 Column Purification 45
2.2.9 Gel extraction 46
2.2.10 NEBuilder HiFi Assembly Cloning 46
2.2.11 Transformation into E. coli 46
2.2.12 Transformation into B. subtilis 46
2.2.13 Site Directed Mutagenesis 47
2.2.14 Sanger Sequencing 47
2.2.15 Whole Plasmid Sequencing 47
2.3 Microscopy 47
2.3.1 Fluorescence microscopy 47
2.3.2 Slide Preparation 47
2.3.3 Vertical cell imaging by nanostructured immobilisation (VerCINI) 48
2.3.4 VerCINI microscopy 49
2.3.5 Image Quantification (Horizontal) 49

2.3.6 Image Quantification (VerCINI) 50
2.3.7 Statistics 50
Chapter 3: Development and design of lacO array for observation of transertion 52
3.1 Introduction 52
3.2 Results 53
3.2.1 Design of lacO48 fluorescent reporter in front of gene des. 53
3.2.2 Quantification and confirmation of lacO48 array exclusion from cell centre. 55
3.2.3 Arrays inserted on different loci around the genome share exclusion from the cell centre 58
3.2.5 Induction of des lacO48 array with cold shock has no effect on gene movement. 61
3.2.5 Antibiotics have negligible effect on lacO48 foci positioning. 65
3.2.6 Design and construction of short array, lac04 68
3.3 Discussion 70
Chapter 4: Analysis of cellular localisation of a gene upon induction 73
4.1 Introduction 73
4.2 Results 74
4.2.1 Effect of lacO4 on foci positioning within cells 74
4.2.2 lacO4 at des shows movement towards the membrane upon induction 77
4.3 Discussion 84
Chapter 5: Analysis of transertion using vertical cell imaging by nanostructured immobilization (VerCINI) 87
5.1 Introduction 87
5.2 Results 88
5.2.1 Use of VerCINI in foci movement tracking 88
5.2.2 des foci position dramatically shifts upon induction 92
5.2.3 Chloramphenicol abolishes foci shift to the membrane 94
5.2.4 Rifampicin abolishes foci shift to membrane 99
5.2.5 Cold shock but not steady state growth in cold results in peripheral des localisation 101
5.2.6 Foci repositioning is dependent on translation 103
5.3 Discussion 105
Chapter 6: Conclusion and future directions 110
Appendix 116
References 117

Table of Tables

Chapter 2:

Table 2.1 List of bacterial strains.

Table 2.2 List of plasmids.

Table 2.3 List of oligonucleotides used.

Table 2.4 List of medias and buffers used with compositions.

Table 2.5 List of antibiotics and working concentrations.

Table 2.6 Filter Cube information.

Table of Figures

Chapter 1

Figure 1.1 *Spatial organisation of nucleoid comparison between species*

Figure 1.2 *Twin supercoiled domain model*

Figure 1.3 *Chromosomal domain boundary formation by transcription.*

Figure 1.4 *Model of coupled transcription-translation.*

Figure 1.5 *SRP RNA structure evolution throughout life*

Figure 1.6 *SRP mediation of protein targeting and insertion into the membrane.*

Figure 1.7 *Model of transertion*

Figure 1.8 *Model of two component Des pathway, DesK-DesR*

Chapter 3

Figure 3.1 *Schematic overview of the lacO48 array marker at des promoter.*

Figure 3.2 *First look at lacO48 array with matching lacI-fusion protein.*

Figure 3.3 *Workflow for manual data quantification with representative scatter plots.*

Figure 3.4 *Quantification of array foci positioning within the cell.*

Figure 3.5 *Location of arrays in different loci around the genome has no effect on exclusion pattern.*

Figure 3.6 *Induction of des lacO48 with cold shock.*

Figure 3.7 *des locus induction by cold shock over time points and returned to 30°C*

Figure 3.8 *Scatter plots showing induction by cold shock at varying time point and return to 30°C.*

Figure 3.9 *Treatment with chloramphenicol and rifampicin have negligible effect on lacO48 location.*

Figure 3.10 *Novel lacO4 short array compared to lacO48 array at locus of des.*

Chapter 4

Figure 4.1 *Effect of chloramphenicol and rifampicin on des locus positioning*

Figure 4.2 *Effect of induction by cold shock on des locus positioning*

Figure 4.3 *Effect of induction at different time points before returning to 30°C.*

Figure 4.4 *Scatter plots showing effect of induction by cold shock at varying time points and return to 30°C.*

Figure 4.5 *Positioning of at membrane positive control p16.7-lacI*

Chapter 5

Figure 5.1 *VerCINI setup to observe and analyse foci positioning.*

Figure 5.2 *Hbs-GFP VerCINI images to determine volume of nucleoid in the cell.*

Figure 5.3 *Cartoon representation of lacO4 array distance to the actual site of transertion.*

Figure 5.4 *Expression dependent localisation of des loci positioning*

Figure 5.5 *Effect of chloramphenicol and tetracycline on des locus positioning in vertical cells*

Figure 5.6 *Treatment with chloramphenicol after induction*

Figure 5.7 *Effect of rifampicin on des locus positioning in vertical cells*

Figure 5.8 *Comparing 15°C grown cells to 30°C grown cells for foci positioning.*

Figure 5.9 *Induction of des foci without start codon.*

Figure 5.10 *inhibition of translation after transertion has been induced.*

List of abbreviations

B. subtilis	*Bacillus subtilis*
Bp	base pair
Cam	Chloramphenicol
CTT	coupled transcription-translation
DAPI	4’,6-Diamidino-2-phenylindole
DNA	Deoxyribonucleic acid
E. coli	*Escherichia coli*
EDTA	ethylene diamine tetra-acetic acid
et al.	*et alia* (and others)
FIS	factor for inversion stimulation
GFP	Green fluorescent protein
HiFi	High fidelity
HiLO	Highly inclined and laminated optical sheet microscopy.
H-NS	histone-like nucleoid structuring protein
IHF	integration host factor
LacO	lac operator
LB	Luria-Bertani medium
LLPS	liquid-liquid phase separation
LoG	Laplacian of Gaussian
Min.	Minutes
mNG	mNeonGreen
mRNA	messenger RNA
NA	Nutrient Agar

NAPs	Nucleoid associated proteins
NDM	normalised distance to the membrane
OD600	Optical Density measured at 600 nm wavelength.
PCR	polymerase chain reaction
RBS	ribosomal binding site
Rif	Rifampicin
RNA	ribonucleoic acid
RNAP	RNA polymerase
ROI	region of interest
rRNA	ribosomal RNA
SIM	Structure Illumination Microscopy
SMC	structural maintenance of chromosomes
SMM	Spitzen Minimal Medium
SOC	Super Optimal broth with Catabolite repression
sRNA	small regulatory RNAs
SRP	signal recognition particle
T3SS	Type III secretion system
TBE	Tris/Borate/EDTA
TIRF	Total Internal Reflection Fluorescence
tRNA	Transfer RNA
VerCINI	Vertical cell imaging by nanostructured immobilisation

Chapter 1: Introduction

1.1The bacterial nucleoid

The bacterial chromosome, upon which genetic information for the cell is stored, is usually a covalently closed circular ring of DNA forming a structure termed the nucleoid. All cells store their genetic information within the cell, which raises the issue size. The average linearised bacterial chromosome is ~1000 times longer than the cell in which it resides, therefore it must be highly condensed and compacted to fit within the confines of bacterial cytoplasmic space. Simultaneously the chromosome must allow for concurrent genomic functions such as transcription, DNA replication and DNA segregation to continue (Toro & Shapiro, 2010; Lagomarsino et al., 2015). The nucleoid overall structure is organised in such a way to accommodate the requirements of condensation as well as DNA associated processes such as transcription, replication and segregation. Compaction of the nucleoid is provided by various proteins, cellular processes and supercoiling of DNA (Badrinarayanan et al., 2015; Verma et al., 2019).

In general, prokaryotic chromosomes are different compared to eukaryotic chromosomes as they lack a membrane envelope surrounding the DNA. In fact, for most bacteria, there are no internal membrane structures at all, allowing the chromosome in principle to freely diffuse in the cytoplasm. Historically this caused the assumption that the nucleoid was not organised, at least not to a degree comparable to eukaryotic cells. However, later studies have highlighted the remarkable degree of chromosome organisation bacterial cells nonetheless achieve. Throughout this introduction, unless stated otherwise, the information provided is focussed on the Gram-negative model organism *Escherichia coli* or the Gram-positive model organism *Bacillus subtilis,* respectively, and they are the best studied bacterial models in this regard. As with chromosome organisation in eukaryotes, the bacterial chromosome organisation manifests itself on different levels; global and local. The nucleoid is organised in such a manner that nonetheless allows access for transcription, translation, DNA repair and replication to occur (Berlatzky et al., 2008;Kleckner et al., 2014). The global internal organisation of chromosome can vary greatly depending on cell cycle and DNA replication stages, or as part or developmental processes such as sporulation in *B. subtilis* (Wang et al., 2017; Badrinarayanan et al., 2015).

Chromosomes can be categorised based on the organisational level. Chromosome domain boundaries further establish distinct areas of the chromosome which are distinguished based on local interactions between gene loci. Such organisational domains are known as chromosomal interaction domains (Dame et al., 2020; Verma et al., 2019).

The spatial organisation of the chromosome on a global level also has effects on DNA replication. Bacteria can broadly be split into two organisational patterns of longitudinal *ori-ter,* such as *C. crescentus* (Viollier et al., 2004) and transverse left-*ori*-ter, such as *E. col,* shown in figure 1.1 (Wang et al., 2006; Nielsen et al., 2006).

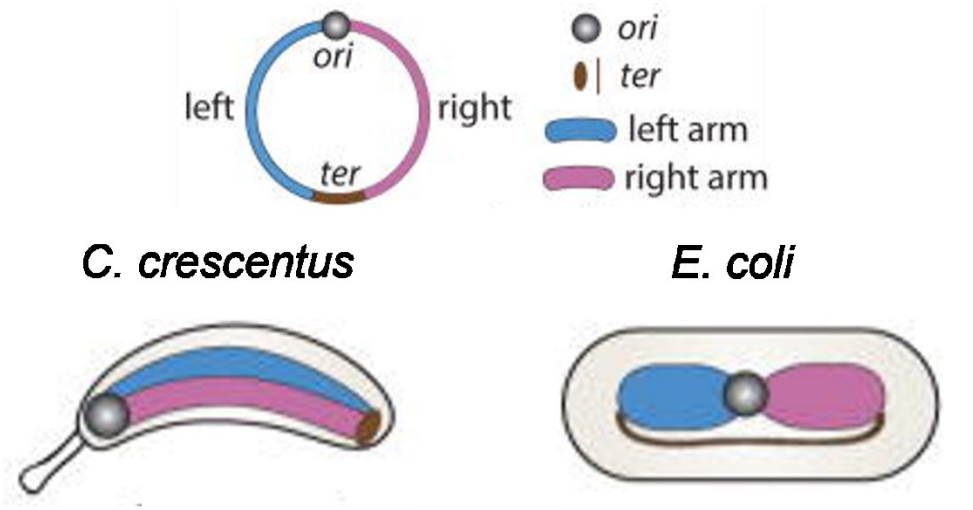

Figure 1.1: Spatial organisation of nucleoid comparison between species
Shown is the two main different organisational patterns, longitudinal (ori-ter) represented by C. crescentus and transverse (left-ori-ter) represented by E. coli. Adapted from (Wang & Rudner, 2014a).

1.1.1 Nucleoid mesh

The nucleoid can be described as a meshwork of DNA and proteins, where an overall condensation of the genetic material interplays with local organisation established by DNA-interacting proteins. Despite lacking a membrane envelope that physically segregates the chromosome away from the cytoplasm, a densely compacted nucleoid can behave in many ways similarly to eukaryotic nucleus. The dense packing of the chromosome results in a nucleoid that is a physically distinct cellular structure with clearly defined overall structure and boundaries (Xiang et al., 2020). For understanding how the nucleoid structure excludes other cellular components,

the spacing between the dense DNA meshwork (DNA mesh size) is a useful concept. Such meshwork has consequences for all chromosomal organisation levels (McLeod et al., 2016; Xiang et al., 2020). Mesh pore size impacts the control of the nucleoid surface by which larger macromolecules such as ribosomes are excluded from the nucleoid interior. Mesh pore size is dictated by the same conditions that act to condense and expand the nucleoid: proteins, supercoiling, processes such as transcription and liquid-liquid phase separation (Gupta et al., 2023).

Nucleoid exclusion of larger molecules can result in cytoplasmic component concentration balance changing and effecting its osmotic pressure. This pressure can also act to compact the nucleoid (Xiang et al., 2020).

The nucleoid can also be regarded as a soluble polymer inside cytoplasm acting as a solvent. In such case, the cytoplasm is a poor solvent, where interactions between the two are not favoured over other interactions taking place in the cytoplasm. Instead, self-interactions of DNA in the chromosome are favoured, further compacting the nucleoid. This is thought to increase compaction by 100-fold (Xiang et al., 2020), accounting for 10% of compacting “pressure” required to fit the chromosome within the individual cell.

Additionally, DNA and RNA can form liquid-liquid phase separation (LLPS) condensates with HU in *E. coli*. Such compartments are phase separated from the cytoplasm, pushing the nucleoid in on itself and potentially acting as a condensing pressure and effecting the organisation of the nucleoid (Nandana & Schrader, 2021; Gupta et al., 2023)

1.1.2 Nucleoid associated proteins

The nucleoid associated proteins (NAPs) make up a large proportion of all DNA binding capable proteins within the cell. In part, the postulated role of a NAP is to bind DNA and condense the chromosome, however the NAPs also fill a broad range of individual functions linked to interactions with DNA and interactions with transcription (Dorman et al., 2020). The nucleoid is highly dynamic and has to accommodate gene expression and DNA replication. NAPs contribute towards local and global organisation of the nucleoid whilst also interacting and interplaying with gene expression processes (Dillon & Dorman, 2010). NAPs are relatively highly conserved between different bacterial species although exception exist (Amemiya et al., 2021). The notable and best studied NAPs are the small proteins transcriptional

dual regulator (HU), histone-like nucleoid structuring protein (H-NS), factor for inversion stimulation (FIS) and integration host factor (IHF) (Hołówka & Zakrzewska-Czerwińska, 2020). Other larger DNA interacting proteins are considered NAPs as well. These include prominently the SMC complexes which for large homodimeric ring complexes that encircle and thus connect two DNA strands (Hoencamp & Rowland, 2023). In *B. subtilis,* proteins MukB in *E.* coli and SMC are responsible for DNA segregation and act as NAPs (Vos et al., 2013; Bock et al., 2021). Both have function in the cell cycle, whereby such complexes reorganise the genome and induce condensation by loop extrusion (Britton et al., 1998;Lioy et al., 2018). However, they both have important roles in chromosomal organisation, such as in *E. coli* the formation of a core from which DNA loops reach from, which contrary to *B. subtilis,* in which SMC aligns the chromosomal arms to either end of the cell (Mäkelä & Sherratt, 2020).

Other NAPs mentioned above such HU, FIS and IHF are responsible for induction of local bends and curves into the DNA strand. HU can in many ways be considered to be functionally similar to eukaryotic histone proteins. HU wraps DNA non-specifically around the protein, thereby inducing sharp bends on the DNA in a manner that contributes to condensation of the overall nucleoid (Nguyen et al., 2009). Roughly 10% of DNA is covered of HU (Dillon & Dorman, 2010). However, HU can also bind to RNA with the same affinity (Stojkova et al., 2019), suggesting possible involvement of HU in transcription regulation as well (Dorman, 2014; Kamashev, 2000). The role of HU in nucleoid morphology should not be understated, as a HUα(triKA) mutant results in an incorrectly segregated nucleoid with increased compaction (Bettridge et al., 2021).

FIS also covers a large proportion of chromosome, binding at AT rich sequence regions to induce bends to the DNA of around 90° (Dame et al., 2020). IHF can introduce more dramatic bends of 160° to the DNA, with implications of IHF bending involved in relocating RNAP closer to regulatory proteins (Ryan et al., 2002; Stojkova et al., 2019).

In contrast to the NAPs discussed above, H-NS introduces bridges between two DNA strands. H-NS can act as a gene silencer of horizontally acquired genes (Scholz et al., 2019; Kahramanoglou et al., 2011). Other proteins unrelated to NAPs, such as Rok in *B. subtilis,* can also introduce such bridges between adjacent DNA strands (Albano et al., 2005).

1.1.3 DNA Supercoiling

The nucleoid is further condensed by supercoiling, whereby DNA is twisted on itself, resulting in continuous loops. Depending on the direction of the twist in relation to the DNA helicity, supercoils can be described as negative or positive. Twist that aligns with the direction of the native helix rotation (of regular B-DNA) result in positive supercoiling whereas counter directional twists lead to negative supercoiling. As the bacterial chromosome is a closed circle unable to relax the coiling at strand ends, DNA supercoiling leads to formation of DNA loops instead (Dame et al., 2020; Toro & Shapiro, 2010). Control of supercoiling throughout the chromosome is essential for the cell to regulate overall nucleoid density. To control supercoiling, the cell utilises various mechanisms, notably the use of topoisomerases and DNA gyrase (Dame et al., 2020; Martínez-Antonio et al., 2009), though HU can also contribute via its bending activity (Woldringh et al., 1995; Stojkova et al., 2019). DNA gyrase is responsible for the active creation of negative supercoils, whilst the opposite is true for topoisomerases which remove negative supercoiling.

1.2 Gene expression

1.2.1 Transcription and RNA polymerase

Transcription is a well-studied cellular process conserved across all life. Transcription synthesizes RNA from the coding DNA by RNA polymerase (RNAP), a large multi-subunit protein. RNA can be split into two main product types: messenger RNA (mRNA) and non-coding RNA (ncRNA). mRNA encodes for an amino acid sequence used as a template for translation by ribosomes. ncRNA encode for a multitude of RNA types: ribosomal RNA (rRNA) for ribosome assembly, tRNAs for use in translation and small regulatory RNAs (sRNA) that regulate gene expression (Guo, 2014; Gottesman & Storz, 2011).

RNAP is conserved throughout all living organisms. Structurally they are well conserved between bacteria. All multi-subunit RNAP possess five subunits in bacteria. There are two alpha subunits which are believed to be a platform from which the other subunits rest. There is a beta and a beta prime subunit which form the catalytic clef between them, forming the iconic RNAP crab claw structure. The omega subunit helps promote assembly of the RNAP (Minakhin et al., 2001). In different bacterial species, there are various types of omega subunits, which can interchange within a species. These five subunits form the core enzyme, which

possesses catalytic activity but cannot yet recognise and bind promoters throughout the genome. Another factor is required for promoter specific transcription initiation known as sigma. Binding the core enzyme with sigma forms the holoenzyme (Murakami et al., 2002). The holoenzyme can recognise, bind and melt DNA at a promoter size by help of the bound sigma factor. Transcription starts where nucleotides enter the active site and are incorporated into the growing RNA chain. After 2-10 nucleotides, the sigma subunit leaves the core enzyme, which can continue to elongate. This is reviewed in Bacterial RNA polymerases: the wholo story by Murakami and Darst (Murakami & Darst, 2003).

After initiation, transcription elongation starts where the RNAP moves down the DNA template to produce the growing RNA transcript. Termination of RNAP can occur in several ways. Primarily, the end of a gene or operon is marked by a terminator sequence, encoding for a hairpin. The hairpin is CG rich for tight binding prefaced by a poly U code in the template (Roberts, 2019). Alternatively, RNAP can pause when transcribing, where if any RNA from the RNAP is free, an RNA helicase known as Rho factor can bind the free RNA. Rho can travel along the RNA, where if it catches up the RNAP, will destroy the complex (Song et al., 2022).

1.2.2 Transcription and the chromosome organisation

Transcription interacts with organisational features of the chromosome, notably with supercoiling. Interactions of supercoiling within the chromosome help regulate the chromosomes organisation. crucially the relationship between transcription and supercoils. Transcription can affect positions of supercoiling sites whilst supercoils can regulate gene expression (Ma & Wang, 2016). Importantly, negative supercoils reduces the energy required to separate the DNA strands, and encourages binding of RNAP (Fogg et al., 2021).

Transcriptional regulation by DNA supercoiling can be regulated by topoisomerases and DNA gyrase (Martis B. et al., 2019). Interestingly, depending on the genes expression rate and level of transcription, alternative topoisomerases will be used. Low output promoters require only topoisomerase I to regulate supercoiling, however increased transcriptional activity at a high output promoter requires management by addition of topoisomerase II (Kouzine et al., 2013). According to the twin supercoiled domain model (Figure 1.2), the act of transcription itself also induces local supercoiling (Forth et al., 2013). RNAP in elongation progresses along the DNA at

the gene, inducing rotation in the DNA, resulting in positive supercoiling downstream of the RNAP, and negative supercoil upstream (Forth et al., 2013). Negative supercoils downstream also further promotes RNAP binding to the area, as negative supercoils DNA strands are easier to melt for initiation. Downstream positive supercoiling induced by the transcribing RNAP can affect roadblocks and positively contribute to transcription processivity. Higher levels of transcription at a locus will induce higher degree of supercoiling (Forth et al., 2013;Lavelle, 2014).

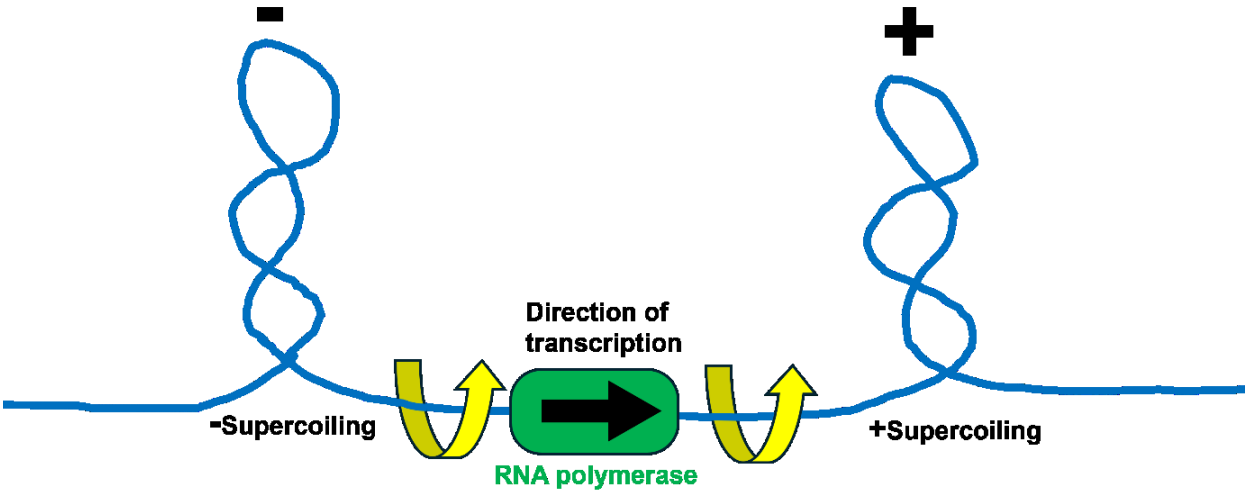

Figure 1.2: Twin supercoiled domain model. *The effect of transcription on local supercoiling upstream and downstream of the elongation complex. Topoisomerase reduces supercoiling to allow RNAP association to transcription start site and initiation. Elongation sees the RNAP twist DNA template inducing positive and negative supercoils downstream and upstream, respectively. Adapted from (Forth et al., 2013)*

Highly expressed genes or operons rely on high RNAP availability and ability to access and bind the promoter (Helmann, 2009). In fact, highly expressed regions of the chromosome participate in the creation of domains boundaries, specifically the chromosomal interaction domains mentioned previously. In this scenario, a gene that requires high expression will be left “open”, whereby supercoiling and condensation will not occur. Due to this, a space is created by the transcribed gene, physically separating genes either side of the “open” gene, highlighted in Figure 1.3 (Le & Laub, 2016). As mentioned previously, the nucleoid is under constant condensation, whereas here transcription contributes slightly to decompaction. In addition, RNAP also has interactions with condensins such as SMC, which must be able to bypass local transcribing RNAPs while sliding along the DNA. While low level of transcription

does not interfere with SMC significantly, highly expressed genes or operons can considerably impede the progress of the SMC complex (Brandão et al., 2019a).

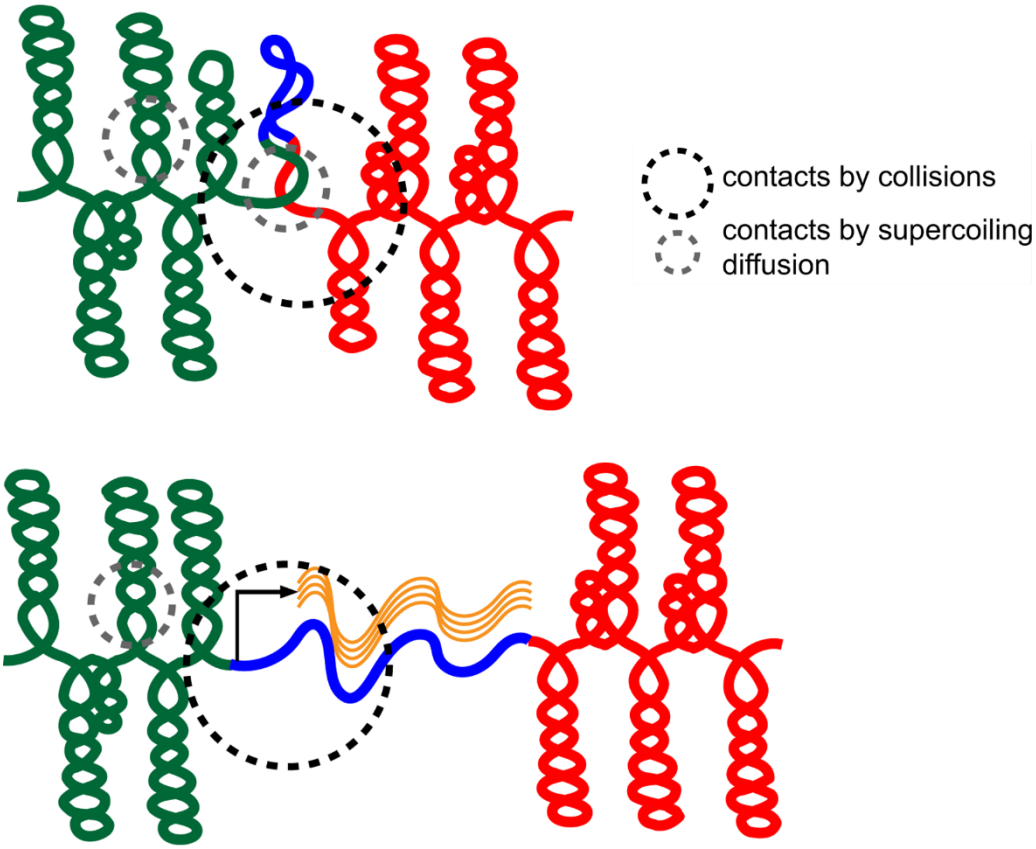

Figure 1.3: Chromosomal domain boundary formation by transcription. *Chromosomal domain boundaries in red and green are physically separated by a highly transcribed region, in blue, thus forming a domain boundary. This locally decompacts DNA, removing collisions contact between red and green domains. Supercoil spreading along the DNA is also supressed by highly transcribed regions. Adapted from* (Le & Laub, 2016).

1.2.3 Translation

Nascent mRNA transcripts as a product of transcription are decoded via tRNAs in the ribosome. Bacterial ribosomes consist of two subunits of 50S and 30S, which upon assembly for translation form the mature 70S ribosome. Both subunits are composed of rRNA and multiple protein units (Gualerzi & Pon, 2015; Zhu & Dai, 2020). Translation initiation requires only the 30S subunit binding the nascent mRNA alongside initiation factors. Initial binding at the 30S is carried out by a specific region of rRNA, the 16S, which undergoes sequence-specific base-pairing with a specific

recognition sequence located in the 5'- untranslated portion of the mRNA with an appropriate distance upstream of the start codon (termed the Shine-Dalgarno sequence, or ribosomal binding site RBS). Once recognised, initiation factors assist binding and the incorporation of the first amino acid (formyl-Methionine), delivered by the corresponding initiator tRNA. This initiation complex is then bound to by the 50S to form the translational complex, as reviewed by Gualerzi and Pon (Gualerzi & Pon, 2015).

After the translational complex is formed, the 70S ribosome starts the elongation process. Triplet codons from the mRNA sequence are matched to by tRNAs, that carry specific amino acids. Upon a matching codon-anticodon pair, the amino acid is deposited and included in the growing peptide chain. Peptide bonds between amino acids of the nascent polypeptide chain are formed by peptidyl transferase activity of the 50S ribosome. Emerging mRNA that has undergone translation can be further bound by other ribosomes, resulting in so-called polysomes. The end of the coding region is recognised by a stop codon, which triggers termination or elongation and release of the polypeptide chain. Following termination or elongation, the 30S and 50S subunits dissociate from mRNA and each other (Deana & Belasco, 2005; Kannaiah et al., 2019). mRNA can be used by following ribosomes or eventually undergoes degradation by RNase. The rate of translation is approximately 20 aa/s in *E. coli* (Zhu & Dai, 2020;Zhu et al., 2016). With approximately 17 aa/s the rate elongation is similar in *B. subtilis* (Johnson et al., 2020).

1.2.4 Coupled transcription translation.

As mentioned previously, most bacteria lack intracellular membrane-based organelles and genomic DNA is, thus, in direct contact with the cytoplasmic components such as ribosomes. This lack of a barrier allows chromosome specific and cytoplasmic based processes to potentially directly interact with each other (Irastortza-Olaziregi & Amster-Choder, 2021;Kannaiah et al., 2019). Unlike their eukaryotic counterparts, bacterial transcription and translation machineries indeed functionally interact in a process termed coupled transcription translation (CTT). In CTT, RNAP produces an mRNA transcript that can interact with a ribosome and serve as a template for translation while the mRNA is still being synthesised. Such interaction forms a complex between DNA, RNAP, nascent mRNA and the ribosome (Figure 1.4). CTT is frequently regarded as a hallmark of bacterial gene expression

although still remains a topic of controversy in various bacterial species (Irastortza-Olaziregi & Amster-Choder, 2021).

CTT as a phenomenon was proposed in 1964 by G. Stent (Stent, 1964). Direct evidence for CTT has since been provided most recently by structural studies that highlight a direct interaction and formation of an expressome (C. Wang et al., 2020). In an expressome model, NusG can form a physical connection between RNAP and a ribosome, both associated with the same mRNA strand(Saxena et al., 2018; Yakhnin et al., 2020). One other model of the expressome argues for interaction based on collision (Kohler et al., 2017). It has been suggested that multiple orientations between RNAP and ribosomes could show various methods of coupling and when coupling can occur (Woodgate & Zenkin, 2023). Both transcription and translation have similar elongation rates (~50 nt/s and ~60 nt/s respectively), thus making collisions between the respective machineries likely (Zhu et al., 2016).

Coupling of transcription and translation offers benefits to each process. Premature transcription termination mediated by the aforementioned Rho factor can bind active RNAP and prematurely disband the complex (Said et al., 2021). NusG is involved in both Rho dependant premature transcription termination as well as RNAP-ribosome interactions. Such interaction leads to competition for NusG, thus less premature termination will occur in CTT (Saxena et al., 2018). CTT also has an effect on stalled RNAP, whereby ribosomes can physically push the stalled transcription complex through roadblocks and backtracks, thus preventing generation of double strand breaks upon collision between transcription complex and the replisome (Lass-Napiorkowska & Heyduk, 2016;Stevenson-Jones et al., 2020). Additionally, in *E. coli,* RNAP transcription rates for rRNA operons have been reported to be higher (~90 nt/s) than for mRNA operons, suggesting that the ribosome might act as a transcriptional regulator for mRNA coding sequences (Vogel & Jensen, 1994).

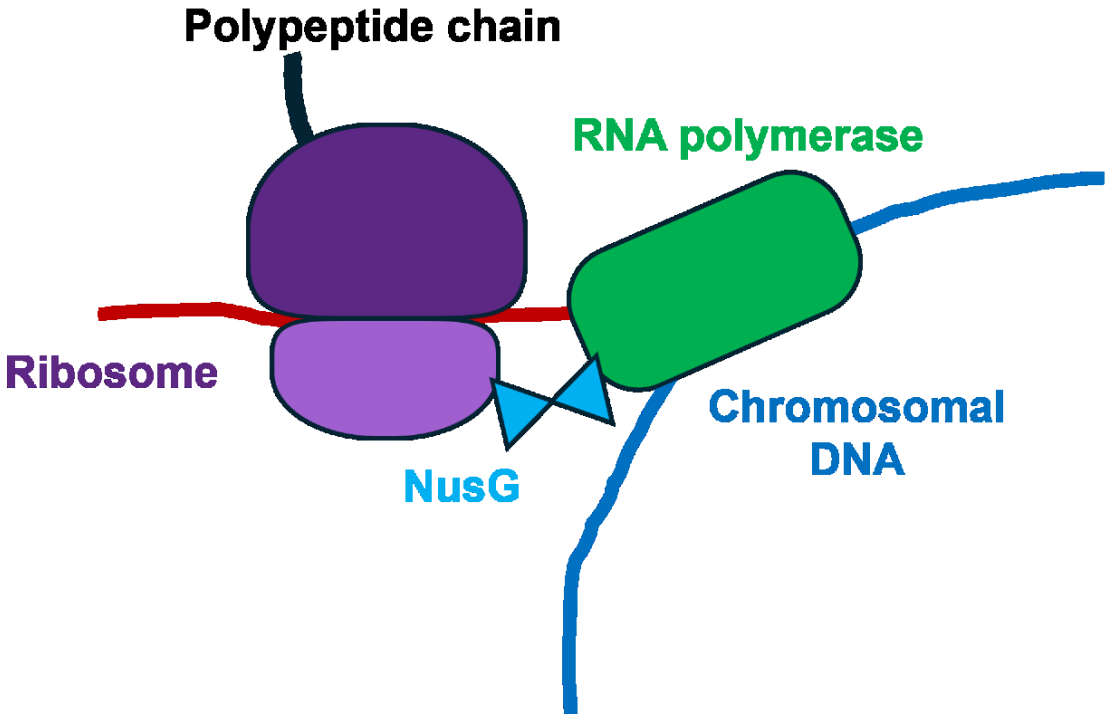

Figure 1.4: Model of coupled transcription-translation. *Transcribing RNAP can physically interact with a ribosome translating along the nascent mRNA. This interaction can be facilitated by NusG.*

CTT can also protect the nascent mRNA by physically shielding the emerging transcript by binding and translating it. This blocks mRNA from degradation via RNase E (Kannaiah et al., 2019). Additionally, co-transcriptional translation of mRNA can suppress re-annealing between RNA and DNA, which could result in formation of problematic so-called R loops (Gowrishankar & Harinarayanan, 2004).

Although CTT is considered a bacterial hallmark and the process has been extensively studied *in vitro*, investigations *in vivo* are underrepresented. The existence of CTT and the expresome however relies on the initial assumption that nucleoid associated processes such as transcription and cytoplasmic processes such as translation are free to interact in a bacterial cell. Evidence of bacterial RNAP localisation suggests that transcription occurs within the nucleoid structure, whilst ribosome location varies somewhat between species. In *C. crescentus,* ribosomes can be found homogenously mixed within the nucleoid with RNAP (Montero Llopis et al., 2010), although this may be a non-typical case, as its genome fills the whole cell akin to decondensed nucleoids in *E. coli* and *B. subtilis* under rifampicin treatment. However, in *E. coli* and *B. subtilis,* ribosomes are strongly segregated away from the nucleoid-occupied space (Lewis, Thaker and Errington, 2000; Cabrera and Jin,

2003). As mentioned above, the nucleoid meshwork and condensed chromosome is postulated to physically prevent large structures and complexes such as the ribosome from penetrating. This results in variation between species of the nucleoid density and ratio with the cytoplasm (Gray et al., 2019). The segregation between nucleoid and ribosomes has been attributed to a multitude of factors: repulsing negative DNA/RNA charges between nucleoid and ribosome (Joyeux, 2016;Somalinga & Roy, 2002), size exclusion from chains of polysomes (Mondal et al., 2011) and finally phase separation-type processes (Joyeux, 2018). Irrespective of the mechanism that underlies the exclusion of ribosomes from the nucleoid, the existence of phenomenon raises the fundamental question how CTT can occur when the processes are spatially separated in a cell?

To answer this, several theories have been put forward. In one model, active genes loci migrate to the nucleoid surface, where ribosomes can bind to emerging nascent mRNA without a requirement for penetration into the meshwork (Yang et al., 2019) (Weng et al., 2019; Ladouceur et al., 2020). In an alternative model, free 30S and 50S ribosomal subunits may be able to penetrate the nucleoid mesh individually, whereby only the 30S is initially required to bind nascent mRNA. Upon successful initiation, binding of 50S to the RNAP-30S complex completes the expressome, resulting in the large 70S ribosome that is excluded from the dense nucleoid (Sanamrad et al., 2014; Gualerzi & Pon, 2015).

That transcription and translation are in fact functionally uncoupled has also been postulated. One investigation into CTT was carried out by Chen and Fredrick where they rationalise the experiment: in CTT only one lead ribosome can engage with RNAP at a time, thus observing the difference between first round and multiple rounds of translation would offer insight into the nature of coupling. In a first round, the ratio between translation products and transcription would be 1:1, however multiple rounds of translation would see the protein product increase by magnitudes. Using this logic, a gene for a self-cleaving ribozyme was used, which would rapidly fold and cleave after translation. Thus, only one round of translation was possible. Multiple rounds were generated by 3 mutations in the ribozyme. In one round translation events, translation to transcription product ratio were 3:1, arguing against strict coupling. Mutant RNAP (I572N) that decreases rate of transcription in the same system however observed a lower ratio closer to 1:1, thus showing CTT can be promoted if the rates match (M. Chen & Fredrick, 2018). Such arguments point out a

potential stochastic model for CTT, not guaranteed. A study looking into mRNA lifetime stability suggests that translation isn't coupled to transcription (Deneke et al., 2013). In these experiments substantial mRNA decays was detected before translation of the transcript has begun, thus arguing against CTT-depedent protection from degradation (Deneke, Lipowsky and Valleriani, 2013).

Additional argument against CTT has been made in *B. subtilis* based on analysis of transcription and translation speeds. Johnson et al. showed that the average transcription rate of *B. subtilis*' RNAP is higher (~75 nt/s) than the ribosomal translation rate (~50nt/s). Thus, the elongation complex runs away from the ribosome rather than collides with it. Additionally, they backed up runaway transcription by showing RNAP is insensitive to translation. This is based on the pattern of trailing ribosomes will block the formation of terminator hairpins. To test this, they removed the stop codon of a highly expressed gene in both *E. coli* and *B. subtilis,* forcing translation through the terminator. Transcription readthrough however was undetectable in *B. subtilis* but was restored in *E. coli* (Johnson et al., 2020). For example, rates between RNAP and Ribosome can be matched in certain scenarios, such as in the presence of RNAP roadblocks and pauses. NusG of *B. subtilis* is also different as its role in this organism is more related to RNAP pausing (Yakhnin et al., 2020), this suggesting that the physical bridge between RNAP and ribosome might not be identical between *B. subtilis* and *E. coli*.

Another argument was made regarding how transcription termination in *B. subtilis* is seemingly insensitive to the effects of translation. In this example, when the ribosome was forced through an intrinsic terminator, transcription run-through product was not observed, suggesting that the ribosome is not regulating termination signals. In fact, a shorter distance between stop codons and intrinsic terminators was also found in *B. subtilis* (Johnson et al., 2020). This short gap was suggested to indicate a lack of ribosome-RNAP interaction as ribosome coupling would block the sites though close proximity and steric clashes. The stop codon-terminator distance was thus used as a signature to determine a lack of coupling. When analysing other bacillota (previously firmicutes), over half of the analysed species bore this potential signature of uncoupled transcription translation. Other Gram-positive clades of bacteria bore the signature as well, though Actinobacteria, Bacteroidetes and some phyla of Proteobacteria have terminators far from the stop codon, not bearing the same signature.

However, it should be noted that a close proximity of the stop codon and the intrinsic terminator site is not exclusive to all genes. 72% of stop codons are located within 12nt of intrinsic terminators (Johnson et al., 2020). *B. subtillis* also possesses mechanisms to avoid intrinsic terminators to regulate the expression of genes, the primary examples being the expression of the tryptophan (*trp)* and bacterial multidrug resistance (*bmr)* operons. Depending on increased or decreased tryptophan levels within the cell, the nascent mRNA encoding for the structural genes can be altered at the secondary structure level to alternate between two competing forms: a terminator or an antiterminator. Such a process is known as attenuation. At higher tryptophan concentrations, the TRAP protein will bind onto the mRNA to prevent formation of the antiterminator, allowing the intrinsic terminator to form and preventing further transcription. In low tryptophan concentrations, the opposite is true, and the TRAP won't bind, leaving the mRNA to form the opposing antiterminator, allowing the RNAP to continue transcribing the entire operon (McAdams & Gollnick, 2014).

Similarly to *trp* expression and attenuation is the multidrug ABC transporter of BmrC/BmrD, which is hypothesized to be regulated by the ribosome coupled interaction with RNAP. In this model, the RNAP is closely followed by the ribosome coupled interaction whilst transcribing the *bmrB* gene. The *bmrB* gene is followed closely by the *bmrC* gene, with an intrinsic terminator between the two. In the absence of antibiotics that target the ribosome, fully efficient translation allows for formation of the intrinsic terminator, thus preventing transcription readthrough into *bmrC*. Upon antibiotic treatment that targets the ribosome, the rate of translation will decrease. This creates a larger space between the RNAP and trailing ribosome on the mRNA, whereby the antiterminator secondary structure can form in place of the terminator, thus RNAP transcription runs through (Reilman et al., 2014).

1.2.5 Bacterial membrane and SRP pathway

The bacterial cell envelope, which encases the cytoplasm can vary significantly in terms of composition and structural organisation. Gram-negative bacteria, such as *E. coli,* possess two separate membrane layers, inner and outer membrane, with a thin peptidoglycan layer found between the two in the periplasmic space (Silhavy et al., 2010). Gram-positive bacteria, such as *B. subtilis,* possess only one membrane layer functionally comparable to the Gram-negative inner membrane, surrounded by a thick peptidoglycan layer interwoven with teichoic acids.

Transferring proteins into and beyond the cytoplasmic membrane a universal requirement. Proteins synthesised destined to be embedded into the cytoplasmic membrane are part of the membranome, whilst those destined to cross the membrane proteins are part of the secretome. In *E. coli*, approximately 22% of the total proteome is part of the membranome and 13% is part of the secretome, totalling 35% destined to the membrane (Green & Mecsas, 2016, Tsirigotaki et al., 2017).

In *B. subtilis*, multiple pathways are used to achieve this. So far, four different pathways have been identified for protein export, namely the twin-arginine translation (Tat) pathway, the ATP-binding cassette (ABC) pathway, a pseudopilin export pathway and most notably the Secretory (Sec) pathway. The Sec pathway is highly conserved and generally divided into three steps: targeting of protein destined for the membrane, translocation to/across the membrane and release (Kang et al., 2014).

Two modes in *B. subtilis* have been identified to recognise and translocate membrane/secretory proteins to the SecYEG translocase. The firstly is SecA, which is generally responsible for delivering secreted proteins to the translocase. SecA itself is an ATPase which recognises and delivers proteins post-translationally (Fiedler & Graumann, 2024), differing itself from the second Sec pathway of the Signal Recognition Particle (SRP). SRP is responsible for recognising emerging nascent polypeptide chains of an integral membrane protein and co-translationally escorting to SecYEG translocase.

1.2.6 SRP structure is universally conserved

SRP is a Ribonucleoprotein (RNP), which has active sites for proteins to bind, unlike the ribosome, another RNP which has RNA active sites. The SRP is highly conserved throughout all form of life, with most studies being conducted on mammalian SRP. It is essential to life and interacts directly with various proteins and the ribosome. Functionally, the SRP acts as a scaffold to bind various functional proteins, that overall, specifically recognises an amino acid sequence emerging from the ribosome, termed the signal anchor. SRP is then also responsible for the pausing and arrest of translation, preventing further peptide additions during transport.

The structure of SRP is highly conserved. The mammalian SRP is a single RNA divided into domains, notably the Alu and S domains found at either end of the RNA structure (Figure 1.4). In mammalians six proteins bind to the SRP RNA at the Alu (SRP9 and SRP14) and at the S domain (SRP19, SRP54, SRP68 and SRP72). In *B.*

subtilis and other Gram-positive bacteria, the structure of SRP RNA (known as the small cytoplasmic RNA) remains similar, with a homolog of the SRP54 protein, Ffh (Fifty-four homologue) still present. However, no homologues for the other SRP proteins are present. Strikingly in *E. coli* and Gram-negatives the SRP RNA is significantly shorter, removing the Alu domain, only leaving the S domain, as highlighted in figure 1.5 (Beckert et al., 2015).

The S domain is highly conserved. This domain is responsible for binding of the Ffh protein, which allows for the function of targeting the ribosome and recognising the emerging signal anchor. Recognition of the signalling anchor is based on hydrophobicity and α-helical conformation of a polypeptide that corresponds to a transmembrane domain once correctly inserted into the membrane (Luirink et al., 2005;Valent et al., 1997), rather than based on a specific amino acid signature. Ffh and the SRP are responsible for the cycling through the stages of the Sec pathway. Ffh achieves signal recognition of the anchor and then transports the SRP-ribosome complex to the cytoplasmic membrane, interacting with the homologue membrane bound receptor FtsY (Moser et al., 1997; Mayer et al., 2021). SRP-Ffh interaction with FtsY binds the entire ribosome complex to the membrane.

Whilst the S domain is highly conserved, the Alu domain is less so, as between species the structure or presence of it varies greatly. Although in mammalian SRP two proteins SRP9 and 14 are found to bind at the Alu domain, they are absent in *B. subtilis.* The Alu domain is proposed to be responsible for translational arrest during SRP/Ribosome interactions, where it blocks aminoacyl tRNA entry. Additionally, the Alu domain can interact with ribosomal translation elongation factors binding sites, for similar translational arrest purposes. The loss of the Alu domain in *E. coli* therefore suggests either the lack of translation arrest or alternative mechanisms to do so outside of Alu/SRP. The Alu domain in *B. subtilis* is similarly not essential, however it does prevent endospore growth and certain secretory proteins such as α-amylase (Nishiguchi et al., 1994).

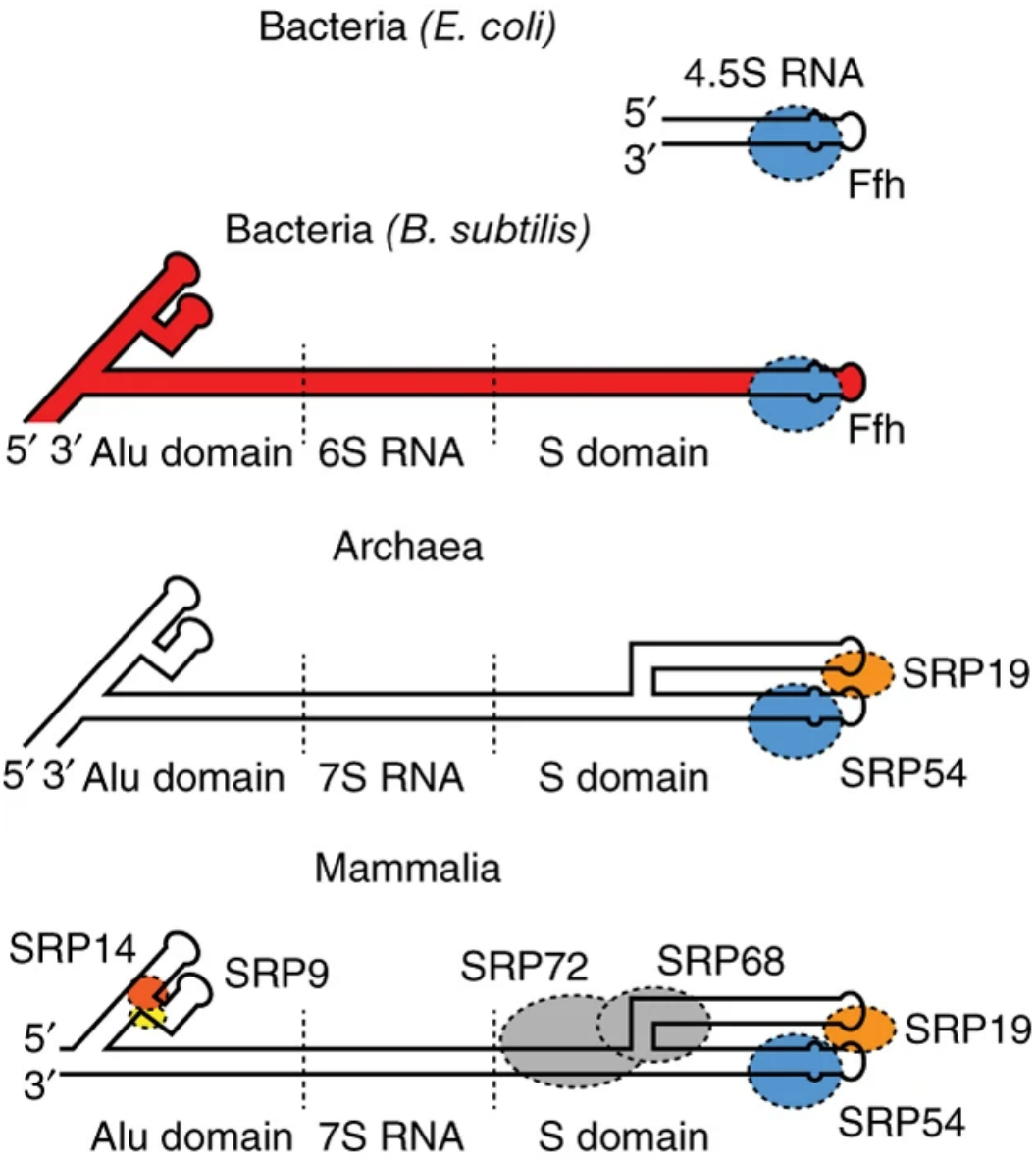

Figure 1.5: SRP RNA structure evolution throughout life. *SRP RNA structure throughout various life forms, highlighting the similarities in the conserved molecule. Notably in blue is the SRP54 and its homologue Ffh (Adapted from Beckert et al., 2015).*

1.2.7 SRP cycle

Ffh and SRP initially recognise the emerging signal anchor. Upon emergence of the signal anchor, the SRP arrests translation (Fiedler & Graumann, 2024), and directs the SRP-translation complex to the membrane SRP receptor FtsY (Kudva et al., 2013). The ribosome-SRP-FtsY complex interacts to the SecYEG translocase,

whereby the paused ribosome is handed over via a switch of GTP between Ffh and FtsY. The GTPase functionality of both proteins results in the release of Ffh and the SRP from the ribosome, relieving translational arrest. Insertion of the nascent hydrophobic polypeptide into membrane, resulting in a correctly folded transmembrane domain, is carried out by translation of the polypeptide directly into the SecYEG translocase, and the secretion activity of SecYEG (Green & Mecsas, 2016).

A minor translocon also able to insert integral membrane proteins to the cytoplasmic membrane is known as YidC, known to both *E. coli* and *B. subtilis* (Saraogi & Shan, 16 2014; Xie & Dalbey, 2008). YidC can be independent or cooperate with SecYEG and is typically used for small membrane proteins with single transmembrane domains only, though YidC can be act post-translationally (Robinson & Woolhead, 2013) or post-translationally where it cooperates with SecYEG and can interact with SRP/ribosomes (Facey et al., 2007).

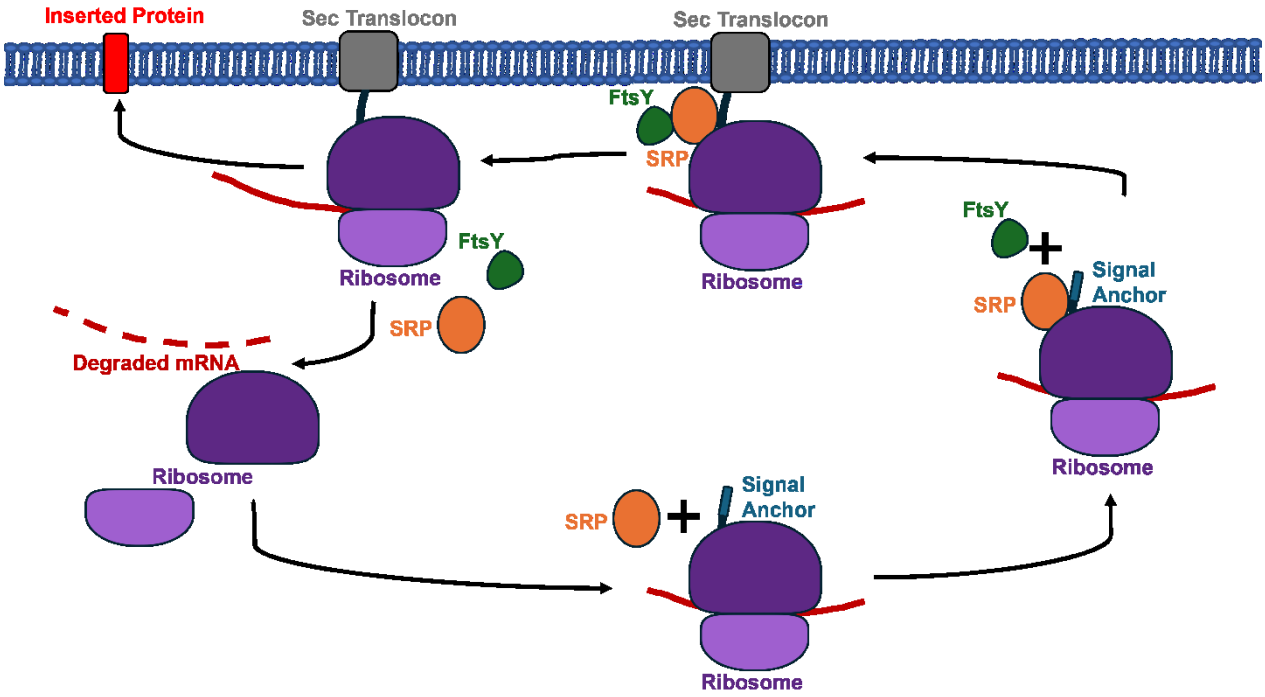

Figure 1.6: SRP mediation of protein targeting and insertion into the membrane. *SRP binds ribosome recognises signal anchor of emerging polypeptide and pauses translation. SRP-Ribosome complex is bound to by FtsY either in cytoplasm or at membrane. SRP-FtsY-Ribosome complex the interacts with the membrane-integral SecYEG translocon. Translation is resumed as SRP and FtsY leave the complex and now feed the polypeptide directly into the SecYEG pore. The process in completed upon translation termination, release of the translated protein to the membrane, degradation of the mRNA, and recycling of the ribosome subunits.*

1.3 Transertion

Transertion a cellular process that involves coupling between transcription, translation, and the co-translational secretion of proteins into the cell membrane via the SRP pathway (or YidC) pathway (Norris, 1995). Historically, transertion is mostly a hypothesis with little direct experimental evidence. Transertion was first postulated in 1995 by V. Norris (Norris, 1995), though it is worth highlighting that RNAP-mRNA-ribosome links have had evidence provided previously, along with speculation by Kleppe et al before (Kleppe et al., 1979) that integral membrane proteins are synthesised at the membrane with the RNAP and ribosome. The molecular mechanism behind how transertion works is clear by combination of CTT and co-translational secretion, however little direct evidence has come out in support of it. DNA association with the membrane has been observed previously however and could also provide alternate mechanisms of transertion. Transcription factors embedded in the inner membrane such as ToxR in *Vibrio cholerae* (Miller et al., 1987), CadC in *E. coli* (Tetsch et al., 2008) or VtrA/C in *Vibrio parahaemolyticus* (Kaval et al., 2023) can all bind DNA from the membrane. Such protein/DNA interaction would be ideal candidates for transertion to take place, but transertion has not been shown to apply to all examples. A limited number of DNA binding and also membrane bound transcription factors are available, making them unlikely as the only sources of transertion. It should be noted that other integral membrane proteins in cells can have DNA binding capabilities and yet might have no role in inducing transertion. In *B. subtilis* with DivVIA (X. Wang & Rudner, 2014b), *Caulobacter. crescentus* with PopZ (Ptacin et al., 2014) and *V. cholerea* with HubP (Yamaichi et al., 2012), tethering of the chromosome to cell poles is essential during chromosome segregation. Whether transertion has any effect here is unclear, but studies have shown a lack of RNAP at the poles, making transertion unlikely at this location (Bakshi et al., 2012). Another protein in *B. subtilis,* Noc, binds to the nucleoid first, before it can then bind to the cell membrane, whereby it inhibits cell division(Adams et al., 2015). Discussion on the matter seem like Noc and transertion are mutually exclusive, however the potential for transertion to leach off Noc's DNA anchoring is a possibility.

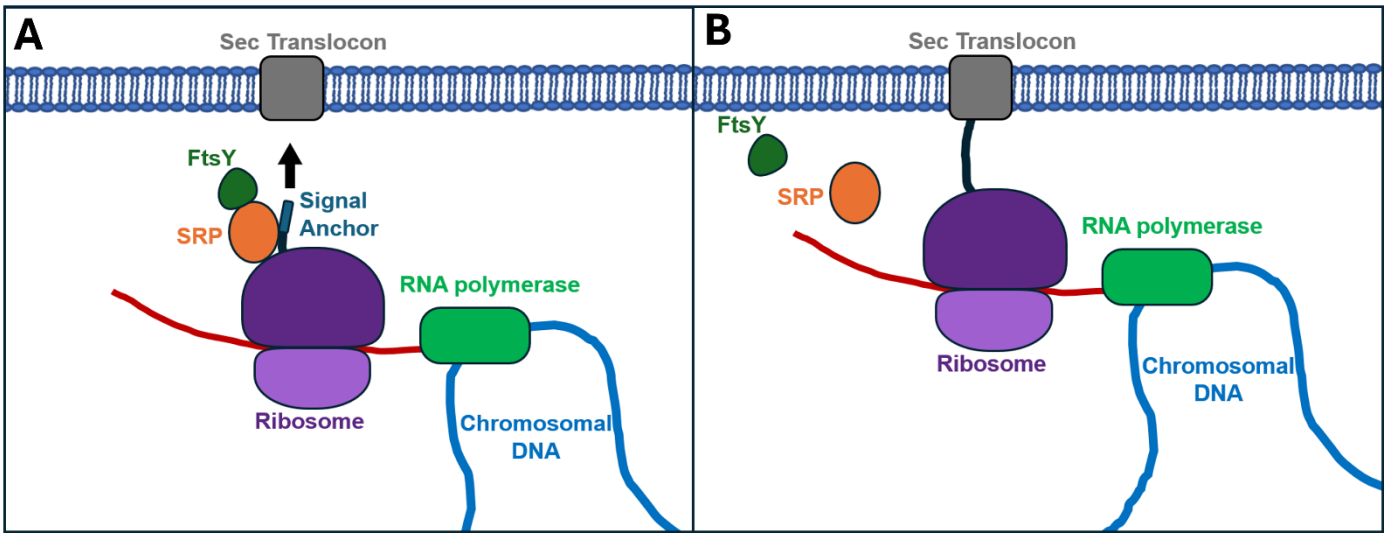

Figure 1.7: Model of transertion. A.) *Translation by a CTT complex results in synthesis of a nascent polypeptide that includes transmembrane protein signal anchor. The anchor is recognised by SRP, which pauses translation and, together with FtsY, escorts the CTT complex to the membrane SecYEG translocon.* ***B.)*** *Translation of the transmembrane proteins continues, thereby tethering the affected chromosomal DNA locus, RNAP, mRNA, and the Ribosome to the membrane.*

1.3.1 Role of transertion in nucleoid structure

If transertion complexes indeed form in vivo, the process would link a chromosomal locus encoding an integral membrane protein, when expressed, to the membrane via the mRNA-RNAP-Ribosome CTT complex. In *E. coli* there are 1,133 integral membrane proteins encoded for by the genome, which are integrated into the inner membrane (Bernsel & Daley, 2009). These genes are distributed throughout the genome allowing coverage of the entire membrane by transertion of integral membrane proteins. Transertion processes would therefore extensively couple the nucleoid with the membrane by physical interactions and this transient, yet frequent tethering could have significant cellular consequences.

The involvement of transertion in nucleoid-membrane tethering has been suggested previously. When translation is inhibited by chloramphenicol or other ribosome-targeting antibiotics, nucleoid compaction can be observed via microscopy. It has been postulated that this is caused by loss of transertion, whereby the DNA is no longer tethering the nucleoid to the membrane (Zimmerman, 2002a). The equilibrium between nucleoid compaction and decompaction could thus be affected by

transertion, with transertion being a major effect promoting nucleoid decompaction and counteracting other forces that drive nucleoid compaction (Woldringh et al., 1995) such as NAPs (Dame, 2005), solubility (Xiang et al., 2020), and supercoiling (Stuger et al., 2002).

A single gene pulled to the inner membrane surface by the transertion process could, in principle, establish a massive complex that can involve tens of RNAP proteins each producing mRNA transcripts to be associated with a large number of ribosomes as a polysome (Matsumoto et al., 2015a). Transertion process can, thus, lead to hyper-structures driving synthesis and secretion of integral membrane proteins, speculated to effect examples such as LacY in *E. coli* (Kennell & Riezman, 1977; Norris et al., 2007).

1.3.2 Role of transertion in cell signalling

Transertion has become an apparent step in signalling and sensing pathways. In the Gram-negative organism *Vibrio parahaemolyticus,* one component signalling systems have links with transertion as part of their mechanism. A two-step transertion system is hypothesised. VtrA/VtrC serve as co-components that assemble at the inner membrane, which have a DNA binding helix-turn-helix motif that captures the target DNA upon bile binding, which activates their DNA binding activity. In the presence of bile, DNA encoding for the Type III secretion system (T3SS) and VtrB, known as the pathogenicity island, is captured at the membrane. Expression of VtrB occurs first, creating the first transertion step. The second transertion step occurs where expressed VtrB clusters act as transcription initiators of T3SS genes at the membrane, where the simultaneous transcription, translation and inner membrane assembly of the T3SS apparatus occurs (Kaval et al., 2023).

1.3.3 Role of transertion in cell division

Additionally, a link between nucleoid complexity and the width of a given cell has been proposed. The width, determined by peptidoglycan, can be affected by the organisation of the nucleoid, which is affected by transertion indirectly (Zaritsky, 2015).

There is also an argument for transertion blocking cell division. As mentioned previously, *B. subtilis* protein Noc is responsible for blocking cell division via large complexes of nucleoproteins physically crowding and blocking FtsZ

recruitment(Adams et al., 2015). Transertion similarly generates large complexes but of DNA-RNAP-Ribosomes at the membrane surface.

A potential role of transertion could also be helping cell differentiation, speculated by Roggiani and Goulian (Roggiani & Goulian, 2015). Here they suggest that transertion creates a positive feedback loop on itself, whereby genes exposed to the membrane are easier to access by transcription factors or by changing the composition of the membrane. In the latter's case, changing the membrane composition could result in activation of integral membrane bound regulatory proteins, which require further transertion at the local site, creating a local difference in membrane composition. This speculation assumes unequal gene expression, such is found for sporulation in *B. subtilis,* allowing transertion to regulate cell differentiation.

1.3.3 Controversies of transertion

Previous experiments in *E. coli* have shown direct observations of transertion (Libby, Roggiani and Goulian, 2012), and recent experiments have shown support for transertion in *V. parahaemolyticus* (Kaval et al., 2023) and experiments previously showing support for the theory. However, this direct evidence for transertion is still limited and requires further validation. Crucially there is to date no direct evidence of transertion in Gram-positive bacteria.

As introduced earlier, the degree of nucleoid condensation is thought to be influenced by the balance between expanding and contracting forces. The expansion is hypothesised to be driven by transertion, whilst the contraction is driven by various factors discussed earlier (Woldringh et al., 1995). Chloramphenicol inhibits protein chain elongation in ribosomes in bacteria. Upon inhibition of translation by chloramphenicol, or other ribosome targeting antibiotics, the chromosome condenses and compacts (Zimmerman, 2002b). This conserved phenomenon, which mechanistically is not well understood, is frequently attributed to the loss of transertion associated with protein synthesis inhibition. (Cabrera et al., 2009). Protein synthesis inhibition could prevent of new transertion events or pause existing ones, followed by the RNAP finishing transcription and being lost from the transertion complex. However, when cells are treated with rifampicin, an antibiotic that targets RNAP and therefore transcription, the nucleoid decondenses instead. This seemingly conflicts with the notion that transertion, which requires active transcription, is able to keep the nucleoid in a more decondensed state.

More recent studies have shone some light on the matter. Rather than potentially just affecting transertion, inhibiting RNAP has multiple effects on the chromosome. Unlike ribosomes and translation, RNAP's contribute to nucleoid organisation at several levels, such as a force for genome segregation (Dworkin & Losick, 2002), interactions with NAPs such as SMC condensing complexes (Brandão et al., 2019) and supercoiling(Forth et al., 2013). Such interactions can in principle lead to both expansion and condensation the nucleoid. Importantly the timescales should also be considered. In a recent paper from the Holden lab (Spahn et al., 2023), treatment with rifampicin showed initial condensation, followed by a later decondensation that has been observed frequently, and by many groups including us. Similar effects have been seen before in other experiments (Dworsky & Schaechter, 1973; Sun & Margolin, 2004). It should also be noted that in X. *doucetiae*, rifampicin also shows a contraction of the nucleoid in the short axis of the cell (Spahn et al., 2023). This observation fits with transertion anchors being detached from the inner membrane.

1.4 Fatty acid desaturase, Des

In this thesis I study the transertion in the Gram-positive model organism *B. subtilis* with focus on the fatty acid desaturase, Des, as the model integral membrane protein potentially affected by transertion. For this reason, the *B. subtilis* Des -system is briefly introduced here.

Regulation of membrane composition in bacteria is essential for adaption to temperature and survival. Changes of the temperature in the environment effect the structure and fluidity of the lipid bilayer. In order to control their own membrane composition and edit it accordingly to temperature shifts, bacteria have developed methods of thermal control of fatty acid synthesis. In *B. subtilis* specifically the regulation is achieved for rapid temperature downshifts via introduction of double bonds of acyl chains into the phospholipids (Weber et al., 2001a). Such process is achieved via Des, a fatty acid desaturase, encoded by the gene *des*. *des* is part of an operon which also encodes for the regulatory pathway consisting of *desk* and *desR* (Daniela et al., 2004).

The genes *desK* and *desR* encode for a two-component regulatory pathway to activate stringent expression of *des* under cold-shock conditions. *desK* encodes for DesK, a membrane sensor kinase, that has both phosphatase and kinase activities. DesK is an integral membrane protein that spans the membrane via five

transmembrane segments, with N-terminal and C-terminal domains that flank either side of the membrane. Each domain contains hydrophilic amino acid motifs, allowing DesK to act as a pair of membrane thickness callipers (Cybulski et al., 2010). This gives DesK its temperature sensory capabilities, as it indirectly senses the temperature shift by the temperatures effect on membrane thickness. In cold conditions, the lipids in the membrane will pack together and increase the membrane thickness, which prevents the hydrophilic motifs of DesK from sensing water, thus activates the kinase abilities of DesK (Vaňousová et al., 2018).

Upon cold shock conditions, DesK will auto-phosphorylate between dimers of itself, with ATP to act as a donor. Following this, the transcriptional activator DesR, encoded for by *desR,* is phosphorylated by DesK. DesR upon phosphorylation acts as a transcription factor, binding to DNA at the DesR transcriptional regulation site upstream of the Des promoter, prompting binding of RNAP to the site. As such, DesR triggers the expression of the *des* operon (Figure 1.8). Once integrated into the membrane, Des desaturase activity results in restoration of the membrane fluidity to pre-shock levels. Thus, under optimal conditions, either by Des activity or return to optimal temperature, the membrane will become thinner. Thinner membranes will allow hydrophilic motifs of DesK to sense hydration again, switching DesK from kinase capabilities to phosphatase, where it will de-phosphorylate DesR, shutting down further des expression (Cybulski et al., 2004).

Of note with regulation of *des* and the operon is the location of terminators. The *des* promoter is followed, in order, by the *des* gene, an intrinsic terminator, *desK* and *desR,* flanked by another intrinsic terminator (Figure 3.1). During cold shock events, RNAP will run through the first intrinsic terminator to transcribe the whole operon. How RNAP ignores this terminator is currently unknown and unexplored, though speculation on attenuation and the relationship with coupled translation could invite answers.

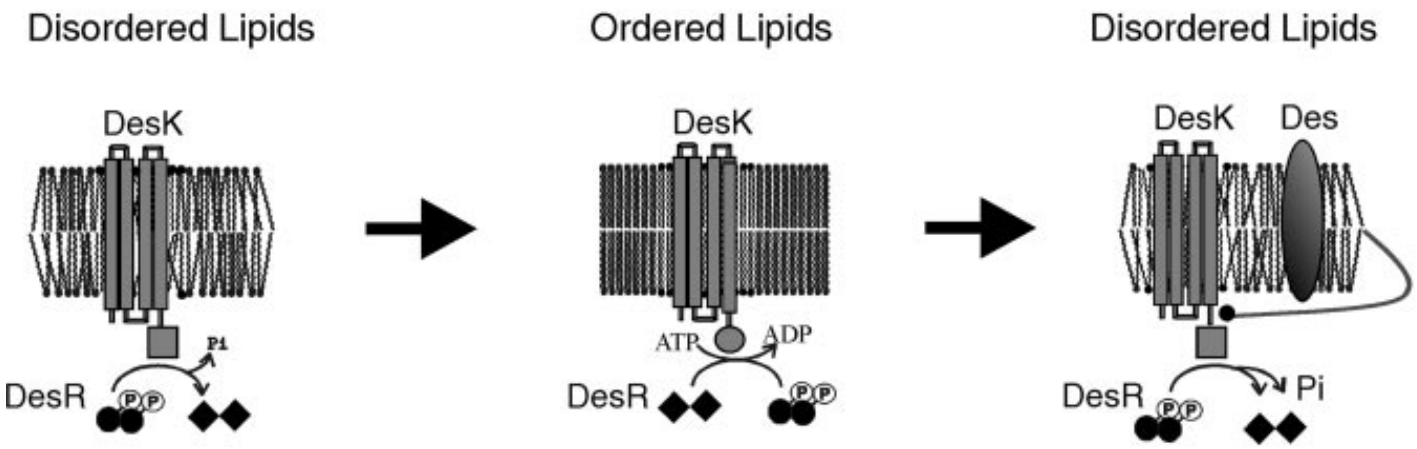

Figure 1.8: Model of two component Des pathway, DesK-DesR. *Pathway showing the action of DesK. Initially, when disordered lipids are present, desk is a phosphotase enzyme, dephosphorylating DesR within the cytoplasm. Upon ordering of the lipids in the bilayer, the thickness increases, sensed by DesK, altering the enzyme into a kinase. Upon phosphorylation of DesR and expression of Des to the membrane, the lipids become disordered again, thinning the membrane, and returning DesK to a phosphatase (Adapted from Cybulski et al., 2004)*

1.5 Aims and Objectives

The primary aim of this study was to study and attempt to directly observe transertion in Gram-positive model organism *Bacillus subtilis.* No previous work aiming to directly observe transertion in *B. subtilis* has, to my knowledge, been carried out. To achieve this, the first aim was to clone and optimise a *lac* operator array near the gene locus of *des*, to be visualised by a new LacI fusion protein utilising a recently developed bright fluorescent protein mNeonGreen (mNG). These novel tools and strains, combined with advanced fluorescence imaging and image analysis, were then applied to analyse the expression-dependent cellular location of the *des*-locus as a model for the analysis of the transertion process.

Chapter 2: Materials and Methods

2.1 Component lists

2.1.1 Bacterial strains

All strains used for this work within this thesis are listed in the following table (Table 2.1). For work in *B. subtilis,* unless stated otherwise, wild type refers to 168ca.

Table 2.1: List of bacterial strains. Transformation of plasmids into a background strain or crossover events are represented as X into Y.

Strain	Species	Genotype	Source or construction
168ca	*B. subtilis*	*trpC2*	(Barbe et al., 2009)
BWX1200	*B. subtilis*	*spoIIIE36*, *yycR*(−7°)::tetO48 (cat), *pelB*(+174°)::lacO48 (kan), *ycgO*::PftsW *tetR*-cfp (spec) terminators *PftsW lacI-mypet*	(Wang & Rudner, 2014)
BWX721	*B. subtilis*	*yycR*(−7°)::tetO48 (erm), *ycgO*::*PftsW tetR-cfp* (spec), *sacA*::*hbs-mypet* (kan)	(Wang & Rudner, 2014)
BWX1206	*B. subtilis*	*spoIIIE36, yrvN*(−120°)::lacO48 (phleo), *ykoW*(+120°)::tetO48 (cat), *ycgO*::*PftsW tetR-cfp* (spec) terminators *PftsW lacI-mypet*	(Wang & Rudner, 2014)
BWX1212	*B. subtilis*	*spoIIIE36, yuxG*(−87°)::lacO48 (phleo), *yhdG*(+87°)::tetO48 (cat), *ycgO::PftsW tetR-cfp* (spec) terminators *PftsW lacI-mypet*	(Wang & Rudner, 2014)
PL070	*B. subtilis*	*AprE::Pxyl*$_{constituative}$*WALP23-mCherry (cat)*	(Lee, unpublished)

CRW593	*B. subtilis*	*trpC2 ycgO::PftsW tetR-mCherry-phleo*	pWX510 into168ca (Wang et al., 2014)
JG254	*B. subtilis*	*trpC2 aprE::cat Pspac-p16.7-msfGFP*	(Grimshaw, 2022)
BJN001	*B. subtilis*	*trpC2 des::lacO48 (kan)*	lacO48 (kan) PCR amplified BWX1200 into 168ca.
BJN002	*B. subtilis*	*trpC2 ycgO::PftsW lacI-mypet* (spec)	BWX1200 into 168ca.
BJN003	*B. subtilis*	*trpC2 des::lacO48 (kan), ycgO::PftsW lacI-mypet (spec)*	BJLN002 into BJLN001.
BJN004	*B. subtilis*	*trpC2 amyE::PftsW lacI-mNeonGreen (Spec)*	pJN11 into 168ca.
BJN005	*B. subtilis*	*trpC2 des::lacO48 (kan), amyE::PftsW lacI-mNeonGreen (Spec)*	BJN004 into BJN001.
BJN006	*B. subtilis*	*trpC2 des::lacO48 (kan), amyE::PftsW lacI-mNeonGreen (Spec), AmyE::Pyxl WALP23-mCherry (cat)*	BJN005 into PL070.
BJN007	*B. subtilis*	*trpC2 amyE::PftsW lacI-mNeonGreen (Spec), AmyE::Pyxl WALP23-mCherry (cat)*	BJN004 into PL070
BJN015	*B. subtilis*	*trpC2 des::lacO4 (kan)*	pJN27 into168ca
BJN016	*B. subtilis*	*trpC2 des::lacO4 (kan), amyE::PftsW lacI-mNeonGreen (Spec)*	pJN27 into BJN004

BJN017	*B. subtilis*	*trpC2 des::lacO4 (kan), amyE::PftsW lacI-mNeonGreen (Spec), AmyE::Pyxl WALP23-mCherry (cat)*	pJN27 into BJN007
BJN018	*B. subtilis*	*trpC2 des::lacO4 (erm), amyE::PftsW lacI-mNeonGreen (Spec), AmyE::Pyxl WALP23-mCherry (cat)*	pJN100 into BJN007
BJN029	*B. subtilis*	*trpC2 Tdes::tetO10 (erm)*	pJN32 into168ca
BJN030	*B. subtilis*	*trpC2 Tdes::tetO10 (erm), ycgO::tetR-mCherry (zeo)*	CRW593 into 168ca
BJN031	*B. subtilis*	*trpC2 amyE::PftsW lacI-mNeonGreen (Spec), ycgO::tetR-mCherry*	BJN004 into CRW593
BJN032	*B. subtilis*	*trpC2 des::lacO4 Pxyl tetO10 (erm), amyE::PftsW lacI-mNeonGreen (Spec), ycgO::tetR-mCherry*	pJN150 into BJN031
BJN043	*B. subtilis*	*trpC2 aprE::Pspac-p16.7-msfGFP (cat), des::lacO48 (kan)*	pJG118 into BJN001
BJN044	*B. subtilis*	*trpC2 aprE:: Pspac-p16.7-lacI-mNeonGreen (cat), des::lacO48 (kan)*	pJN200 into BJN001
BJN045	*B. subtilis*	*trpC2 aprE:: Pspac-p16.7-lacI-mNeonGreen (cat), des::lacO4 (kan)*	pJN200 into BJN032
BJN046	*B. subtilis*	*trpC2 aprE::Pspac-p16.7-lacI-mNeonGreen (cat)*	pJN200 into168ca

BJN047	*B. subtilis*	*trpC2 sacA::hbs-GFP (kan), AmyE::PyxI WALP23-mCherry (cat)*	PL070 into BWX721
BJN055	*B. subtilis*	*trpC2 des::lacO4-desM1K (kan), amyE::PftsW lacI-mNeonGreen (Spec), AmyE::PyxI WALP23-mCherry (cat)*	pJN207 into BJN007
DH5α	*E. coli*	*fhuA2 Δ(argF-lacZ)U169 phoA glnV44 Φ80 Δ(lacZ)M15 gyrA96 recA1 relA1 endA1 thi-1 hsdR17*	(Taylor et al., 1993)

2.1.2 Plasmids

Table 2.2: List of plasmids

Plasmid	**Genotype**	**Source or construction**
pUC18	*bla lacZ*	(Taylor et al., 1993)
pSHP2	*bla amyE:: mNeonGreen*	(S.H.Peeters, unpublished)
pJG118	*bla cat aprE:: Pspac-p16.7- msfGFP*	(Grimshaw, 2022)
pJN11	*bla amyE::PftsW lacI-mNeonGreen Spec*	This work (2.2.1)
pJN26	*bla Pdes*	This work (2.2.1)
pJN27	*bla Pdes::*lacO4 *kan*	This work (2.2.1)
pJN32	*bla Tdes::* tetO10 *erm*	This work (2.2.1)
pJN98	*bla erm*	This work (2.2.1)

pJN99	*bla lacO4 Pxyl erm*	This work (2.2.1)
pJN100	*bla Pdes::*lacO4 *Pxyl erm*	This work (2.2.1)
pJN150	*bla des::*lacO4 *Pxyl tetO10 erm*	This work (2.2.1)
pJN200	*bla aprE:: Pspac p16.7-lacI mNeonGreen cat*	This work (2.2.1)
pJN207	*bla Pdes::*lacO4-*desM1K kan*	This work (2.2.1)

2.1.3 Oligonucleotides

Table 2.3: List of oligonucleotides used.

Primer	**Sequence**	**Use**
JN01	GTTGATGACTCTATTTCGCTCG	Sequencing for *yycR* locus *B. subtilis* genome
JN02	CCATTATTGGATGCTTTCTTGGC	Sequencing for *yycR* locus B. subtilis genome
JN03	CGGTTTCTCGGTAATTGTTTCGGC	Sequencing for *pelB* locus B. subtilis genome
JN04	ATGAATGCTTCAAGTGCGAGGG	Sequencing for *pelB* locus

		B. subtilis genome
JN05	GCTGCCTGATCCGGAAGACCCACTTTCACATTTAAG	*tetR* amplification with overhang for pSHP2 insertion
JN06	AAGGAGATTCCTAGGATGATGTCTAGATTAGATAAAAG	*tetR* amplification with overhang for pSHP2 insertion
JN07	GCTGCCTGATCCGGACTGCCCGCTTTCCAG	*lacI* amplification with overhang
JN08	AAGGAGATTCCTAGGGTGAAACCAGTAACGTTATACG	*lacI* amplification with overhang
JN09	CCTAGGAATCTCCTTTCTAGATGC	Linearisation of pSHP2
JN10	TCCGGATCAGGCAGC	Linearisation of pSHP2
JN11	CTGAAGTCTGGACATTTATTTATACAGCTCATCCATACCACCCG	*mScarlet-I* amplification
JN12	TCAGGCAGCGGATCAATGGTATCCAAAGGAGAGGC	*mScarlet-I* amplification
JN13	TGATCCGCTGCCTGATC	Linearisation of pUC18 for pJLN11
JN14	ATGTCCAGACTTCAGATCCACTAG	Linearisation of pUC18 for pJLN11

JN15	GGAGACGAAATCCGGATCGTG	Upstream flank of *des* promoter
JN16	TAGATGTCTGCTG+AGCTGCATAGCCGATTGCGCTAAAAAAG	Upstream flank of *des* promoter
JN17	CGTGATGTTCATGAGCAACTTCAAGC	Downstream flank of *des* promoter
JN18	GAGGGATCCGAATTCTGCCGCACGAGACATGAC	Downstream flank of *des* promoter
JN19	CACGTTCCCTATAGGAGGAACATG	*lacO* sequencing
JN20	GTTTCAGGCTGAGCAAATGCAG	*lacO* sequencing
JN21	GAATTCGGATCCCTCGAGCC	*LacO48* array amplification
JN22	GCTAGCAGACATCTAAATCTAGGTACTAAAAC	*LacO48* array amplification
JN23	CTAAAACAATTCATCCAGTAAAATATAATATTTTATTTTC	*Kan* cassette amplification
JN24	CAATTACCCGTACATAATTGAATCGGCTCCGTAGATAC	*Kan* cassette amplification
JN25	CATAGCGATAACGAGCTCCCTATC	*tetO25* amplification
JN26	TCCAGTGCAGGAGCTCTGTAGCTC	*tetO25* amplification
JN27	TTACTGGATGAATTGTTTTAGTGCATAGCCGATTGCGCTAAAAAAG	*lacO4* flank upstream matching reverse
JN28	CAATTATGGACGGGTAATTG	*lacO4* amplification

JN29	GAATTCGGATCCCTCGAG	*lacO4* amplification
JN30	GCTTGTCTGTAAGCGGATGC	Sequencing of pUC18 based plasmids
JN31	GGGGTGCCTAATGAGTGAGC	Sequencing of pUC18 based plasmids
JN32	CAGTTTTCGCAATCCACATC	Sequencing for *lacO4* plasmid
JN33	GCTGAATCGAGATCCGAGTGTGC	Sequencing for *tetO25* plasmid
JN34	CAATAAAGCGTCCTCTTGTG	Sequencing for *lacI*
JN35	GGATATAACATGAGCTGTCTTCGG	Sequencing for *lacI*
JN36	GCAGTTGTTGAAAGTGCCCGAGCTCGAATTCGTAATCATGG	pUC18 linearisation with overhangs for *tetO25*
JN37	CAA GTTTTAGCCTGGCCTGGCCGTCGTTTTACAACG	pUC18 linearisation with overhangs for *tetO25*
JN38	GCTCATGAACATCACGCCGAGCTCGAATTCGTAATCATGG	pUC18 linearisation with overhangs for *lacO4*

JN39	CCGGATTTCGTCTCCCTGGCCGTCGTTTTACAACG	pUC18 linearisation with overhangs for *lacO4*
JN40	CCTAGGATGAAATATGTAACGTTATACG	*lacI* mutation Ser3->Tyr3
JN41	CGTATAACGTTACATATTTCATCCTAGG	*lacI* mutation Ser3->Tyr3
JN42	GCGCGCCTAGGATGAAACCAGTAACGTTATACGATG TCG	*lacI* -11aa truncation
JN43	GCGCGGAATTCCAGCTGCATTAATGAATCGGC	*lacI* -11aa truncation
JN44	CTGACGATGGAACATTCAAAGG	*tetO25* upstream flank
JN45	CCAGTCTTTTATTGGGCTGTTAAC	*tetO25* upstream flank
JN46	AGCACAAAAGAAAAACGAAATGATACACC	Erythromycin cassette amplification
JN47	GGGACCTCTTTAGCTCCTTG	Erythromycin cassette amplification
JN48	GAGCTAAAGAGGTCCCCCTGAATCGCACATAAAGAA AAAC	*TetO25* downstream flank
JN49	GCACTTTCAACAACTGCATTCG	*TetO25* downstream flank
JN50	AATGGGGAAGAGAACCGCTTAAG	*amyE* amplification

JN51	ATGTTTGCAAAACGATTCAAAACCTC	*amyE* amplification
HS03	ATGCCGCGATTTCCAATGAG	Sequencing pSHP2
HS84	GGCAACAAACTAATGTGCAACTTAC	Sequencing pSHP2
JN52	TTGAAAGTGCCCGAGCTCGAATTCGTAATC	pUC18 linearisation
JN53	CCATCGTCAGCTGGCCGTCGTTTTACAAC	pUC18 linearisation
JN54	GCTGGCTTAACAATTATGGACGGGTAATTG	*lacO4* amplification for SIP/pJLN98
JN55	TGAAGCATGCGAATTCGGATCCCTCGAG	*lacO4* amplification for SIP/pJIN98
JN56	CTTTTGTGCTGCGTATCACGAGGCCCTTTC	pJLN98 linearisation
JN57	AAGAGGTCCCGATAATAATGGTTTCTTAGACGTCAG GTG	pJLN98 linearisation
JN58	CGGCTATGCACTCCCGGAGACGGTCACAG	pJLN99 linearization
JN59	TTTCGTCTCCAACGCGCGAGACGAAAGG	pJLN99 linearization
JN60	CTCGCGCGTTGGAGACGAAATCCGGATCG	Flank region pJLN100 insert amplification
JN61	TCTCCGGGAGTGCATAGCCGATTGCGCTAAAAAAG	Flank region pJLN100 insert amplification

JN62	CATTATTATCGGGACCTCTTTAGCTCCTTG	Erythromycin cassette amplification
JN63	CGTGATACGCAGCACAAAAGAAAAACGAAATGATAC	Erythromycin cassette amplification
JN64	CGTATCAATAGATCTTGTAAAAGCC	*lacO48*/ kanamycin cassette amplification
JN65	CAAGAAACCATAGGCCGAAG	*lacO48*/ kanamycin cassette amplification
JN66	CTCACTCATGAGCAGATTGCTC	*lacO48* specific sequencing
JN67	CTCGAGGGATCCGAATTCTG	kanamycin cassette specific sequencing
JN68	GCTGGCTTAAGCATGCTTCAAAGCCTGTC	Pxyl amplification with overhangs
JN69	ATGCAAGCTTCCTAGGAATCTCCTTTCTAGATG	Pxyl amplification with overhangs
JN70	GCGCGCCTAGGATGGATTACAAAGAGACTGCAAAAC	*sacP* amplification
JN71	GCGCGGAGCTCTCATTTTTTCCTCTCCTCATCCT	*sacP* amplification

JN72	GCGCGCCTAGGATGAAACGACTTTGTTTATGGTTC	*pelB* amplification
JN73	GCGCGGAGCTCTCAGTAGCCAAATACCAGAGTTG	*pelB* amplification
JN74	GAAAAAATGAGAGCTCGAATTCGTAATCATGG	SIP4 linearisation
JN75	TGTAATCCATCCTAGGAATCTCCTTTCTAGATGC	SIP4 linearisation
JN76	ATCCGAATTCGCATGCTTCAAAGCCTGTC	Pxyl overhangs with *lacO4*
JN77	CGAGGCCCTTTCGTCTC	SIP plasmid sequencing
JN78	CTGTAAGCGGATGCCGGG	SIP plasmid sequencing
JN79	GTGAGTTAGCTCTACTCATTAGGCAC	SIP plasmid sequencing
JN80	GATTCCTAGGATGGAAAAGCTATTTAAAGAAGTTAAACTAG	*sunA* amplification
JN81	ATTCGAGCTCTTATCTGCAGAATTGACGATAGTTTTG	*sunA* amplification
JN82	GATTCCTAGGATGCTGCTAATCGGCTACTTTG	*putP* amplification
JN83	ATTCGAGCTCTTATTGCGACATTGTATCTTGGTAG	*putP* amplification
JN84	GATTCCTAGGATGAATGAGCAGATTCCACATGAC	*cypC* amplification
JN85	ATTCGAGCTCTTAACTTTTTCGTCTGATTCCGCTC	*cypC* amplification
JN86	GATTCCTAGGATGATGAATCATCAATTTTCAAGTCTTG	*glpD* amplification
JN87	ATTCGAGCTCTTATTGCTCAAGCGGTACGAC	*glpD* amplification

JN88	GATTGAAGATGATTATATGTCAGACATC	pJLN100/SIP sequencing
JN89	CTTTTGTTTATAAGTGGGTAAACCG	pJLN100/SIP sequencing
JN90	GAGCTCGAATTCGTAATCATGG	pJLN100/SIP linearisation (for genes)
JN91	CCTAGGAATCTCCTTTCTAGATGC	pJLN100/SIP linearisation (for genes)
JN92	GATTCCTAGGAAACGACTTTGTTTATGGTTC	*pelB* amplification (ATG deletion)
JN93	AAGGAGATTCCTAGGATGAATGAGCAGATTCCACATG	*cstA* amplification
JN94	TATGACCATGATTACTTAACTTTTTCGTCTGATTCCGC	*cstA* amplification
JN95	AAGGAGATTCCTAGGATGAGAAATGGATTCGGCAAAAC	*pbuX* amplification
JN96	TATGACCATGATTACTTAGACTGCTGTTTTTTGTTCAGC	*pbuX* amplification
JN97	AAGGAGATTCCTAGGATGATTTACACTGTAACACTTAATCC	*fruK* amplification
JN98	TATGACCATGATTACCTATAGACGTGTGACCTTAACTTC	*fruK* amplification
JN99	AAGGAGATTCCTAGGATGATGAAGAAACCGATTCAAG	*yesT* amplification
JN100	TATGACCATGATTACTTATACATGTTCTTTTCCCTCCC	*yesT* amplification
JN101	TTCGTCTCGCGCGTTGCTGGTTGAAAAAAGCTTAGAAC	*rrn* amplification flank

JN102	GACCGTCTCCGGGAGAACACCTTCAGTTGTCTAAGTC	*rrn* amplification flank
JN103	TTCGTCTCGCGCGTTATTCTTACAAATCCCCCAATCC	*rpoB* amplification flank
JN104	GACCGTCTCCGGGAGCTGATTCACCCCTCAAATCATG	*rpoB* amplification flank
JN105	GTTGATCCAGCATAGGGAAACCTGTCGTGCCAG	pJLN100/SIP linearisation (for pJLN150)
JN106	TATTGGGCTGTTAACACCCCAGGCTTTACACTTTATG	pJLN100/SIP linearisation (for pJLN150)
JN107	TGTAAAGCCTGGGGTGTTAACAGCCCAATAAAAGACTGG	Amplification of *TetO10*/ Erythromycin cassette/flank region for pJLN150)
JN108	GCACGACAGGTTTCCCTATGCTGGATCAACTCTTTCAG	Amplification of *TetO10*/ Erythromycin cassette/flank region for pJLN150)
JN109	CAGGAAACAGCTATGACCATGATTAC	pJLN150 linearisation (for gene)
JN110	GTTAACAGCCCAATAAAAGACTGG	pJLN150 linearisation (for gene)

JN111	CGTTAGAACGCTTAGGTTATCG	pJLN150 sequencing (for gene)
JN112	AAGTGGGTAAACCGTGAATATCG	pJLN150 sequencing (for gene)
JN113	GAACATGTGAGCAAAAGGCC	pJLN150 sequencing (for integration)
JN114	GGTTTCTTAGACGTCAGGTGG	pJLN150 sequencing (for integration)
JN115	GGTCATAGCTGTTTCCTGATGAATGAGCAGATTCCACATG	*cstA* amplification (pJLN150 overhangs)
JN116	TCTTTTATTGGGCTGTTAACTTAACTTTTTCGTCTGATTCCGC	*cstA* amplification (pJLN150 overhangs)
JN117	GGTCATAGCTGTTTCCTGATGAGAAATGGATTCGGCAAAAC	*pbuX* amplification (pJLN150 overhangs)
JN118	TCTTTTATTGGGCTGTTAACTTAGACTGCTGTTTTTTGTTCAGC	*pbuX* amplification (pJLN150 overhangs)
JN119	GGTCATAGCTGTTTCCTGATGAATTTACACTGTAACACTTAATCC	*fruK* amplification (pJLN150 overhangs)

JN120	TCTTTTATTGGGCTGTTAACCTATAGACGTGTGACCTTAACTTC	*fruK* amplification (pJLN150 overhangs)
JN121	GGTCATAGCTGTTTCCTGATGATGAAGAAACCGATTCAAG	*yesT* amplification (pJLN150 overhangs)
JN122	TCTTTTATTGGGCTGTTAACTTATACATGTTCTTTTCCCTCCC	*yesT* amplification (pJLN150 overhangs)
JN123	CCATAGAAAACACACAGCTG	*ycgO* sequencing
JN124	CGTTTGTTTCCAAAAGAAAAAAATGG	*ycgO* sequencing
JN125	CTCGAGTAAGGATCTCCAGG	dCas9 (pJMP1) linearisation
JN126	GTCACCTCCTAGCTGACTC	dCas9 (pJMP1) linearisation
JN127	TCAGCTAGGAGGTGACTCCGGATCAGGCAGCGG	Halo-tag amplification with linker
JN128	GGAGATCCTTACTCGAGTTAGCCGCTGATTTCTAAGGTAGAAAGC	Halo-tag amplification with linker
JN129	GGCGTTAGCCCAAGCGC	pJG118 linearisation
JN130	GCCGCTTCCTGAGCCTTTC	pJG118 linearisation

JN131	CTCAGGAAGCGGCATGAAACCAGTAACGTTATACGATGTC	*lacI-mNG* with flex linker amplification
JN132	CTTGGGCTAACGCCTCACTTATAGAGTTCATCCATACCC	*lacI-mNG* with flex linker amplification
JN133	GAGAGGATACTTACTAAAACTGAACAAACCATTGC	*lacO4* quick-change ATG->AAA
JN134	GCAATGGTTTGTTCAGTTTTAGTAAGTATCCTCTC	*lacO4* quick-change ATG->AAA

2.1.4 Medias and buffers

Table 2.4: List of medias and buffers used with compositions.

Media	**Components**
LB	10 g Tryptone 5 g yeast extract 10 g NaCl 1 L Distilled water
SMM basic salts	0.2% Ammonium sulphate 1.4% Di-potassium hydrogen phosphate 0.6% Potassium dihydrogen phosphate 0.2% Sodium citrate dihydrate
SMM transformation media	10 ml SMM basic salts 120 µl 40% glucose solution 60 µl 1M MgSO4 100 µl of 2% tryptophan 10 µl 20% Casamino acids 10 µl of 2.2mg/ml Ferric-ammonium citrate solution.
SMM Dilution Media	10 ml SMM basic salts 120 µl of 40% glucose 60 µl 1M MgSO4

SMM microscopy media	10 ml SMM basic salts 240 µl 40% glucose solution 60 µl 1M MgSO4 100 µl of 2% tryptophan 10 µl 20% Casamino acids 100 µl of 2.2mg/ml Ferric-ammonium citrate solution.
TBE (5x)	54 g Tris base 27.5 g boric acid 20 ml 0.5M EDTA (pH 8.0)

2.1.5 Antibiotics

Table 2.5: List of antibiotics and working concentrations.

Antibiotic	**Working concentration for *B. subtilis***	**Working concentration for *E. coli***
Ampicillin	-	100 µg/ml
Chloramphenicol	5 µg/ml	10 µg/ml
Erythromycin	1 µg/ml	-
Kanamycin	5 µg/ml	25 µg/ml
Tetracycline	10 µg/ml	-

2.2 Cloning

2.2.1 Plasmid construction

Plasmid pJN11 was constructed by using a gene block synthesised by IDT: *amyE::PftsW lacI-mNeonGreen spec* which was inserted into pUC18 linearised by oligos JN13 and JN14, via NEBuilder assembly. pJN26: upstream *Pdes* flank amplification by oligos JN15 and JN16, downstream *Pdes* flank amplification by JN17 and JN18 were inserted into pUC18 linearised by oligos JN52 and JN53, via NEBuilder assembly. pJN27: lacO4 amplified by oligos JN28 and JN29 and kanamycin cassette amplified by oligos JN23 and JN24 were inserted into pJN26 linearised by oligos JN38 and JN39, via NEBuilder assembly. pJN32: synthesised gene block by IDT *des::*tetO10 *erm* was inserted into pUC18 linearised by oligos JN52 and JN53, via NEBuilder assembly. pJN98: erythromycin cassette amplified by oligos JN62 and JN63 and inserted into linearised pUC18 by oligos JN52 and JN53, via NEBuilder assembly. pJN99: lacO4 amplified by JN54 and JN55 with P*xyl*

amplification by oligos JN68 and JN69 both being inserted simultaneously into pJN98 linearised by oligos JN56 and JN57, via NEBuilder assembly. pJN100: *des* flank region amplified by oligos JN60 and JN61 inserted into pJN99 linearised by oligos JN58 and JN59, via NEBuilder assembly. pJN150: tetO, erythromycin resistance cassette and flank region amplified from plasmid pJN32 by oligos JN107 and JN108 inserted into pJN100 linearised by oligos JN105 and JN106, via NEBuilder assembly. pJN200: pJN11 fragment amplified by oligos JN131 and JN132 inserted into pJG118 linearised with oligos JN129 and JN130, via NEBuilder assembly. pJN207: oligos JN133 and JN134 were used to mutate via site directed mutagenesis.

2.2.2 Strain growth conditions

Overnight cultures of strains were carried out at 37°C or 30°C shaking in LB media supplemented with 0.2% glucose.1/100 dilution was made into LB or fresh SMM microscopy media. Culture was grown until desired optical density. For most experiments an optical density of 0.3 was sufficient. 200 µl of cells were then transferred into a 2 ml Eppendorf test tube with an air hole and incubated with necessary dye or antibiotic. When used, membrane stain Nile red and nucleoid stain DAPI were added to cells at 1 ug/ml for 15 minutes at 30°C whilst shaking. Antibiotics, unless stated otherwise, were incubated for the same time.

2.2.3 Genomic DNA extraction

Genomic DNA for *E. coli* was purified using Blood & Cell Culture DNA Mini Kit from QIAGEN according to the manufacturer's instructions.

Genomic DNA for *B. subtilis* was purified from by using a modified version of the Promega Wizard® Genomic DNA Purification Kit protocol. Single colony was inoculated overnight in 5 ml LB in 37°C, shaking. Overnight cells were spun down and pelleted to be resuspended in 500 µl 50 mM EDTA, then adding 5 µl RNase and 10 µl lysozyme (10 mg/ml) before incubating at 37°C for 60 minutes. 600 µl of Nuclei lysis solution was added and incubated for 5 minutes at 80°C. Samples were left to cool to room temperature and 600 µl of protein precipitate solution added. The mixture was vortexed and placed on ice for 10 minutes. Samples were spun down at 13,000 x *g* for 10 minutes, supernatant transferred to a fresh tube with 600 µl room temperature isopropanol. Samples were gently inverted until a visible precipitate could be seen. Samples were spun another 10 minutes at 13,000 x *g*, disposing the supernatant and gently washing the pellet with 500 µl of 70% ethanol. The sample

was spun as before, removing the supernatant and allowing to air dry for 15 minutes. 100 µl of water was added and the DNA resuspended.

2.2.4 Plasmid DNA extraction

Plasmid extraction was carried by using QIAprep Spin Miniprep Kit also from QIAGEN, by following the manufacturer's instructions.

2.2.5 Polymerase Chain Reaction

Q5® High-fidelity DNA polymerase was used for most PCR reactions according to the manufacturer's instructions within a thermocycler. This was primarily used for amplification of inserts and linearisation of plasmid templates.

For colony PCR, Taq® DNA polymerase was used. This was carried out with select colonies, which were heated to 95°C for 15 minutes, before following the manufacturers instruction for Taq DNA polymerase PCR.

2.2.6 Restriction Enzyme Digest

Analysis of plasmids by linearisation was done via restriction enzymes. Enzymes were chosen depending on exact DNA sequence. Chosen enzymes specifically underwent different temperatures, buffers and heat inactivation, determined by NEBcloner online tool.

DpnI was routinely used, adding 20 units of Dpn1 (NEB), 5 µL 10X rCutSmart Buffer (NEB) and 1 µg DNA for a 50 µl reaction. The reaction was incubated for 3 hours at 37°C then heat inactivated at 80°C for 20 minutes.

2.2.7 Agarose Gel Electrophoresis

1% agarose gels were formed with 1x TBE. Nancy-520 was added, exact volume dependant on gel volume. 2 µl of 6x Gel loading dye, Blue 6X (NEB) was added to 10 µl of sample before loading and running on gel. Gels were typically run between 80V to 150V. Samples for gel extraction were done in 0.8% gels at 80V.

2.2.8 Column Purification

Products of PCR were purified via the QIAquick PCR Purification Kit (QIAGEN). Purifications were done according to the manufacturer's instructions.

2.2.9 Gel extraction

Some PCR products required Gel extraction via Monarch® DNA Gel Extraction Kit Protocol (NEB #T1020). These were achieved via the manufacturer's instructions.

2.2.10 NEBuilder HiFi Assembly Cloning

Plasmids throughout were constructed via NEBuilder® HiFi DNA Assembly. Primers were designed specifically to linearise plasmids and amplify DNA fragments with homologous DNA overlaps. Both the insert DNA fragment and the linearised DNA vector were PCR products (2.2.3). Insert and vector were both column purified and DpnI treated. Inserts were gel extracted to separate from oligomers further. Both insert and vector were then combined in specific molar ratios calculated by the NEBioCalculator online tool for calculating ligation reactions. Reactions were mixed then with the recommend quantity of NEBuilder® HiFi DNA Assembly Master Mix via the instructions from the NEBuilder HiFi DNA Assembly Reaction Protocol. The reactions were incubated at 50°C for at least 1 hour. The reaction was then transformed into *E. coli.*

2.2.11 Transformation into E. coli

E. *coli* transformations were done into chemically competent NEB commercial DH5α cells done via the NEBuilder transformation protocol. DNA was added to thawed cells and left on ice for 30 minutes. Cells underwent heat shock at 42°C for 30 seconds, then placed back in ice for 2 minutes. 950 µL of room temperature SOC media was added to the cells before outgrowth at 37°C for 60 minutes. Cells were streaked onto LB agar plates with appropriate antibiotics for overnight growth at 37°C.

2.2.12 Transformation into B. subtilis

Transformation into *B*. *subtilis* was achieved using SMM transformation medium. The appropriate strain was grown overnight on a plate before being inoculated into 5 ml of SMM transformation media, left to incubate for 3h at 37°C whilst shaking. Culture was then diluted with 5 ml of pre warmed SMM dilution medium, then shaking at 37°C for 2 further hours. 400 µl of culture was taken and 8 µl of DNA was added, then left to shake at 37°C for 1 hour. Cells were then spread on appropriate selection antibiotic plates overnight at 37°C or for 48 hours at 30°C.

2.2.13 Site Directed Mutagenesis

Q5® Site-Directed Mutagenesis Kit (E0554) was used to perform direct mutations according to the manufacturer's instructions.

2.2.14 Sanger Sequencing

Sanger Sequencing was achieved via Eurofins Genomics. Primers used by Eurofins to perform this are included in table 2.1.3 above. To prepare, a plasmid DNA extraction or PCR were performed before following Eurofins's sample preparation instructions.

2.2.15 Whole Plasmid Sequencing

Whole genome sequencing was performed by Plasmidsaurus, utilising Oxford Nanopore. To prepare, a genomic or plasmid DNA extraction were performed before following Plasmidsaurus sample preparation instructions. All plasmids in this project were analysed by whole plasmid sequencing.

2.3 Microscopy

2.3.1 Fluorescence microscopy

Fluorescence microscopy was done on a Nikon TI2 using NIS Elements imaging software. Horizontal microscopy was done exclusively using a pE-4000 light source with a Kinetix camera at the following wavelengths: 365nm, 435nm, 470nm and 580nm. Nikon CFI Plan Apo Lambda 100x/1.45 NA Oil Ph3 objective was used. Depending on what was needed a Semrock GFP-4050B filter cube (GFP), a Semrock mCherry-C (mCherry), Semrock CFP-2432C (CFP) or Semrock DAPI-5060C (DAPI) were used for their respective fluorophore. Each filter cube's specific information is found in table 2.6.

2.3.2 Slide Preparation

To prepare for microscopy, the microscope chamber was set to the temperature required for the temperature (30°C or 37°C). Slide preparation had 1.2% agarose dissolved in the media of the cell culture. Once melted, agarose was added to a multi-spot slide (Hendley-Essex), which was then compressed against another slide attached with a gene frame (Thermo Fisher) to allow an even agarose surface. Once set, the gene-frame slide was removed and 0.5 µl of cell culture added. Multi-spot slides allowed for various cultures to be analysed at once. The culture was left to dry for 3 minutes before a coverslip was added and pressed down. Cells were then

transferred to the microscope. All cell work was done at 30°C during preparation of slides unless stated otherwise (te Winkel et al., 2016).

Table 2.6: Filter Cube information

Filter cube	Excitation filter	Dichroic mirror	Emission filter
GFP	466/40	495lp	525/50
mCherry	562/40	593lp	641/75
CFP	438/24	458lp	483/32
DAPI	377/50	409lp	447/60
488 nm (laser)	488/10	488lp	525/50+500
561 nm (laser)	461/10	561lp	600/50+575

2.3.3 Vertical cell imaging by nanostructured immobilisation (VerCINI)

Cells were prepared as described in 2.3.2. To prepare for vertical immobilisation, a gene-frame was mounted onto a glass slide. 6% agarose in growth media was prepared. Once dissolved, the agarose was left in a 90°C water bath for 3 minutes to remove bubbles. Wide bore pipette tips (1000 µl tips with ends cut off) were used to pipette 800 µl of agarose onto the micropillar wafer, directly onto the pillars. Micropillar wafers were kindly provided by the Whitely lab. Immediately the glass slide was pushed down for 20 seconds until the agarose has polymerised. The slide was then left at imaging temperature.

Once cells and slide had been prepared, all following steps were completed at imaging temperature, notably 30°C and 15°C. 1 ml of cells at OD600 of 0.3 were transferred into 1.5 ml Eppendorf test tubes, then spun down for 1 min at 13.000 x *g*, supernatant removed and resuspended in fresh SMM microscopy media. The micropillar wafer was removed from the slide. 8 µl of cells were added to the imprinted agarose.

Slides are then centrifuged on a flat bottomed 96-well plate rotor for 4 minutes at 4000 x *g*. Non trapped cells were washed away with the same imaging media. Samples were left to air dry for 3 minutes before cutting away non-imprinted agarose regions for oxygen pockets and sealing with a coverslip. All information on VerCINI can be found in the paper (Whitley et al., 2022).

2.3.4 VerCINI microscopy

VerCINI was done on a Nikon TI2 using NIS Elements imaging software. For vertical cells a Nikon CFI SR HP Apo TIRF 100x/1.49 NA Oil objective was used with 488nm and 561nm laser sources, for GFP or mCherry signal respectively, with the Kinetix camera. Information on each source can be found in table 2.6. TIRF objective allowed illumination via HiLO to increase signal to noise ratio. Highly inclined and laminated optical sheet microscopy (HiLO) increases signal to background noise ratio via inclining the laser beam, penetrating the specimen at an angle. Therefore, illumination of the specimen is laminated as a thin optical sheet (Tokunaga et al., 2008a).

2.3.5 Image Quantification (Horizontal)

Image's taken for horizontal cells were analysed and quantified utilising programs Ilastik and FIJI. Images taken via 2.3.1, in order to correct for any chromatic aberration between wavelengths, a scaling factor was applied to the red channel. Images were then put through Ilastik, (Berg *et al.* 2019), which segments the cells. Membrane probability maps were generated from this. FIJI (Schindelin, J *et al, 2012*) was used for the rest of image quantification. In Fiji, images underwent gaussian blur with a sigma of 2 for first enhancing contrast before then minimum thresholding of pixel dilation. Cell regions of interest (ROI) were determined from these previous steps. Fluorescence intensity values had the mean fluorescence intensity of the background subtracted.

Foci were tracked via the Fiji plugin, Trackmate (Ershov et al, 2022; Tinevez et al, 2017). Within Trackmate, foci were filtered by prominence and chosen only within one cell ROI. Foci localisation at a subpixel level was achieved by Laplacian of Gaussian (LoG). Foci positioning was then determined within the context of the cell by drawing lines bisecting the Foci and passing through the membrane determined via the ROI's. This is iterated every 10 degrees. Each line has X and Y coordinate information, along with angle and length. This is generated from a plot of a fluorescence intensity profile along this line, which is used to calculate the full width half maximum of gaussian fit of this intensity profile. The shortest distance between them is full width half max, where the quality of the gaussian curve is quality checked by the R^2 value. The midpoint of the cell is defined by the gaussian equation of the line for the ROI and membrane. This determines the centre line of the cell where the

distance of the foci to the membrane is contextualised. Distance between the foci and membrane is calculated by:

$$\text{Distance} = \sqrt{(X_1 - X_2)^2 + (Y_1 - Y_2)^2}$$

Pole distance is further calculated after the foci has been determined to be within the cell and a distance to the membrane has been calculated. The line is rotated by 90° and iterated outwards until membrane is hit at the poles.

The foci are also checked to determine whether it is in focus or not. 6 iterations from 0° to 150° are taken, at 30° intervals. Full width half maximum of the foci for each angle is taken. Focus is then checked via three methods: sum of residuals squared, the standard deviation and the R^2. Other values are also outputted for manual evaluation, namely the focus values as mentioned and the mean intensity, whereby the foci brightness is compared to the backgrounds. All of the above is available at https://github.com/NCL-ImageAnalysis/FociToMembraneDistance.git.

2.3.6 Image Quantification (VerCINI)

Quantification for VerCINI is mostly similar to the flatpad method (2.3.5) with the changes listed below. No Ilastik was required to determine segmentation due to the nature of VerCINI. Local thresholding was changed from Gaussian blur to Bernsen local thresholding with 15° for the circular ROI's. Each ROI is checked for circularity, where 0.8-1.0 values are acceptable. Cell sizes are also checked, only ensuring they are larger than 0.5.

The cell ROI's midpoint is determined via gaussian curve and used to calculate the distance of the foci. A line is drawn emerging from the ROI centre and out, bisecting the membrane. Where the foci sit on this line is calculated from the intensity curve. All the above is available at https://github.com/NCL-ImageAnalysis/FociToMembraneDistance.git.

2.3.7 Statistics

Statistics were performed on graphs within the program GraphPad prism 10. Primarily an unpaired t-test was done, using a nonparametric Mann-Whitney test. P values were summarised on graphs with ns ($P>0.05$), * ($P \leq 0.05$), ** ($P \leq 0.01$), *** ($P \leq 0.001$) and **** ($P \leq 0.0001$). Experiments were done in triplet unless stated otherwise.

Chapter 3: Development and design of lacO array for observation of transertion

3.1 Introduction

Transertion, despite a long-standing hypothesis, has had minimal direct experimental evidence. The first direct evidence for transertion was observed in *Escherichia coli (Libby et al., 2012),* whereby genes were directly observed in live cells to shift from the midcell to the cell periphery. More evidence pertaining to transertion has been directly observed in another Gram-negative bacterium *Vibrio parahaemolyticus (Kaval et al., 2023)*, whilst super-resolution microscopy of *E. coli* cells has shown tethering of nucleoid to the inner membrane, supporting transertion (Spahn et al., 2023). In Gram-positive bacterium *Bacillus subtilis,* however, no previous research into the field of transertion has been achieved. In the introduction, arguments against transertion were inferred only through arguing against coupled transcription-translation in *B. subtilis.* In this case the argument of RNAP outpacing the ribosome in *B. subtilis* (Johnson et al., 2020) does not directly infer against transertion. Regardless of evidence against CTT, there is no direct experimental evidence for or against transertion in *B. subtilis*.

Live cell imaging of genomic loci through light microscopy has been in use as a technique by other studies to understand chromosomal organisation and replication for decades. To test this, *lac* operator sequences have consistently been used for this very purpose.

The *lacO* binding site, a 21bp sequence of DNA is bound to by the lacI protein; a homotetramer, where two dimers of lacI come together. A monomer of lacI consists of an N-terminal DNA binding domain, characterised by a Helix-turn-helix motif, a hinge region, followed by a core for binding lactose and a C-terminal tetramerization domain (M. Lewis et al., 1996). LacI can also from tetramers whereby a dimer of dimers can form. A fusion protein expression of *lacI* with a fluorescent protein allows for imaging of the gene locus with fluorescent microscopy.

In this chapter I aim to use *lac* operator arrays to image and visualise a gene locus shift towards the membrane or nucleoid edge within *B. subtilis.* This chapter also aims to optimise these *lacO* array tools further in *B. subtilis*. Imaging of foci will allow visualization of gene locus movement with the cell, observing potential locus location shifts. Such will allow determination of transertion or gene movement in *B. subtilis.*

Therefore, this chapter will also establish how the foci positioning was quantified to be able to determine the location of loci shift.

3.2 Results

3.2.1 Design of lacO48 fluorescent reporter in front of gene des.

To observe gene locus movement, operator arrays were utilised to image the chromosomal loci of choice in live cells. Previous experiments observing chromosomal loci have used *lac* operator (*lacO*) and *tet* operator (*tetO*) sequences of multiple repeats. Repetitions of such *lacO* and *tetO* arrays vary in size, from 240 repeats to newer reduced number of operator site of 48 repeats. Longer repeats of arrays have been shown to cause blocks in the progression of the replisome (Bernard et al., 2010). To this end, the shorter 48 repeats of *lacO* and *tetO* from Wang et al were utilised (Wang et al., 2014).

To image transertion, the *lacO48* array would need to be placed at a suitable site, and for this purpose the *des* gene locus was chosen. *des* encodes for protein Des, a fatty acid desaturase which regulates membrane fluidity. Des is incorporated into the membrane to adapt the cell to sudden drops in temperature (Weber et al., 2001a). Des expression is controlled by a two-step signalling system. DesK sits in the membrane as a sensor of membrane fluidity. Upon cold shock the lipid bilayer's fluidity is altered, into ordered state. Sensing this, DesK phosphorylates DesR dimer, which allows DesR to interact with the binding region upstream of *des* promoter. Binding of DesR to the DNA binding site promotes RNAP binding and activates *des* transcription. Upon insertion of Des into the membrane, enzymatic activity of Des changes the phospholipid membrane fluidity and eliminating signally of DesK and downregulating further Des expression (Cybulski et al., 2004) As *des* encodes for an integral membrane protein and its promoter is induced by its own unique regulatory sensor pair, it was deemed an ideal candidate for conditional observation of gene movement. Additionally, *des* operon is located near the terminus of chromosomal replication. DNA replication in *B. subtilis* undergoes multi-fork replication, where freshly divided cells possess two origins of replication. Thus, genes located near the origin of the cell will have two copies, whereas genes at the terminus will have one (X. Wang et al., 2014b). Due to this, *des* being located at the chromosome terminus is an advantage for experiments for quantification due to only one foci per cell a majority of the time.

To be able to observe the gene locus without interrupting the expression, the lacO48 array was transformed upstream of the *des* promoter (Figure 3.1). I developed a strain with *lacO48* integrated upstream of *des* promoter, further confirmed by colony PCR and sanger sequencing. Sequencing data showed several repeats of lac operator sequence had undergone single point mutations, however, this only effected 4 out of 48 total *lacO* repeats, which was deemed unlikely to affect results. Sequencing also confirmed the array was located in the correct location at *Pdes* as designed.

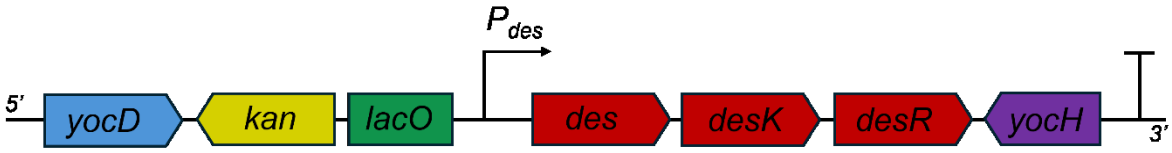

Figure 3.1: Schematic overview of the lacO48 array marker at des promoter. *The lacO48 array was integrated at the des locus, upstream of the promoter in B. subtilis by homologous recombination, with the kanamycin resistance for selective pressure (kan). The kan is situated upstream of lacO48, with its expression facing the opposite direction to that of des, to avoid read through into the operon. Neighbouring genes are shown either end of the overview. desK encodes for an integral membrane protein and yocH encodes for a secreted protein, both potentially having a knock-on effect on foci location. Intrinsic terminators can be found after des and desR.*

In order to image the array, the matching *lacI* fusion protein was required. To this end, I initially utilised lacI fusion protein with myPET, a YFP, from strain BWX1200. Fluorescent microscopy of the strain (Figure 3.2) showed foci, which are lacI-myPET at *lacO48* arrays upstream of *des*. Cells were additionally stained with membrane stain Nile-red and nucleoid stain DAPI to contextualise foci location within the cell. Initially, it was thought that the *des* locus should be located within the nucleoid interior without induction of expression. However, foci were observed by eye to be located towards the nucleoid edge and membrane without induction.

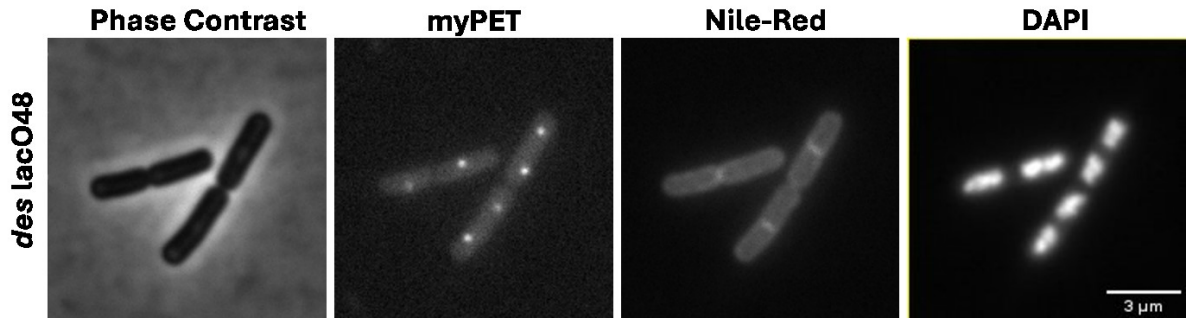

Figure 3.2: First look at lacO48 array with matching lacI-fusion protein*. Fluorescent images of B. subtilis cells expressing lacI-myPET under a constitutive promoter of P_{ftsW}, binding to lacO48 array at des locus. Scale bar 3µm. Strain: BJN003 (lacO48, lacI-mNG).*

3.2.2 Quantification and confirmation of lacO48 array exclusion from cell centre.

Using microscopy images taken of cells, foci of the *lacO48*/*lacI-myPET* complex at *des* appeared to be shifted towards the periphery of the cell (Figure 3.3A). To be able to further confirm this, foci distance to the membrane required quantification. Manual quantification of foci distance to the membrane was achieved by determining fluorescent intensity peak values from the foci and the membrane stain. Distance was measured between foci and the closest membrane peak and converted into percentage value towards the membrane (Figure 3.3C). A midline of the cell was determined down the long axis of the cell to act as a baseline by also using membrane peak intensity (Figure 3.3B).

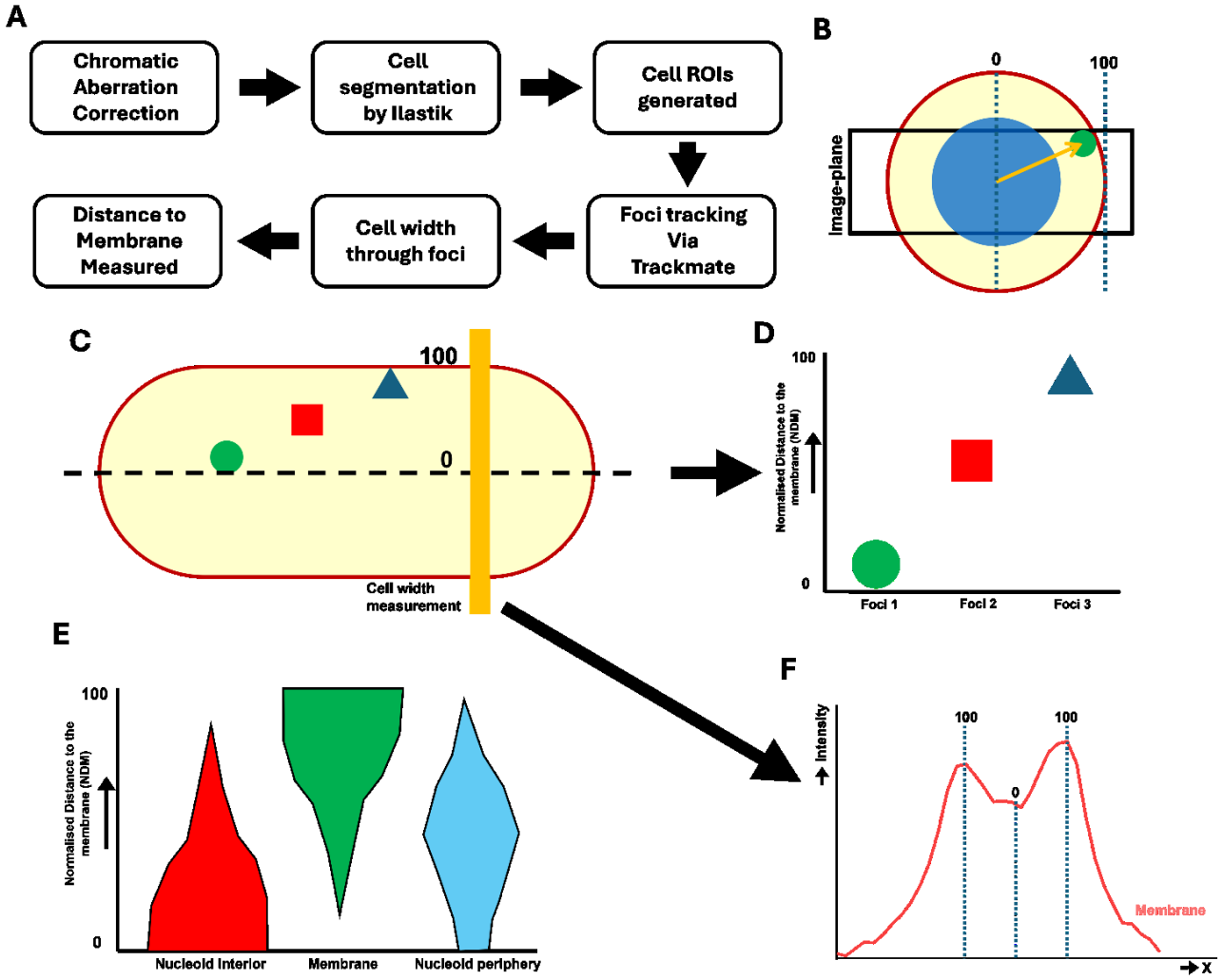

***Figure 3.3: Workflow for manual data quantification with representative scatter plots**. **A.)** Simplified workflow for measurement of foci distance and quantification based on chapter 2.3.5 **B.)** Cartoon representation of focal imaging plane for horizontal cells from the side of the cell, where 0 is the midcell and 100 is the membrane, demonstrating the curved membrane edge and potential geometric issues. **C.)** Cartoon representation of cell with 3 foci distances, then represented in a scatter plot in D.). Yellow line shows measuring tool to generate line scan plot of membrane shown in F.). **D.)** Simplified scatter plot representing where each "foci" from C.) would be plotted on a graph. **E.)** Cartoon demonstration of what certain localisations might look like, where each coloured area represents a scatter plot population. Red shows estimated nucleoid interior associated foci, green shows estimated membrane associated foci and blue shows estimated foci at the nucleoid periphery. **F.)** Fluorescent intensity line scan of membrane stain with context of Normalised distance to the membrane values, where cell midline is 0 and membrane is 100.*

The change was made to automatic image quantification as described (2.3.5) for analysis of large data pools of foci for statistics and unbiased foci measurements within cells. Cell geometry was also determined to be a potential issue, whereby foci at poles of the cell would be recognised simultaneously at the membrane and the cell midline. To test this, pole distance of foci was measured and represented against normalised distance to the membrane (NDM), where poles were deemed not to have a material effect to warrant another filter step (Figure Appendix 1).

Using data from the fluorescent microscopy fields of view (Figure 3.4A) and quantified by the above-described quantification macro, foci positioning within the cell was represented in a scatter plot (Figure 3.3C). *lacO48* at *des* showed a median of 39 NDM, from cell midpoint towards the membrane. Foci are located throughout the cell homogenously mixed, confirming the initial observation that foci appeared to be preferentially away from cell centre.

Further additions to strains were made throughout. To increase the brightness of each focus, the lacI fusion with fluorescent protein mNeonGreen was developed (Shaner et al., 2013). To this end, the fusion lacI-mNeonGreen (lacI-mNG) was constructed. Additionally, the Nile-red membrane dye was replaced by a more effective membrane fluorescent signal with expression of helical transmembrane peptide WALP23 fused to mCherry (Matalon et al., 2013; Gohrbandt et al., 2022).

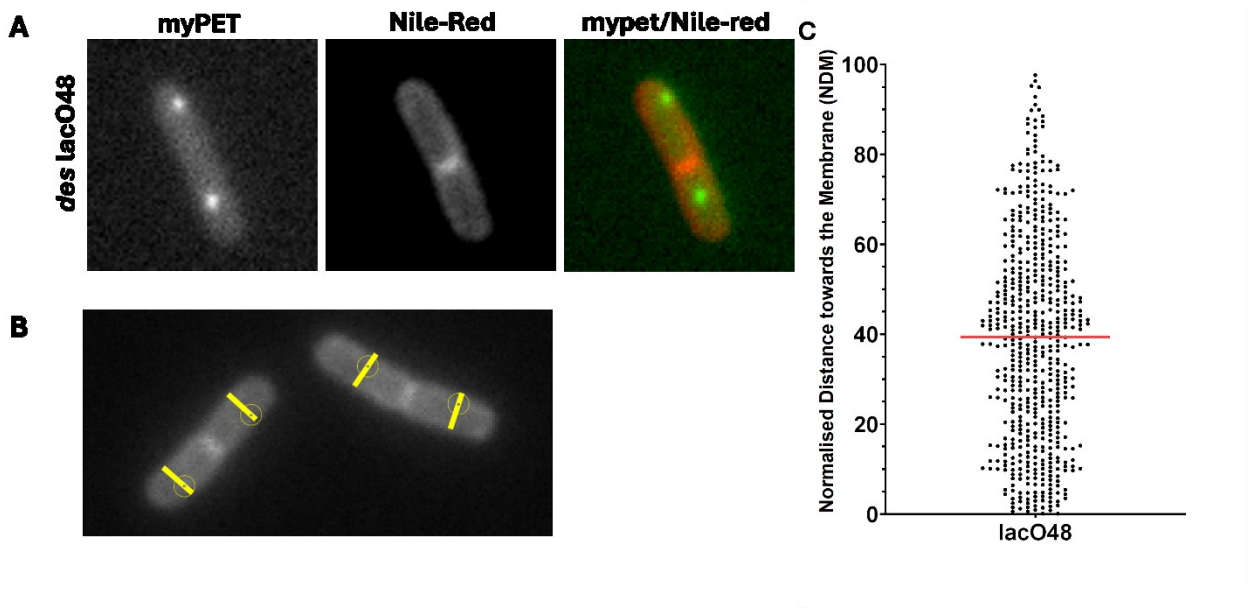

Figure 3.4: Quantification of array foci positioning within the cell. A.) *Representative lacO48 arrays located at des promoter within cells. For quantification, only the foci and membrane channels were utilised.* ***B.)*** *Representative image showing foci detection via macro in circles, with cell width measured through foci via yellow line, to give exact positioning of foci within the cell.* ***C.)*** *Quantification of cells in one experiment as a scatter plot. Red line shows median. Strains used: BJN003 (lacO48, lacI-myPET).*

3.2.3 Arrays inserted on different loci around the genome share exclusion from the cell centre.

To determine if *lacO48*/*lacI-mNG* complex was excluding *des* from the nucleoid centre, other previously utilised *lacO* and *tetO* arrays were looked at. Previous work has commented on arrays causing blockage to the replisome in *E. coli*, whereby shorter arrays *lacO48* and *tetO48* were designed to mitigate this issue. As discussed above, Above observation suggest that foci are not moving, though this is premature and requires further evidence. Alternatively, *des* locus itself could be responsible. To determine if *lacO48*/*tetO48* arrays are responsible for exclusion or if the specific location of the gene on the chromosome is responsible, strains possessing arrays at locations *yycR* (-7°/Ori), *ydhG* (87°), *ycoW* (120°), and *yuxG* (-87°), thus distributed throughout the genome.

Fluorescent microscopy images of each locus, aswell as *des,* were collected (Figure 3.5A). As expected, arrays positioned at the chromosomal origin, *yycR*, showed to have multiple foci per cell, compared to foci at the chromosomal terminus, *des.* As discussed previously, multi-fork replication in growing *B. subtilis* cells results in two origins per cell on average. Thus, foci near the ori would have more copies per cell.

Foci were measured and quantified via macro and represented in scatter plot (Figure 3.5B). Locus *yycR* showed a median of 35 NDM, *ydhG* a median of 36 NDM *ycoW* a median of 36 NDM and *yuxG* a median of 25 NDM. Comparatively *des* showed a median of 39 NDM. With the exception of *yuxG*, all strains showed minimal shift deemed not to be relevant compared to *des* locus localisation. The exception, *yuxG,* comparatively to *des* had a median difference of 14 NDM, showing a small relevant distance between foci populations. The specific gene location of *yuxG* might be the source of foci located closer to 0 NDM and the cell midline.

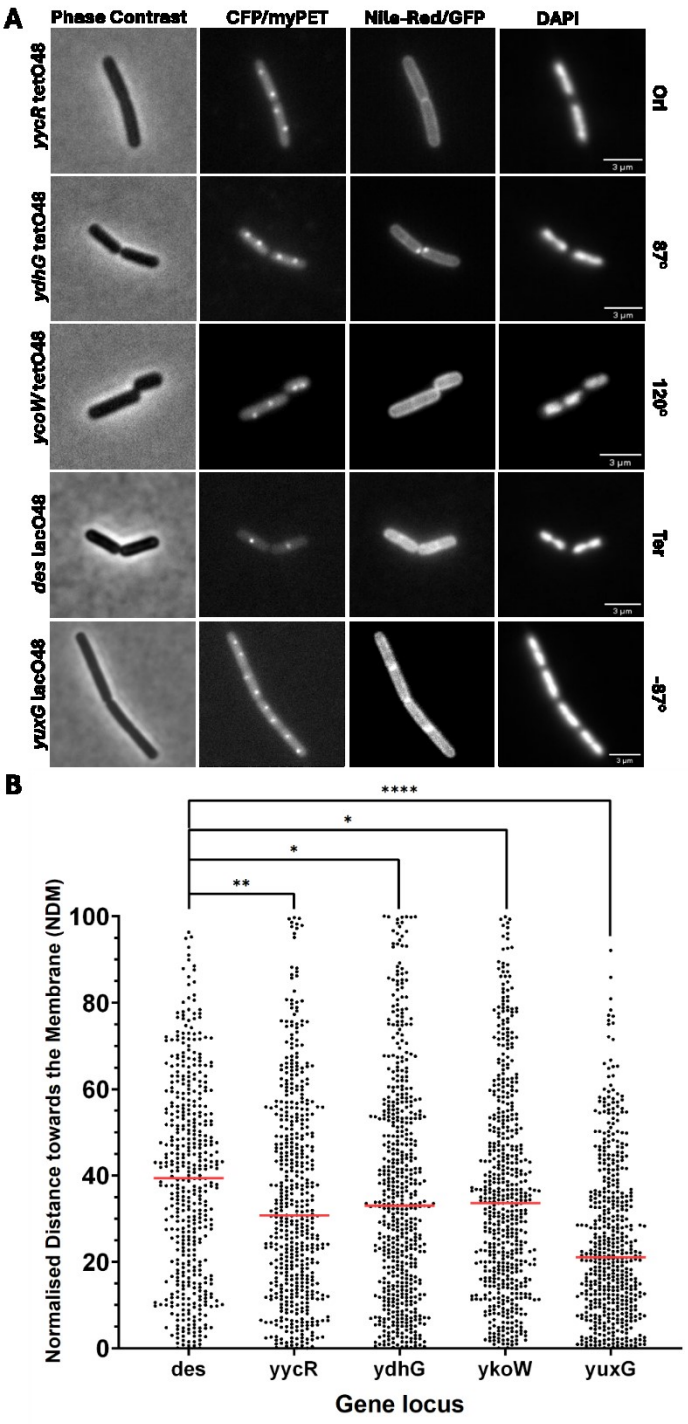

Figure 3.5: Location of arrays in different loci around the genome has no effect on exclusion pattern. A.) *Phase contrast and fluorescent images of B. subtilis cells with either tetO48 or lacO48 arrays inserted at different loci around the genome. For lacO, lacI-myPET, for tetO, tetR-CFP. Positioning within the genome is labelled on the Y-axis. Cells were grown at 30°C to* OD_{600} *0.3 and treated with DAPI. Nile-red was also used for lacO48 constructs. Scale bar 3µm.* ***B.)*** *Quantification of foci positioning from cells. Distance was represented Normalised Distance to the Membrane (NDM), where normalised foci position is placed from midcell (0) to membrane (100). Red line shows median of NDM. Strains: BWX721 (yycR tetO48, tetR-CFP), BWX1212 (ydhG tetO48, tetR-CFP/yuxG lacO48, lacI-myPET), BWX1206 (ykoW tetO48, tetR-CFP) and BJN003 (des lacO48, lacI-myPET).*

3.2.5 Induction of des lacO48 array with cold shock has no effect on gene movement.

One of the primary aims of the project was to observe the effect of transertion. Observation of this in previous work in *E. coli* (Libby et al., 2012) managed to image foci at the membrane after induction of *lacY* expression, where they shift towards the membrane from cell midpoint. In my experiments, lacO48 foci location appeared to already show a clear shift towards the membrane and nucleoid edge (Figure 3.4C). To test if induction shows a further shift, I took advantage of *des* promoter which uses cold shock temperatures to regulate expression of *des* by its own regulatory sensor pair.

Previous work with Des expression used temperature shifts from 37°C to 22°C, or 30°C to 15°C for 15 minutes (Gohrbandt et al., 2022) Aguilar et al., 1999). In this work, I chose to grow cells at 30°C for fluorescent protein folding, thus cold shock induction was determined to be at 15°C.

Using data collected by fluorescent microscopy (Figure 3.6A), numerous foci locations were measured from both temperatures, then analysed from the resulting scatter graph (Figure 3.6B). Firstly, *lacO48* at *des* at 30°C has a median of 38 NDM compared to the median observed at 15°C of 34 NDM. This shows no relevant difference between uninduced and induced populations.

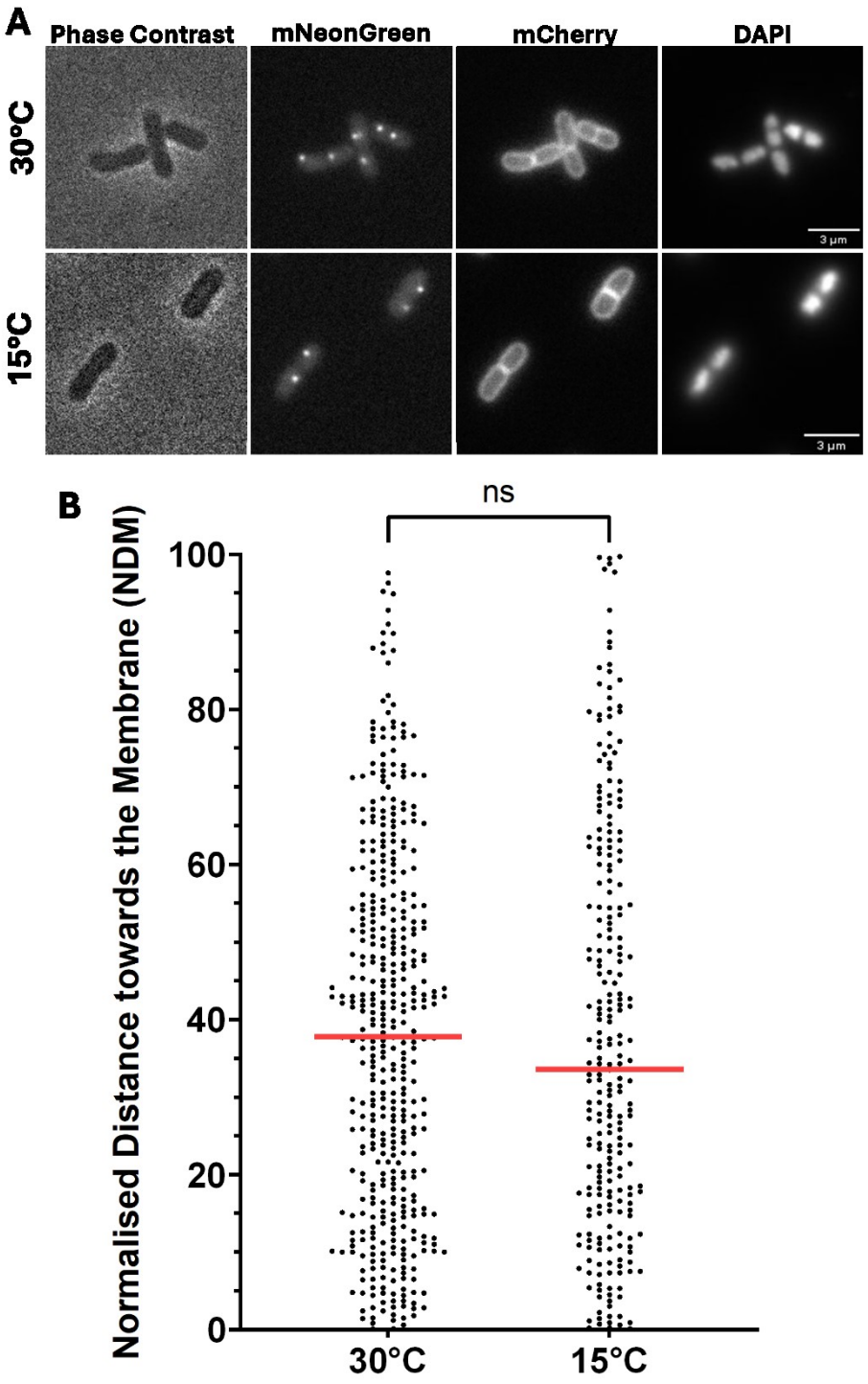

Figure 3.6: Induction of des lacO48 with cold shock. A.) *Phase contrast and fluorescent images of B. subtilis cells with des lacO48 array. Cells constitutively express WALP23-mCherry and lacI-mNG. Cells were grown at 30°C to* OD_{600} *0.3 and treated with DAPI. Induction by cold shock carried out at 15°C for 15 minutes. Microscope kept at room temperature. Scale bar 3µm.* ***B.)*** *Quantification of foci positioning from cells. Distance was represented Normalised Distance to the Membrane (NDM), where normalised foci position is placed from midcell (0) to membrane (100). Red line shows median of NDM. Red line shows median. Strain: BJN006 (lacO48, lacI-mNG).*

To determine if time scale was a factor in induction of *des* by cold shock, cells expressing *lacI-mNG* with *lacO48* were imaged after an increase or decrease 15°C incubation time. An additional factor of recovery was also considered. If *des* moves to the membrane for transertion under cold shock, return to 30°C after cold shock shuts down expression and make the foci move down towards the cell centre (Figure 3.7).

The data collected from microscopy underwent quantitative data collection (as described in 2.3.5) and represented scatter graphs (Figure 3.8). When induced for a shorter period of time at 5 minutes, the median measured at 38 NDM. At 30°C for time point 0 was 39 NDM, 15 minutes at 15°C showed a median of 39 NDM and increasing induction time to 30 minutes showed a median of 37 NDM. Finally, after incubation at 15°C, cells were incubated back at 30°C for 30 minutes. Recovery showed a slightly lower median of 36 NDM. When compared against the standard conditions at 30°C at time point 0, no substantial change is observed between any induction timepoint or recovery.

The above argues against transcription dependant shifting of gene loci. This is surprising however as comparatively, uninduced gene loci are shown to be at the nucleoid periphery or closer to the membrane. It is plausible that a shift has already occurred in uninduced gene loci. Such a shift could be due to the *lac* operator array size at the gene locus, where foci would be seen at the nucleoid surface or membrane irrespective of transcription due to size. However, such conclusion is premature and requires validation. As such this could be tested via mass spectrometry analysis of lipid membrane, to determine whether the *lac* operator array changes the composition.

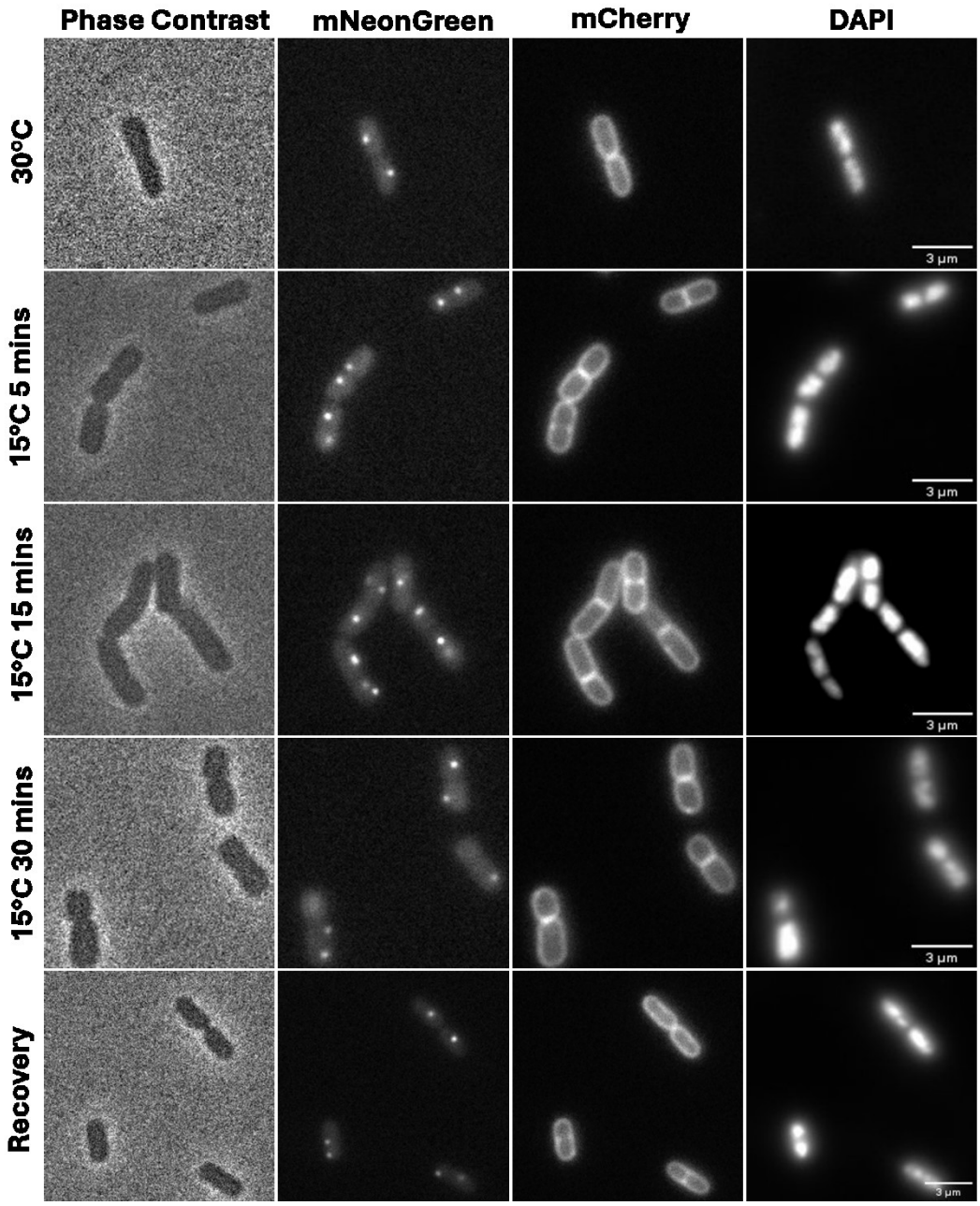

Figure 3.7: des lacO48 induction by cold shock over time points and returned to 30°C. *Phase contrast and fluorescent images of B. subtilis cells with des lacO48 array. Cells constitutively express WALP23-mCherry and lacI-mNG. Cells were grown at 30°C to OD_{600} 0.3 and treated with DAPI. Cells were then incubated at 15°C for the respective time for induction as indicated above. Recovery marks 15°C for 30 minutes before then returning to 30ºC for further 30 minutes. Scale bar 3µm. Strains: BJN006 (lacO48, lacI-mNG).*

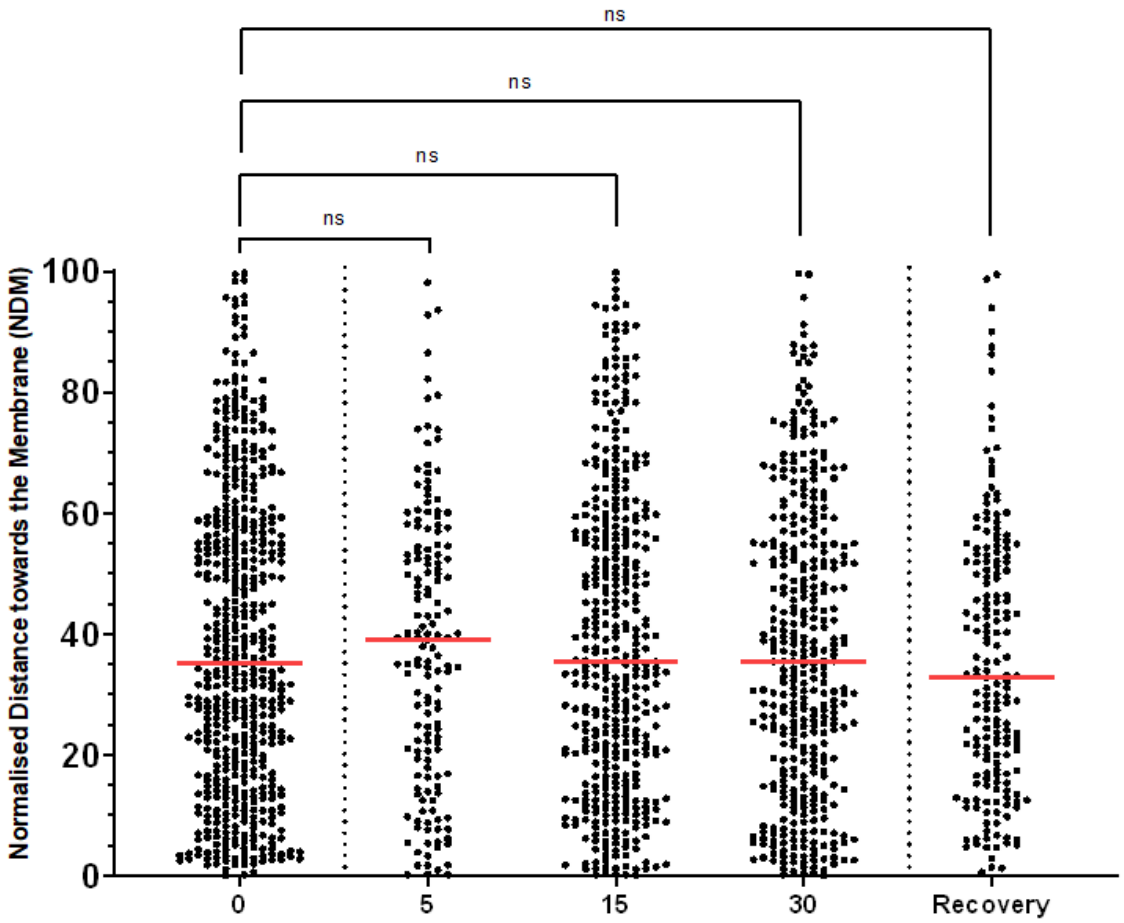

Figure 3.8: Scatter plots showing induction by cold shock at varying time point and return to 30°C. *Scatter plots of quantification of foci position from B. subtilis cells. Cells were incubated at 15°C for the respective time as indicated above. Recovery marks 15°C for 30 minutes before then returning to 30ºC for further 30 minutes. Distance was represented Normalised Distance to the Membrane (NDM), where normalised foci position is placed from midcell (0) to membrane (100). Red line shows median of NDM. Strains: JBN006 (lacO48, lacI-mNG).*

3.2.5 Antibiotics have negligible effect on lacO48 foci positioning.

Data shown in previous subsections above have shown the location of *lacO48*/*lacI-mNG* complex at *des* locus to be outside the nucleoid interior, independent of gene induction. Foci at the periphery could be due to transertion at this site already taking place at the locus from neighbouring genes or crucially from membrane associated protein DesK (Figure 3.1). To determine if transertion was in fact already playing a role, the antibiotic transcription inhibitor rifampicin and translation initiation inhibitor chloramphenicol were used. Additionally, rifampicin and chloramphenicol are known to have an effect on nucleoid morphology, hypothesised to be due to inhibition of transertion (Bakshi et al., 2014;Spahn et al., 2023). Changing nucleoid morphology by chloramphenicol results in condensation and by rifampicin, results in decompaction/expansion. Such changes in morphology would highlight the location

of *lacO48* complex in comparison to the nucleoid. Fluorescence microscopy was used to observe *B. subtilis* cells affected by either chloramphenicol or rifampicin (Figure 3.9A).

DAPI stain was used to confirm nucleoid morphology changes, whereby when compared to untreated, chloramphenicol treated cell nucleoids were condensed and rifampicin treated cell's nucleoid expanded. Foci data was quantified and represented on scatter plots (Figure 3.8B). Untreated cells had a median value of 39 NDM, which slightly increased to 43 NDM for chloramphenicol treated cells. For rifampicin treated cells, there was a 2-point decrease compared to untreated, at 37 NDM. Condensation by chloramphenicol and decondensation by rifampicin did not meaningfully shift the foci distance to the membrane.

This minor difference between untreated and chloramphenicol suggests there is no disruption of any existing transertion at *des* locus. The compaction of the nucleoid is a more likely candidate for foci being further excluded. The lack of difference between rifampicin and untreated is more surprising. Rifampicin treatment has been thought to either expand the nucleoid outwards or dissolve the structure. Foci not being further shifted towards the membrane suggests the latter. The data is consistent with exclusion of large complexes from the nucleoid interior; therefore, transertion dependant changes of foci location are undetectable.

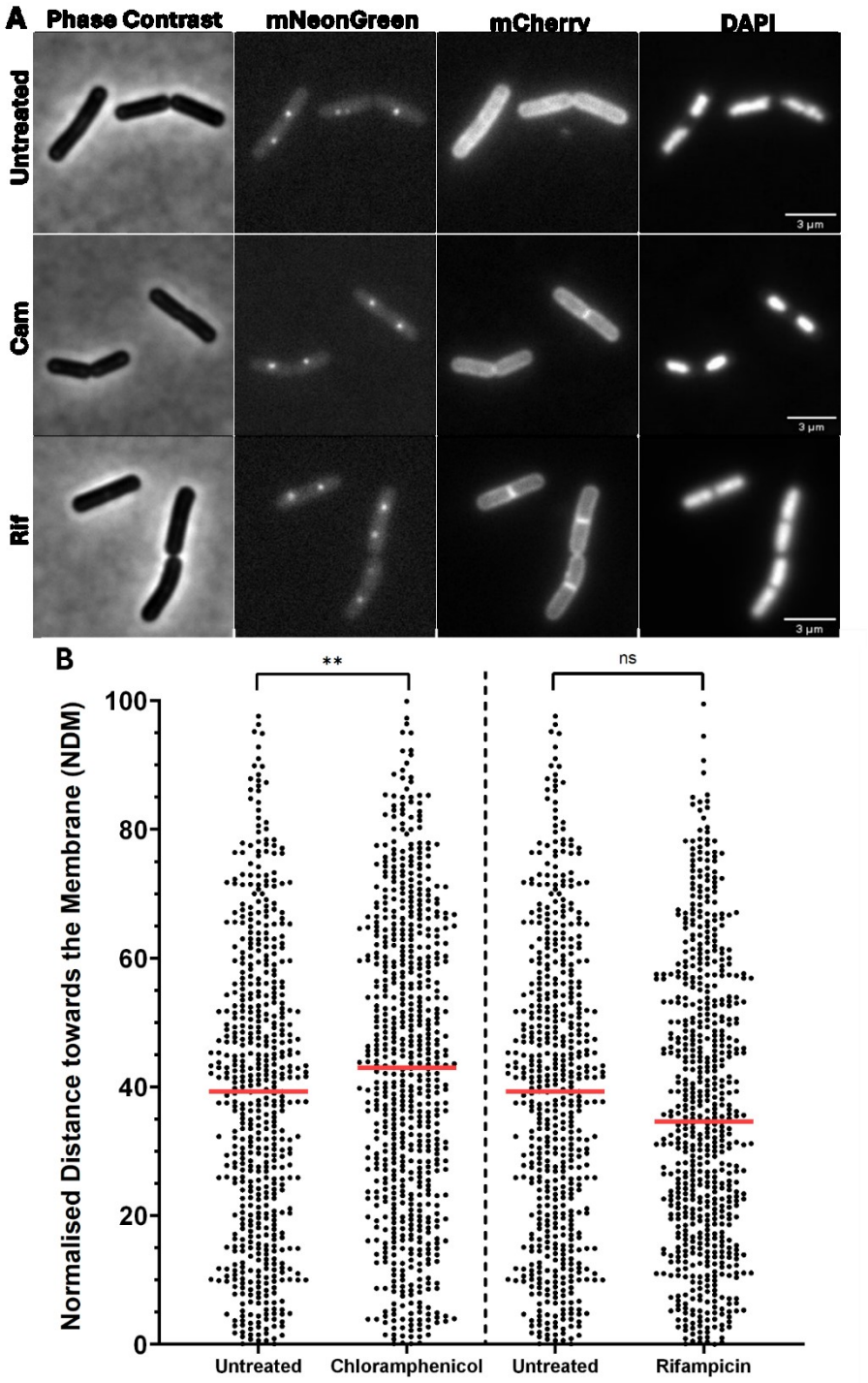

Figure 3.9. Treatment with chloramphenicol and rifampicin have negligible effect on lacO48 location A.) *Phase contrast and fluorescent images of B. subtilis cells either untreated or treated with chloramphenicol or rifampicin. Cells were expressing lacI-mNG localising to lacO48 arrays at des locus, and WALP23-mCherry. Cells were grown at 30°C to* OD_{600} *0.3 and treated with DAPI. Scale bar 3µm.* ***B.)*** *Quantification of foci positioning from cells. Distance was represented Normalised Distance to the Membrane (NDM), where normalised foci position is placed from midcell (0) to membrane (100). Red line shows median of NDM. Strains: BJN006 (lacO48, lacI-mNG).*

3.2.6 Design and construction of short array, lac04

To explore the hypothesis that the lacO48/lacI-mNG complex is responsible for excluding *des* locus from the nucleoid, the effect of a smaller array was looked into. As so far, *lacO* arrays as mentioned above, were larger with the smallest current array being at 48 repeats. Multiple repeats allowed more possible binding opportunities for *lacI-mNG*, to increase brightness. The new brighter fluorophore of *mNeonGreen* in fusion with *LacI* meant foci brightness would not be sacrificed when reducing the number of operator arrays, allowing testing into whether array count had an effect on foci positioning.

To test this, novel *lacO4* short array was developed. Utilising the same design principles as *lacO48* (Figure 3.1), *lacO4* was integrated into *B. subtilis* upstream of *des* promoter, in the background of WALP23-mCherry and lacI-mNG. Colonies were selected and sequenced. No changes in array sequence were detected, unlike with 48 *lac* operator repeats. *lacO4* array localisation was then observed via fluorescence microscopy where foci were detected (Figure 3.10A). Foci were bright though a noticeably weaker fluorescence signal than the *lacO48* counterpart as expected.

Quantification of cell images (Figure 3.10B) for *lacO48* and *lacO4* showed significant differences in foci location. *lacO48* maintained a median value of 39 NDM. In stark contrast, *lacO4* had a median of 21 NDM, a 19-point shift towards cell midpoint compared to *lacO48*. Overall, the *lacO4* showed significant difference in foci cellular location. Specifically, a majority of *lacO4* foci were determined to be tending towards the cell centre.

This shift of *lacO4*/*lacI-mNG* foci towards the cell midpoint compared to *lacO48* demonstrates that large arrays are preferentially shifted outside of the nucleoid interior. The small *lacO4* array is able to remain within the nucleoid interior, therefore suggesting that this small array is more similar to that of the native locus. Closer resemblance of the native locus therefore means *lacO4* is a more trustworthy

representation of gene locus location. Throughout this project going forwards, *lacO4* is always used.

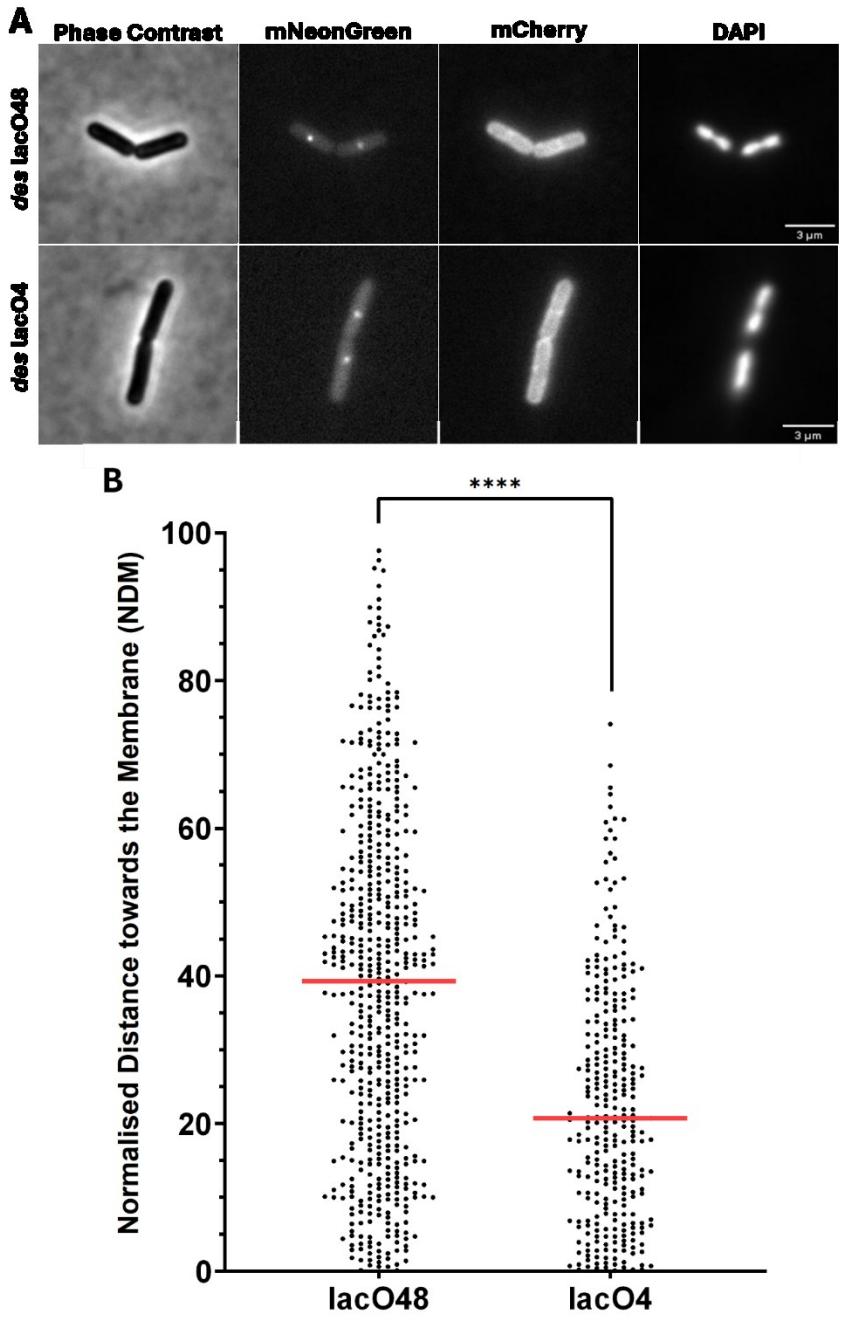

Figure 3.10: Novel lacO4 short array compared to lacO48 array at locus of des. ***A.)*** *Phase contrast and fluorescent images of B. subtilis cells with des lacO48 array. Cells constitutively express WALP23-mCherry and lacI-mNG. Cells were grown at 30°C to* OD_{600} *0.3 and treated with DAPI. Scale bar 3µm.* ***B.)*** *Quantification of foci positioning from cells. Distance was represented Normalised Distance to the Membrane (NDM), where normalised foci position is placed from midcell (0) to membrane (100). Red line shows median of NDM. Strains: BJN006 (lacO48, lacI-mNG), BJN017 (lacO4, lacI-mNG).*

3.3 Discussion

Since the first studies on live cell imaging on chromosomal loci, utilising *lacO* or *tetO* arrays have been a staple of the technique, notably looking at DNA replication in *B. subtilis* (Lee & Grossman, 2006;*Webb et al., 1998)* and later looking at transertion(Libby et al., 2012). Here, we utilised intermediate sized array *lacO48*, yet still our analysis has shown that inclusion of a *lacO48* array in tandem with partner lacI fusion protein is shifted outside of the nucleoid interior and is consistently shifted towards the membrane. Such exclusion from the nucleoid interior and midcell can be hypothesised to be due to several reasons in the surrounding area of *des.* Surrounding genes in the operon's location could be responsible for influencing locus movement, as other integral membrane proteins, notably DesK, could be undergoing transertion and therefore influencing local genomic area location. Alternatively, the kanamycin resistance cassette used for selection is directly next to *lacO48*, where active expression of the resistance cassette could influence *lacO48* location.

The *lacO48* itself must be considered, however. Evidence from alternative gene loci with arrays present shows exclusion as well (Figure 3.5). The *lacO48* is a ~2100bp long repetitive sequence that is bound by up to 48 dimers of *lacI-mNG* fusion protein, which is positioned immediately upstream of *Pdes.* As mentioned in chapter 1, the nucleocytoplasmic ratio of *B. subtilis'* nucleoid can exclude larger cellular equipment from the centre. The shifted gene loci to the surface means imaging of transertion is not possible with *lacO48* arrays at *des,* as the gene locus is already excluded. Thus, the large complex of DNA and protein of *lacO48*/*lacI-mNG* might work as an excluding factor. The observation of *lacO4* array seems to confirm this, whereby the 12-fold reduction in number of binding sites no longer is pushing *des* and the array away from the nucleoid centre. Of note should also be lacI protein. The lacI tetramer is combined with protein mNeonGreen for a vast number of experiments. Per *lacO* binding site, a large tetramer of *lacI-mNG* could be a significant factor in exclusion. In future, experimenting with truncation of lacI to prevent dimerization of the protein could be looked into.

Induction of *des* locus with a *lacO48* array results in no detectable foci shift (Figure 3.6). Detection of transertion or gene locus movement would be impossible with this array setup. Lack of foci shift could coincide with *lacO48* array exclusion from the nucleoid interior, as the gene locus has already been shifted from the localisation of

the native locus. Therefore, changing the inducing time (Figure 3.6) would have no further effect on gene loci movement, as is seen (Figure 3.7).

Chloramphenicol treated cells see the compaction of the nucleoid but no substantial shift of gene locus location (Figure 3.8). As discussed in chapter 1, the nucleocytoplasmic ratio is important for determining what is excluded from the nucleoid interior. Compacting the nucleoid further via chloramphenicol would only further condense the nucleoid, excluding large complexes. As no substantial change is seen, this supports the above theory that the *lacO48* is excluded due to size.

Rifampicin treatment of cells inhibits transcription and decondenses the nucleoid, which also results in no gene locus shifts being observed compared to untreated cells. Rifampicin either expands the nucleoid or the nucleoid is dissolved homogenously throughout the cell. Foci not shifting towards the membrane with rifampicin treatment suggests nucleoid is dissolved. In such case, size exclusion from the nucleoid is no longer relevant, as nucleoid organisation ceases to exist. Comparatively, untreated cells still retain organisation. In the case of data shown, no shift between treated and untreated therefore further confirms that *lacO48* foci are shifted from nucleoid interior. It should be noted that both rifampicin and chloramphenicol have major pleiotropic effects on cell function, limiting how much information can truly be extracted only from inhibition of transertion on *des.* This is explored further in later chapters.

Any cell takes up a 3D space. However, our analysis observes foci and the cell from a 2D plain. Foci will travel in any direction, irrespective of our top-down perspective, notably in the Z-plane. To combat this and prevent bias of data, we threshold images through the macro to exclude out of focus foci. However, it should be noted that despite this, foci are still not all in the same Z-plane upon foci recognition. Foci close to the membrane in actuality may be further away from the membrane in 2D images due to the angle of foci in the Z-plane. Foci at the membrane will have a broader distribution than those at the cell midline. Foci throughout the nucleoid will have a degree of distribution as they can move in the Z-plane (Figure 3.1E). The exact degree of this distribution is unknown.

The results of this chapter show that *lacO4*, the smaller array, avoids such exclusion issues presented by *lacO48*, due to its small size and lacI binding reduction. *lacO4* foci shifting to the midcell comparatively to *lacO48* means that the longer array

location within the cell is not equivalent to the native locus location. *lacO4* therefore is the closest to native array available. Due to this, *lacO4* marks the ideal array candidate to continue the observation into gene locus movement in *B. subtilis.* In future lacO4 is the only acceptable array size for DNA locus experiments. In the following chapters, the intention is to examine gene locus movements only using *lacO4* arrays.

Chapter 4: Analysis of cellular localisation of a gene upon induction

4.1 Introduction

Attempting to observe gene locus dynamics within live cells with *lacO48* resulted in the discovery that larger arrays are shifted from the nucleoid interior independent of induction. This discovery led to the construction of an optimised short array, *lacO4*, which now should now allow more robust analysis of cellular location of gene locus upon induction.

A previous observation of transertion, which utilised arrays of operator sequences, was achieved in *E. coli (Libby et al., 2012),* where the *lac* operon was labelled with a *tetO* array of unknown length. Upon induction, a population of foci location shifted closer to the membrane. However, no such experiments have been conducted for *B. subtilis.* As *B. subtilis* is argued to not exhibit coupled transcription-translation (Johnson et al., 2020), this would imply that transertion is also not. However, this generalised conclusion is not generally accepted. The interest is to test the core tenants of the transertion hypothesis through direct observation to build a strong case for or against transertion.

Previously in chapter 3, use of antibiotics chloramphenicol and rifampicin were used to alter the nucleoid density to observe how gene locus location would alter in comparison. The intention in this chapter is to further this with a novel *lacO4* array*,* comparing foci positioning during nucleoid expansion or condensation to foci with *lacO48* arrays. Such comparison could further suggest the more native like nature of *lacO4* arrays. Additionally, use of antibiotics for potentially inhibiting transertion in neighbouring genes at *des* would show if the gene locus is shifted due to this.

The aim of this chapter is to investigate the possibility of *des* gene locus movement when induced. The first aim was to evaluate if activating expression of *des* would result in foci location change from the nucleoid interior to either the nucleoid edge or the membrane. Secondly, the intention is to observe if the repositioning of *des* locus could be reversed once the induction condition is removed. Such an effect should be observed as gene loci recovery once the gene is no longer needed to be expressed. I also aimed to create a positive control that undergoes foci tethering to the membrane without induction to demonstrate that des locus can be pulled towards the membrane. Thus, showing what stable persisting tethering to the membrane would look like.

4.2 Results

4.2.1 Effect of lacO4 on foci positioning within cells

From chapter 3, it was observed that the *lacO4* array was not excluded from the nucleoid, tending closer to the cell midline compared to the predecessor *lacO48* (Figure 3.9). Thus, gene locus location shifts were now directly observable within *B. subtilis* cells*,* previously difficult to establish due to *lacO48* foci exclusion interfering independently from induction. As previously mentioned, the transertion affecting products of neighbouring genes, such as *desK* (Figure 3.1) could influence the positioning of foci*.*

To inhibit transertion, both the ribosome inhibitor chloramphenicol and the RNAP inhibitor rifampicin were used. Both antibiotics also have effects on the overall nucleoid morphology and density, making them less than ideal for testing transertion as well as having other pleiotropic effects. Observations show that *lacO4* foci interact differently with condensed and decondensed nucleoids compared to *lacO48*. Such observation further indicates that lacO4 is not excluded by size. Cells were treated with chloramphenicol, rifampicin or remained untreated and then were imaged by fluorescent microscopy (Figure 4.1A). DAPI staining confirmed nucleoid morphology. The nucleoids of chloramphenicol treated cells were compacted whilst rifampicin treated cells nucleoids were expanded across the cell. Quantification of foci of a population into scatter plots (Figure 4.1B) showed untreated cells with *lacO4* foci at a median of 21 NDM. Chloramphenicol treated cells had a negligible increase to 22 NDM compared to untreated. Rifampicin treated cells showed a substantial 12-point increase from untreated, at a median of 32 NDM. This is contrary to what was seen before with *lacO48* array, where no relevant changes in normalised distance to the membrane were observed under different antibiotic pressures, thus further arguing for use of small array *lacO4*.

No relevant shift between untreated and chloramphenicol treated cells suggests no transertion from neighbouring genes at *des* locus. Nucleoid compaction by chloramphenicol has also made no effect on foci position, likely owing to the foci already being present within the nucleoid interior. Comparison between rifampicin and untreated showed a substantial change in foci shift location. The previous argument for rifampicin action in chapter 3, states that rifampicin dissolves the nucleoid structure, thus no longer affecting array positioning. As the foci shifted toward the membrane

when affected by rifampicin, mixing homogeneously through the cell, this argument is further supported. This also indicates that transertion was not present at neighbouring genes during this experiment. Thus, only rifampicin's action on the nucleoid structure is responsible for the gene locus shift. *lacO4* foci can then be said to be largely unaffected from exclusion observed for *lacO48* arrays.

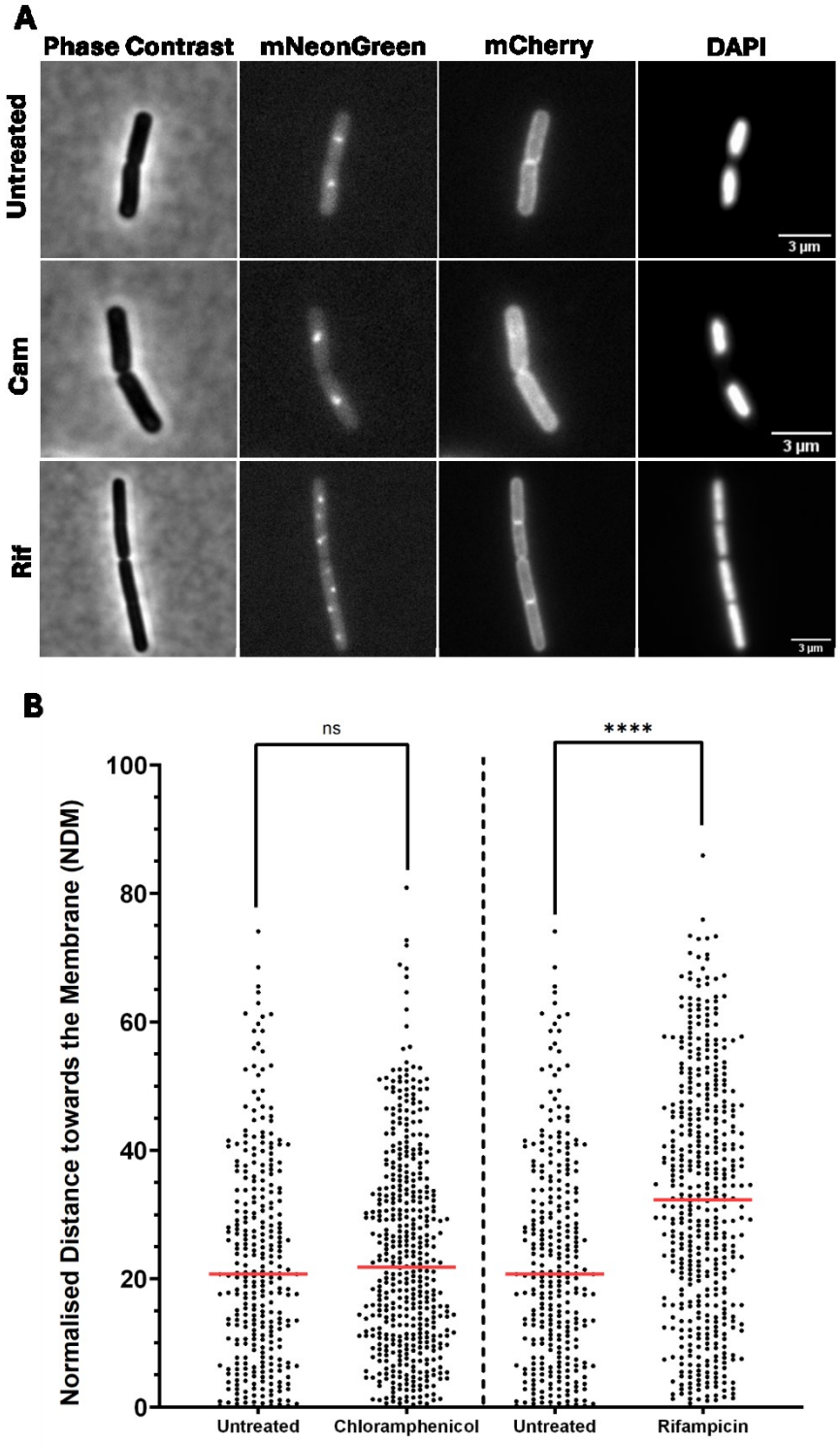

Figure 4.1: Effect of chloramphenicol and rifampicin on des locus positioning ***A.)*** *Phase contrast and fluorescent images of B. subtilis cells either untreated or treated with chloramphenicol or rifampicin. Cells were expressing lacI-mNG localising to lacO4 arrays at des locus, and WALP23-mCherry. Cells were grown at 30°C to* OD_{600} *0.3 and treated with DAPI, then incubated with 100µg/ml Rifampicin or 100µg/ml Chloramphenicol. Scale bar 3µm.* ***B.)*** *Distance was represented Normalised Distance to the Membrane (NDM), where normalised foci position is placed from midcell (0) to membrane (100). Red line shows median of NDM. Strains: BJN17 (lacO4, lacI-mNG).*

4.2.2 lacO4 at des shows movement towards the membrane upon induction

lacO4 has now enabled the hypothesis of transertion and gene repositioning to be experimentally determined. If transertion occurs a shift in the foci population would be present tending towards the membrane would be observed. To achieve this, a strain with *lacO4* at *des* locus with *lacI-mNG* (BJN017) was grown, before being incubated at 15°C (induced) or kept at the same temperature of 30°C (Uninduced), before fluorescent microscopy.

Cells were imaged by fluorescent microscopy (Figure 4.2A) and then were quantified by automated macro as described (2.3.5). When subjected to cold shock, *des* locus foci shifted closer to the membrane (Figure 4.2B). Foci measured after 15°C (Induced) incubation resulted in a median value of 49 NDM. Foci analysed at 30°C (Uninduced) were positioned closer to midline of the cell; median percentage value towards the membrane was valued at 21 NDM. The median shift difference between the two populations resulted in 29-point increase from 30°C to 15°C. The above suggests that induction of *des* moves the gene locus from the nucleoid interior outwards towards either the nucleoid periphery or membrane. The difference between uninduced and expressed are substantial and imply the existence either of transertion or repositioning of genes to the nucleoid surface upon induction. Such resolution of which exactly is not possible in this current set up.

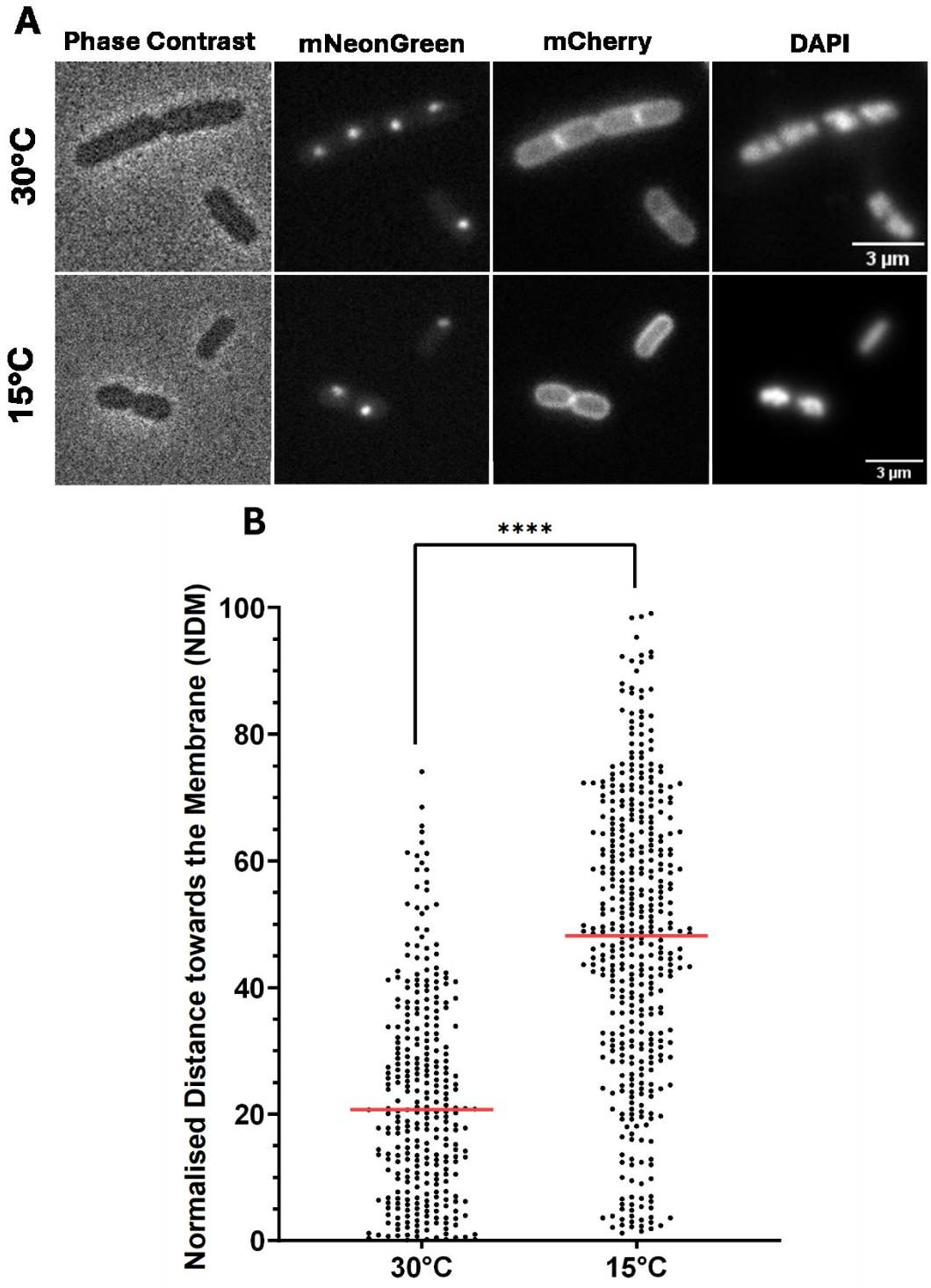

Figure 4.2: Effect of induction by cold shock on des locus positioning A.) *Phase contrast and fluorescent images of B. subtilis cells with des lacO4 array. Cells constitutively express WALP23-mCherry, and lacI-mNG. Cells were grown at 30°C to* OD_{600} *0.3. Induction by cold shock carried out at 15°C for 15 minutes. Microscope kept at room temperature, samples were transported and kept at 15°C for as long as possible. Scale bar 3µm.* ***B.)*** *Quantification of foci positioning from cells. Distance was represented Normalised Distance to the Membrane (NDM), where normalised foci position is placed from midcell (0) to membrane (100). Red line shows median of NDM. Strains: BJN17 (lacO4-lacI-mNG).*

Previous work with *des* cold shock used 15 minutes incubation time, as discussed in chapter 3. Des expression is controlled by a regulatory pair of proteins: DesK and DesR. Cold shock alters the membrane fluidity and thickness, which is detected by DesK. DesK then phosphorylates DesR dimers to bind upstream of the Des promoter to facilitate RNAP binding. The timing of this system came under question, as in cold temperatures, cell processes slow down significantly. Altering the time that cold shock is applied to the cells could have substantial effects. 5-minute incubation for Des expression might be too quick whilst 30 minutes of cold shock might recruit further gene loci towards the membrane. Directly imaging can determine if time of cold shock has an effect on Des expression. Strain BJN017 containing *lacO4* at *des* promoter with accompanying *lacI-mNG*, was grown at 30°C and kept at 30°C. This marked time point 0. Cells were induced at 15°C for 5-, 15- and 30-minute time points as indicated (Figure 4.3). Additionally, another question was asked in regard to foci dynamics. Foci were able to relocate upon induction for Des to be expressed, however would the foci remain at said location upon the loss of expression. To answer this, another time point was added, whereby after 15-minute cold shock incubation, cells were returned to 30°C for a further 30 minutes to allow recovery from expression shut down. Alternative temperature shifts were not considered due to previous work undertaken with Des.

In cold shocked cells, foci appear to move towards the periphery of the cell for all timepoints, before expression shut down (recovery) then showed foci to return to the nucleoid interior (Figure 4.3). Foci across each time point immediately show that time of cold shock is not a factor in overall foci population shifts towards the membrane (Figure 4.4). Initial time point 0, before 15°C (induction) incubation, showed a median of 25 NDM, whereas upon 5 minute of cold shock induction increases by 23-points to a median of 48 NDM. This substantial shift up was replicated upon 15 minutes of cold shock, whereby the median value at 49 NDM. There was no relevant change between time points of cold shock. Increasing the time of incubation further had no effect on foci shift towards the membrane, at a median of 49 NDM for 30-minute incubation at 15°C. Strikingly, upon returning cells to 30°C for 30 minutes, the foci median dropped down by 22-point to a value of 27 NDM. Comparison between time point 0, where no cold shock had occurred yet, and recovery shows negligible difference, demonstrating loss of expression shifts foci back into the nucleoid interior.

The shift of population towards the membrane matches with the transertion hypothesis. Time of induction played no factor in the population shift, which could indicate that cold shock is responsible for a shift, not maintaining exposure to 15°C. DesK recognises the shock via temperature downshift, thus activating DesR, which actives Des expression. Altering the time that DesK is detecting membrane thickness has no effect on furthering expression of Des. Keeping the cells at the lowered temperature resulted in *des* staying located towards the membrane, suggesting expression was still occurring after the initial temperature shock. Alternative efforts to move away from the Des promoter are ongoing, which could further confirm the kinetics of gene foci movement without interference from temperature.

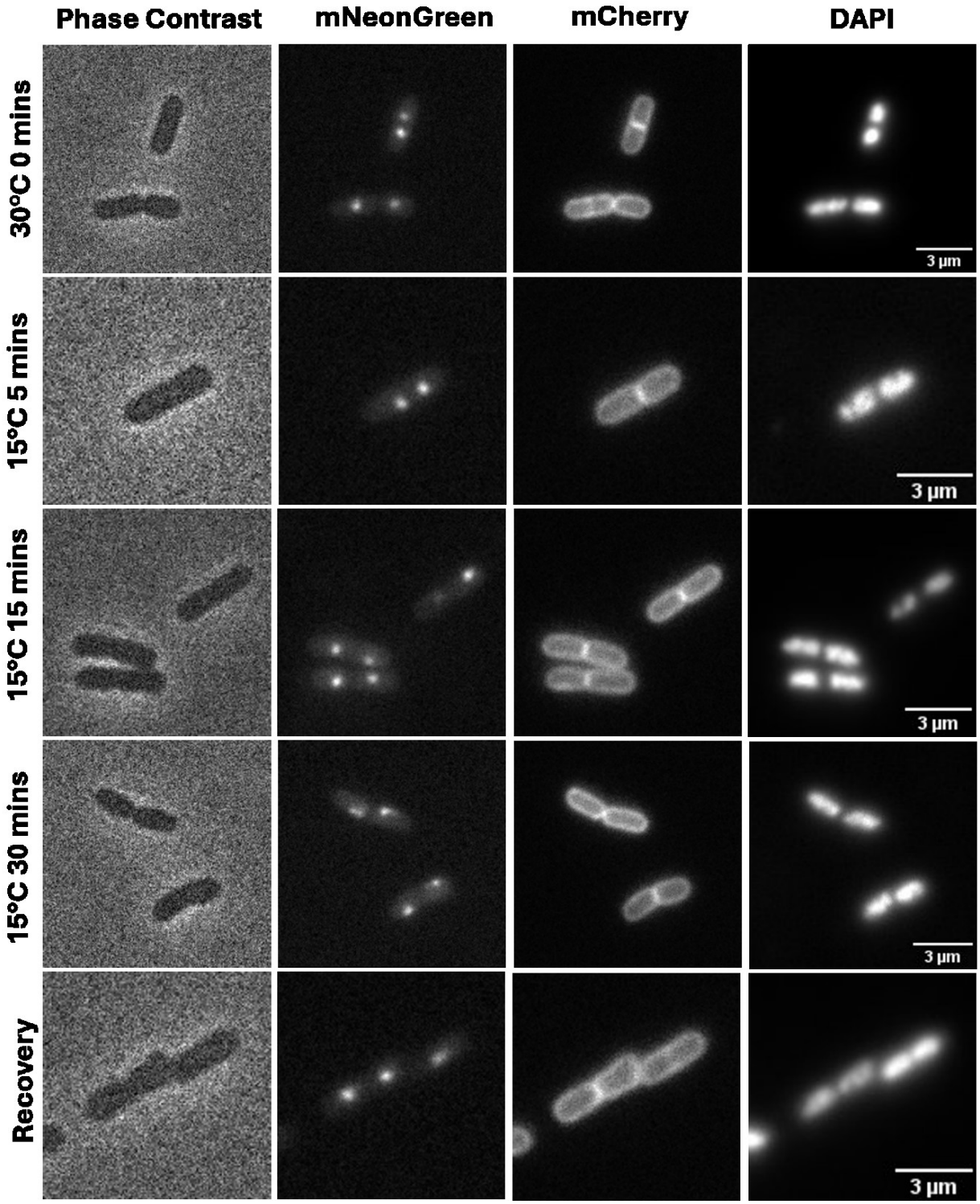

Figure 4.3: Effect of induction at different time points before returning to 30°C. A.) *Phase contrast and fluorescent images of B. subtilis cells with des lacO4 array. Cells constitutively express WALP23-mCherryy and lacI-mNG. Cells were grown at 30°C to* OD_{600} *0.3. Induction by cold shock carried out at 15°C for the respective time as indicated above. Microscope kept at room temperature, samples were transported and kept at 15°C for as long as possible. Scale bar 3µm.* ***B.)*** *Quantification of field of views taken of cells. Distance was represented as percentage value towards membrane, with 0% representing the cell midpoint and 100% representing membrane peak intensity. Red line shows median. Strains: BJN17 (lacO4, lacI-mNG).*

Returning cells to 30°C results in loss of Des expression as determined by return of foci towards cell centre. Returning cells to 30°C results in membrane fluidity and thickness changing back, whereby DesK is no longer sensing the change in thickness. Thus, DesR is not phosphorylated, not binding upstream of *des* promoter and not promoting RNAP binding. As no transcription is occurring, no transertion can occur, thus gene loci shift to nucleoid interior.

Foci positioning within the cell at the moment cannot be accurately determined either at the membrane or at the nucleoid periphery. Evidence of membrane tethering by DNA would help indicate what foci at membrane would look like. To test this, a positive control using *lac* array tools that acts to show membrane tethering was created. This was created utilising P16.7, a non-native to *B. subtilis* membrane protein with an N-terminal transmembrane domain (Serna-Rico et al., 2002). *P16.7-GFP* fusion in *B. subtilis* produces an even fluorescent membrane akin to membrane stains.

The gene of *P16.7* was inserted into the plasmid pJN200, as a fusion to the C-terminal domain of *lacI-mNG,* to form *P16*.7-*lacI-mNG.* This plasmid was transformed into *B. subtilis* to integrate at the *amyE* locus. Fluorescent imaging of *P16*.7-*lacI-mNG* expressed in *B. subtilis* (BJN046) is shown in figure 4.5. Another strain was constructed where *P16*.7-*lacI-mNG* was expressed with *lacO4* present at *des* locus (BJN045), also shown in figure 4.5, where multiple foci are seen. A strain lacking the *lacI* but retaining *P16.7-GFP* and *lacO4* was also constructed (BJN43) and imaged. This strain no longer presenting foci but a smooth membrane stain. Foci formed only in the presence of *lacO4* and *lacI*. Additionally, foci were observed to be localised to the membrane, demonstrating that *des* locus was mobile and could tether to the membrane.

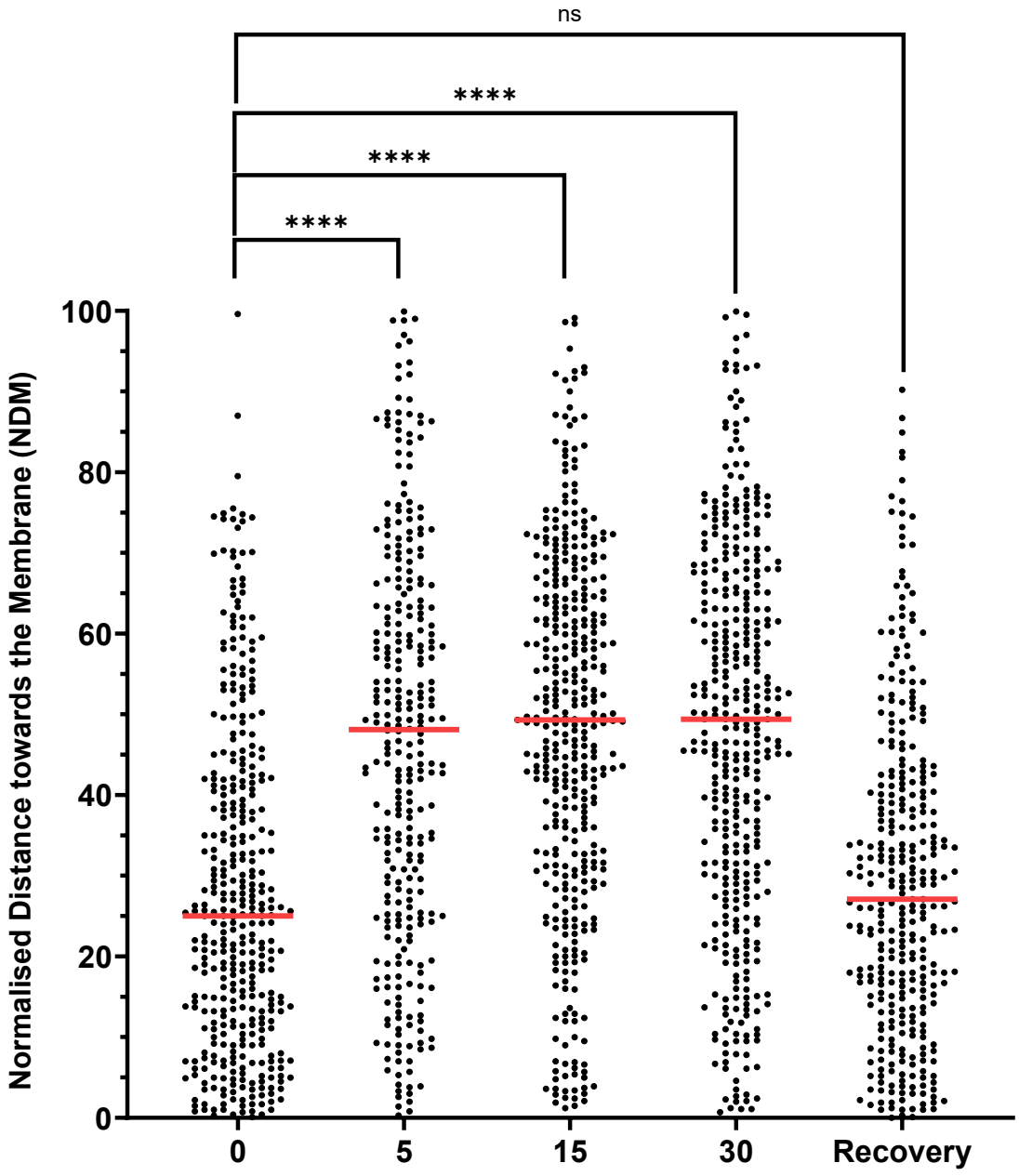

Figure 4.4: Scatter plots showing effect of induction by cold shock at varying time points and return to 30°C. *Quantification of foci positioning from cells. Cells were incubated at 15°C for the respective time as indicated above. Recovery marks expression shut down, achieved by 15°C for 30 minutes before then returning to 30ºC for further 30 minutes Distance was represented Normalised Distance to the Membrane (NDM), where normalised foci position is placed from midcell (0) to membrane (100). Red line shows median of NDM. Strains: BJN17 (lacO4, lacI-mNG).*

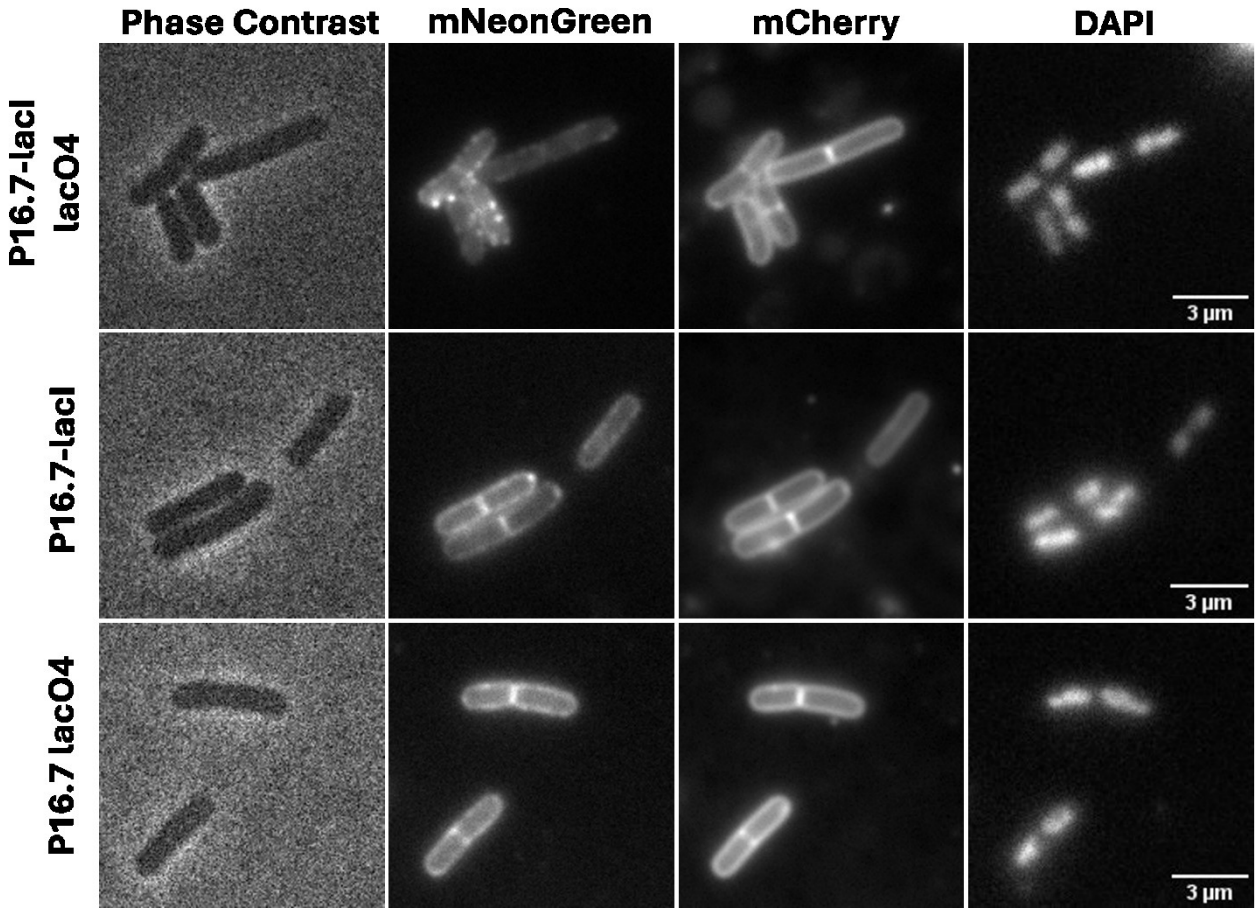

Figure 4.5: Positioning of at membrane positive control p16.7-lacI *Phase contrast and fluorescent images of different B. subtilis strains. Cells were expressing P16.7-lacI-mNG or P16.7-GFP and WALP23-mCherry. Cells were grown at 30°C to OD_{600} 0.3 and treated with DAPI. Scale bar 3µm. Strains: BJN45 (lacO4, P16.7-lacI-mNG), BJN046 (P16.7-lacI-mNG), BJN043 (lacO48, P16.7-msfGFP).*

4.3 Discussion

The development of the short *lacO4* array in chapter 3 has allowed the in-depth investigation on cellular localisation of a gene upon induction. The first experiments were repetitions of previous work carried out with *lacO48* to observe the arrays positioning within the cell. Notably examining the effect of both chloramphenicol and rifampicin upon the shorter array before the observation of gene shifting. As before for *lacO48*, *lacO4* array was tested with chloramphenicol. The longer array showed negligible difference between untreated, and chloramphenicol treated, though both data sets were diffusely spread throughout the cell, perhaps owing to the exclusion by size. *lacO4* untreated and chloramphenicol treated are also of no notable difference, however this time it can be proposed that this is due to the *lacO4* remaining in the nucleoid interior, as foci for both remain close to the midcell and 20 NDM. Rifampicin treatment for *lacO4* arrays showed a substantial increase, which, as

suggested above, might be the loss of nucleoid structure by rifampicin, thus homogeneously mixing foci throughout the cell. When compared to *lacO48* from chapter 3, *lacO4* analysis is consistent with the notion of lacO48 shifting towards the membrane and out of the nucleoid interior. Indeed, induction is now observed to result in a shift of *lacO4* based foci towards the cell periphery. Of importance, this approach does not possess the resolution currently to be able to determine whether foci shift to the nucleoid edge or to the membrane, an important point to distinguish if transertion is to be observed. Exact positioning of foci in regard to nucleoid or the membrane needs to be determined, which will be touched on in chapter 5 with use of a high-resolution microscopy option.

It should be noted, as mentioned above, that whilst foci shifting is seemingly abolished by both rifampicin and chloramphenicol treatment, that this alone does not support the determination of transertion. This is due to the significant pleiotropic effects on cell function found by both antibiotics. Chloramphenicol treatment will affect a majority of ribosomal function within the cell, thus also pausing other regulatory gene expression for adaptation to cold shock and heavily disrupting various control mechanisms throughout the cell. Additionally, this applies to rifampicin, which will disrupt RNAP and transcription. Various genes expressed under cold shock are required to stabilise translation, thus potentially having hidden effects in these experiments. Going forward, whilst antibiotics can provide useful control experiments, a more direct disruptor of both transcription and translation of *des* will be required, such as *des* specific mutations. In particular, deletion of the *des* promoter or the deletion of the DesR binding site upstream of the promotor would specifically inhibit transcription of *des*. Site directed mutagenesis of the ATG start codon of *des* would directly inhibit the translation of only *des.*

Upon induction by cold shock, the observation of foci repositioning towards the periphery of the cell can be seen. Regardless of the length of cold shock, induction occurs as quickly as 5 minutes, with further incubation having no effect on foci movement. This can be seen as the cell responding to the initial cold shock, responding by expressing Des into the membrane to alter the fluidity (Weber et al., 2001b). DesK can sense and signal for Des expression as quickly as 5 minutes. Longer 30-minute incubation at 15°C results in no change of gene locus location. Thus, DesK might still be signalling for Des expression, or current Des expression at the membrane due to transertion is still being carried out, with the feedback loop not

yet stopping Des expression. It is important to note this is likely due to cold temperatures affecting cell process rates. Upon returning cells to 30°C, Des transertion into the membrane would no longer be required by the cell, as DesK will no longer sense the thickness change. Thus, DesR phosphorylation does not occur, DesR binding upstream of promoter does not occur and RNAP binding to the *des* promoter does not occur. Loss of transcription would prevent transertion or coupled transcription translation, thus movement of the gene back to the nucleoid interior is observed. This observation however does not confirm that it is transertion that is responsible for movement nor that the foci seen are directly in the membrane. Alternatively, Des when expressed, could be repositioned to the nucleoid surface. Additionally, although not considered for this work, different temperature shifts could be considered as alternatives to 30°C to 15°C, such as 37°C to 22°C.

Whilst induction does affect cellular localisation of *des,* the question must also be asked for other genes, whether encoding for other integral membrane proteins or for cytoplasmic based genes. To test this, the goal was to observe alternate genes with a system to also observe different chromosome loci and controlled under another inducible promoter. Addition plasmids with *lacO4*, xylose inducible promoter and a multiple cloning site to rapidly confirm various gene loci (pJN100) have also been tested. This work is currently ongoing. Various mutants of the *des* operon, such as *desK* with no transmembrane domains, have shown to stay in the kinase form, keeping DesR in its phosphorylated state and therefore upregulating *des* expression.

Finally, is should be noted that current experimental method with horizontal cells offers disadvantages to our aims. Notably the lack of resolution to reveal exact gene loci positioning and the cell geometry. On cell geometry, the cylindric cells in our current orientation are problematic. Foci moving in the Z-axis towards the membrane could be miss-represented as foci in the nucleoid interior, foci at the membrane cannot be accurately determined due to the membrane curvature and foci moving to the poles or septum can create difficulties. To this end, in chapter 5, the technique of VerCINI will be used. This technique offers high resolution and foci moving in the Z-axis not affecting location. Thus, VerCINI will make a valuable addition to analysis, with the downside of lower cell counts for analysis.

Chapter 5: Analysis of transertion using vertical cell imaging by nanostructured immobilization (VerCINI)

5.1 Introduction

As initial observations had shown movement of foci upon induction, I explored further whether the gene locus shifts to the nucleoid edge or to the membrane, and by what molecular mechanism is found responsible for the repositioning of genes. To this end, the choice was also made to utilise a recently developed method of imaging cells vertically: VerCINI (Whitley et al., 2022).

Vertical cell imaging by nanostructured immobilisation (VerCINI) is a novel technique allowing observation of cells under the microscope down the long axis of the cell, from pole to pole. Previous work on *B. subtilis* with FtsZ and MreB dynamics utilised this technique to great benefit (Whitley et al., 2021;Middlemiss et al., 2024). Utilising vertical cells for observations offers several benefits. As foci previously moved from the cell centre outwards, imaging along the long axis of the cell would provide better resolution for foci positioning. Additionally, VerCINI ignores cell geometry issues stated previously in chapter 4, where foci measurement towards the membrane is minimally impacted by foci positioning in the Z-plane. To our knowledge, VerCINI has not previously been used for gene loci positioning or to observe transertion directly.

Chloramphenicol inhibits protein chain elongation in ribosomes in bacteria. When the *E. coli* nucleoid treated with chloramphenicol is analysed, the genome is condensed and crucially, in terms of transertion, is no longer linked to the membrane (Spahn et al., 2023). Such experiments suggest the existence of transertion in *E. coli*; therefore, it can be hypothesized that in *B. subtilis,* where chloramphenicol has the same nucleoid condensing effect, transertion can exist (Matsumoto et al., 2015). However, as chloramphenicol inhibits all ribosomes within the cell, it cannot be claimed that observed foci positioning is due to the inhibition of translation of only the Des protein. This logic holds true for rifampicin as well for transcription.

Use of point mutations and deletions at *des* would allow direct testing specifically for transcription or translation for only Des. Thus, helping distinguish coupled transcription-translation (CTT) dependent recruitment to the nucleoid surface from transertion dependent recruitment to the membrane. VerCINI helps through the higher resolution possible regarding the membrane.

The aim of this chapter is to further investigate *des* gene movement by using VerCINI techniques with *lacO4* array developed and analysed in chapters 3 and 4. This chapter will optimise VerCINI for imaging gene loci positioning and fluorescent imaging, induction of foci in vertical cells, whether coupling of transcription and translation are directly involved in foci induction dependent shift observed in chapter 4. *Des* start codon mutation distinguishes transcription dependent movement from transcription-translation couple dependent movement. Such a mutation shows that transcription isn't enough for a shift, where at least CTT is required for a foci shift to the nucleoid periphery and transertion for a foci shift to the membrane.

5.2 Results

5.2.1 Use of VerCINI in foci movement tracking

To provide better imaging of foci movement tracking I used vertical cell imaging with VerCINI. Foci in VerCINI would have increased resolution and when measured, are mostly unaffected by cell geometry. To observe foci using this technique, cells were loaded into an agarose micro-hole pad (Figure 5.1A) as described in chapter 2.3.3. Cells immobilised by this method were imaged using fluorescent microscopy (Figure 5.1B). Initial microscopy observed high background fluorescence, to which highly inclined and laminated optical sheet microscopy (HiLO) was utilised to help. HiLO yields a higher signal/background intensity ratio by inclining the laser from a total internal reflection, thus penetrating the sample at an angle in a thin optical sheet (Tokunaga et al., 2008b).

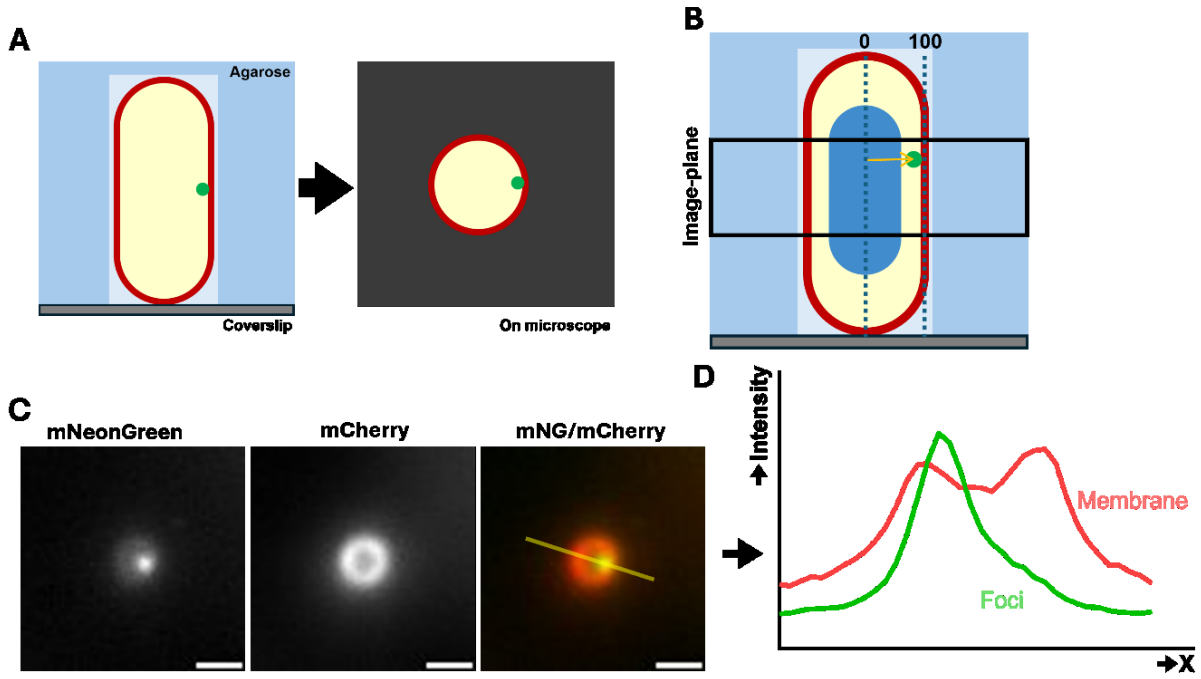

Figure 5.1: VerCINI setup to observe and analyse foci positioning A.) Representation of cell setup vertically in VerCINI. ***B.)*** Cartoon representation of focal imaging plane for VerCINI, where 0 is the midcell and 100 is the membrane, demonstrating the straight membrane edge and geometric advantages over horizontal orientated cells. ***C.)*** *Representative single cells of B. subtilis cells constitutively expressing lacI-mNG and WALP23-mCherry. lacO4 arrays located at Pdes. Yellow line represents measurement line to plot profile of line scan in D.)* ***D.)*** *Plot of fluorescent intensity line scan comparing membrane stain with lacI-mNG signal from foci from C.). Quantification of foci is achieved using at this plot. Cells imaged with HiLO fluorescence microscopy. Scale bar 1µm. Strain: BJN17 (lacO4, lacI-mNG, WALP23-mCherry).*

Cells imaged via HiLO fluorescent microscopy (Figure 5.1C) were then used for quantification of foci positioning. Initial quantification was achieved using manual measurement of difference between foci centre and membrane intensity peaks, which represent the accurate positioning of the membrane plane in VerCINI unlike for horizontal cells (Figure 5.1D). Automated macro quantification was developed from the framework of the horizontal cell macro, as described (2.3.6). VerCINI allowed for a streamlined macro, whereby segmentation by Ilastik was no longer required, as vertically immobilised cells are already segregated based on micro-hole agarose (Figure 5.1B). Observation in a specific plane meant only one foci or no foci per cell were observed, meaning gene location within the genome and DNA replication were no longer factors to consider, as mentioned in chapter 4.

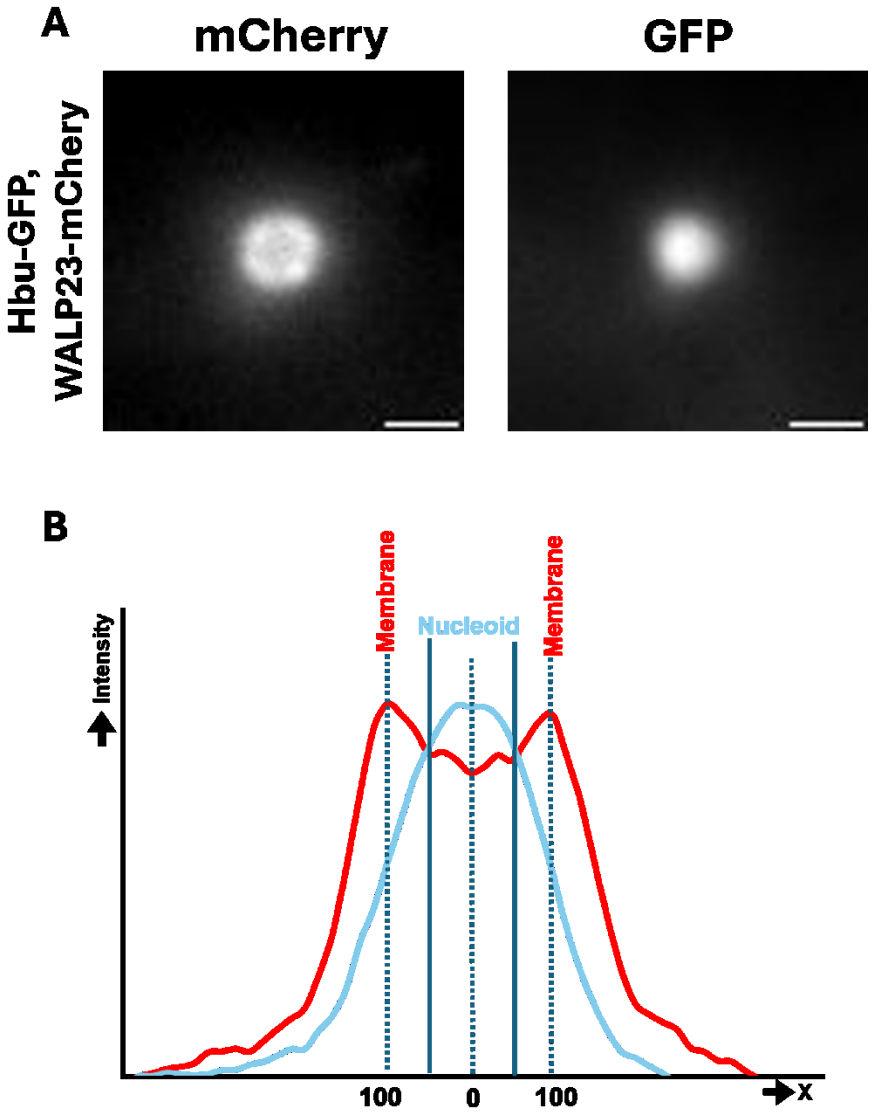

Figure 5.2: Hbs-GFP VerCINI images to determine volume of nucleoid in the cell. A.) *HiLO fluorescent images of individual B. subtilis cells. Cells were constitutively expressing Hbs-GFP and WALP23-mCherry. Cells were grown at 30°C to OD_{600} 0.3, before undergoing VerCINI prep as per 2.3.5. Scale bar 1µm.* ***B.)*** *Line scan of fluorescent intensity of both Hbs-GFP nucleoid signal and WALP23-mCherry membrane signal. 100 represents membrane peak and 0 represents cell midline. Solid lines represent area nucleoid represents between membrane peaks. Nucleoid volume of cell was normalised for distance to the membrane, where 25 cells mean average gave a NDM value of ~60. Strains: BJN047 (Hbs-GFP, WALP23-mCherry)*

Additionally, DAPI staining was no longer possible for use with HiLO and VerCINI, as the correct laser wavelength for DAPI was not present. Due to this an alternative solution was sought. The solution was utilising nucleoid associated protein Hbs fused with GFP or mCherry, which imaged as a uniform nucleoid stain. Hbs-GFP clashed with the current strain, where use of red and green lasers by WALP23-mCherry and lacI-mNG respectively. Therefore, Hbs-GFP and lacI-mNG could not be

simultaneously imaged in the same strain. To establish where the nucleoid is positioned a strain with Hbs-GFP and WALP23-mCherry was used (Figure 5.2A). From images of the strain, the fluorescent intensity line scan of membrane and nucleoid were compared (Figure 5.2B). This allowed determination of nucleoid volume of the cell, whereby on a scale of normalised distance to the membrane (100) from the cell midpoint (0), the nucleoid was observed from 0 to ~60. Membrane fluorescence in VerCINI as determined to be at 100. Inaccuracy of the membrane, as highlighted and described in Figure 5.3, determines that ~80 to 100 of normalised distance towards the membrane can be said to be at the membrane.

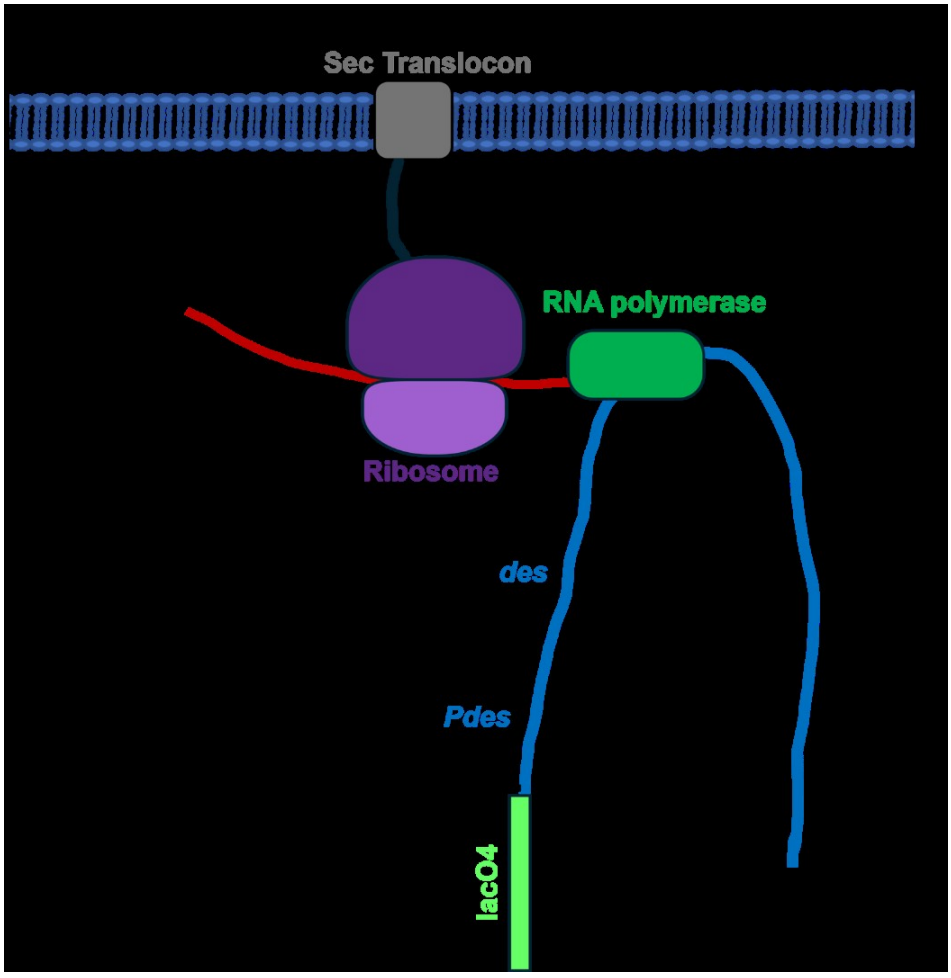

Figure 5.3: Cartoon representation of lacO4 array distance to the actual site of transertion. *In this experimental design, foci are formed from lacI-mNG binding to the lacO4 array (Green). Foci cannot represent the exact location of transcription, translation, and insertion. lacO4 is located upstream of des promoter, which is upstream of des gene, therefore unable to be at the location of RNAP and the expresome. The distance from array to membrane can alter depending on DNA folding, angle, and distance through transcription. At the end of transcription of des, the array could potentially be as far away as ~30% of the cell.*

5.2.2 des foci position dramatically shifts upon induction.

Utilising VerCINI with novel *the lacO4* array meant that it was possible to determine the exact positioning of the *des* gene loci within the cells. Movement from nucleoid interior outwards had been previously visualised in chapter 4, although limitations on the quantification due to cell geometry and resolution emerged. To test this utilising VerCINI, strain with *lacO4* at *des* promoter with *lacI-mNG* was grown at 30°C before being transferred into micro-hole agarose pads (2.3.5). Cells on microscope slide were incubated at 15°C or 30°C for 15 minutes and imaged with HiLO fluorescent microscopy (Figure 5.4A).

Acquired images were analysed by automated macro quantification, whereby they visualised by plotting onto a scatter graph (Figure 5.4B). At 30°C, foci within cells average localisation pattern spread around the cell midline, with a median value of 50 NDM. This is exclusion from the midline where foci are positioned halfway from the midline to the membrane. Foci when compared to flatpad horizontal cells at 30°C (Figure 4.2B), appear further out from the midcell, as expected from elimination of cell geometry issues by VerCINI. Throughout all plots, foci are rarely found from values 0 NDM to 10 NDM. As discussed, the nucleoid extends to ~60 NDM which means a majority of foci are found to be in the fraction occupied by the nucleoid. Induction by cold shock at 15°C for 15 minutes resulted in foci being preferentially located towards the membrane. Incubation of cells at 15°C resulted in a median of 74 NDM, a 24-point increase from the median of 30°C cells. By the median, 50% of foci are located above 74 NDM median. The membrane fraction of NDM is between ~80 NDM and 100 NDM. Therefore, it can be said that a majority of foci are outside of the nucleoid and shifted to the membrane. The above shows that induced foci are not located in the nucleoid interior and shift towards the membrane. It should be noted that the *lacO4* array is not an exact representative of *des* locus location, with it being only in close proximity to it. Indeed, the array can never be directly at the membrane (Figure 5.3). This is consistent with tethering of DNA to the membrane, not being directly at it. Additionally, upon returning cells from 15°C to 30°C for 15 minutes, thus shutting down expression (Recovery), the foci median position shifted back down to 51 NDM, a 23-point decrease from induction. The above confirms observations made previously in chapter 4 that suggests that inducing *des* shifts the gene locus towards the cell membrane. In vertical cells, the NDM shift difference of magnitude between 30°C, 15°C and recovery of shift is similar to before in horizontal cells.

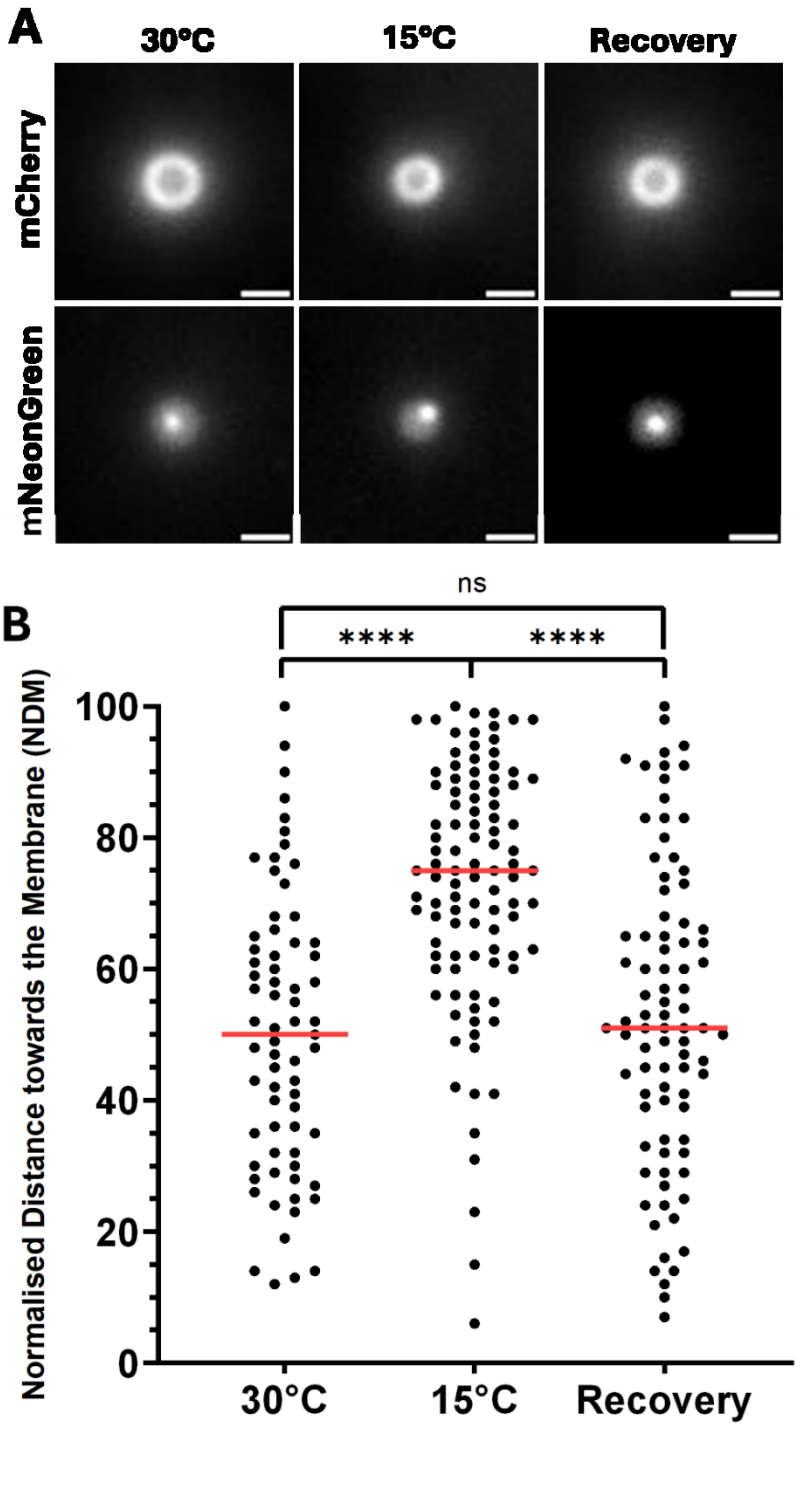

Figure 5.4: Expression dependent localisation of des loci positioning A.) *HiLO fluorescent images of individual B. subtilis cells with lacO4 array. Cells were constitutively expressing lacI-mNG and WALP23-mCherry. Cells were grown at 30°C to OD_{600} 0.3, before undergoing VerCINI prep as per 2.3.5. Cells were induced for 15 minutes at 15°C in slides. Scale bar 1µm.* ***B.)*** *Quantification of field of views taken of cells. Distance was represented as percentage value towards membrane, with 0% representing the cell midpoint and 100% representing membrane peak intensity. Red line shows median. BJN17 (lacO4, lacI-mNG, WALP23-mCherry).*

5.2.3 Chloramphenicol abolishes foci shift to the membrane.

To further characterize foci repositioning and the potential role of transertion, vertical cells were treated with chloramphenicol. Previous treatment with chloramphenicol showed foci positioning within cell volume occupied by nucleoid at 30°C, thus in absence of gene induction. Chloramphenicol was shown to have no effect on the positioning of foci within the cell, however, previous work with chloramphenicol was not carried out in inducing conditions (15°C). As induction shown in absence of chloramphenicol a substantial shift towards the membrane, and that goes beyond the nucleoid surface the movement argues for transertion. Transertion requires multiple processes working in tandem to work, notably translation by the ribosome. Inhibition of the ribosome by chloramphenicol would disrupt cell wide translation as well as any transertion interactions occurring within the cell. To test this hypothesis, *B. subtilis* cells were grown at 30°C and incubated with chloramphenicol. Cells were then immobilised in VerCINI micro-holes and then incubated at 15°C (induced) or 30°C (uninduced) for 15 minutes on the slide, before imaging. Foci and membrane stain were observed (Figure 5.5A).

Quantification of foci distribution in vertical cells were represented on a scatter plot (Figure 5.5B). Foci at 30°C when treated with chloramphenicol were evenly distributed throughout the cell, with a median of 48 NDM. Compared to previous work at 30°C in VerCINI (Figure 5.4B), this is a negligible decrease. Upon induction of *des* at 15°C, another negligible shift is observed to a median of 54 NDM. Previous work in absence of chloramphenicol showed a substantial shift (Figure 5.4B) where a shift towards the membrane was observed, by 26-points. It could be determined that inhibition of translation blocks the foci shift seen previously, heavily implying the requirement of translation in the mechanism of foci shifts away from the nucleoid interior towards the membrane.

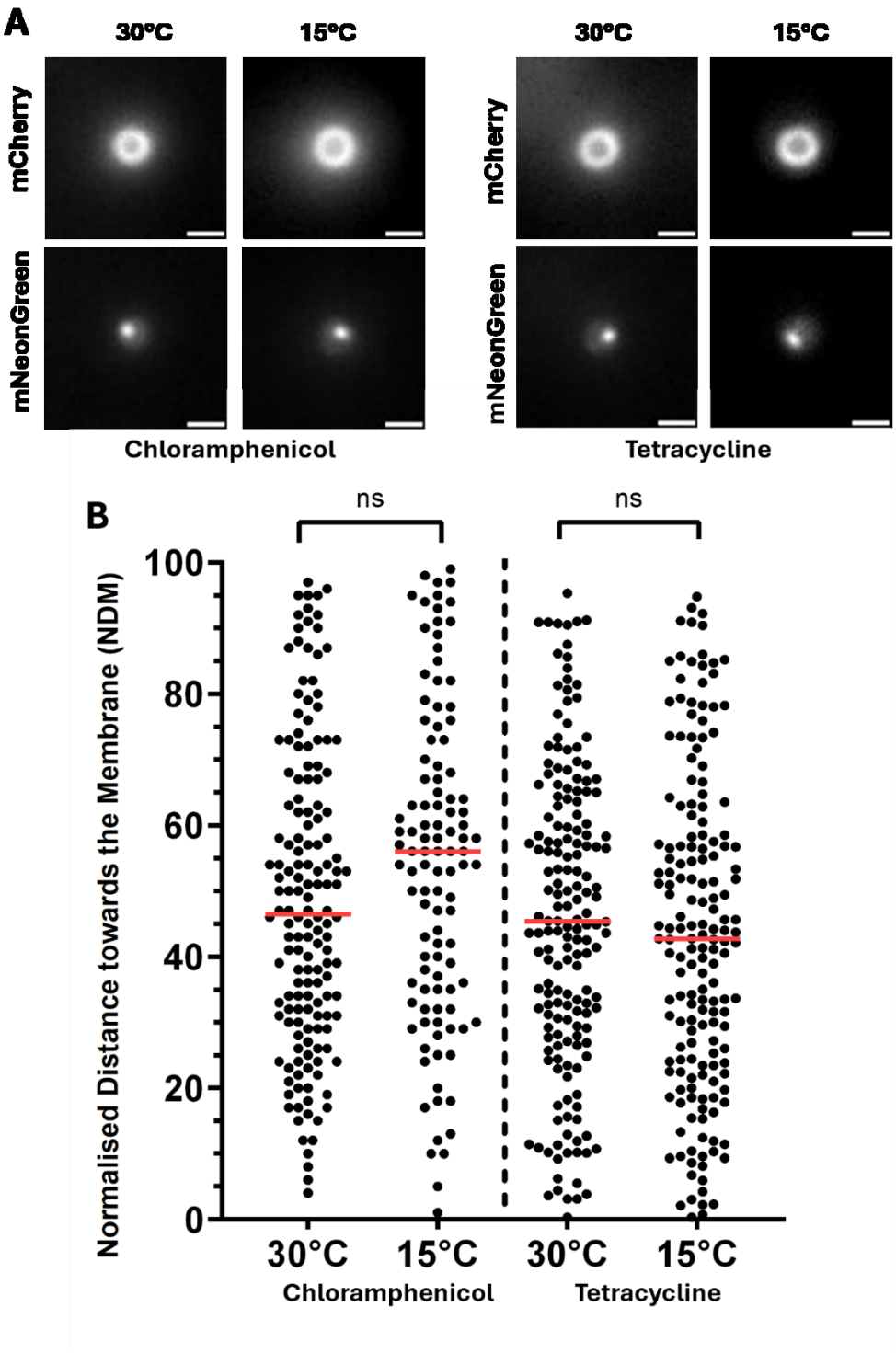

Figure 5.5: Effect of chloramphenicol and tetracycline on des locus positioning in vertical cells A.) *Phase contrast and HiLO fluorescent images of B. subtilis with lacO4 array. Cells were constitutively expressing lacI-mNG and WALP23-mCherry. Cells were grown at 30°C to OD_{600} 0.3, then incubated with 25µg/ml Tetracycline or 100µg/ml Chloramphenicol before undergoing VerCINI prep as per 2.3.5. Cells were induced at 15°C for 15 minutes on slide. Scale bar 1µm.* ***B.)*** *Quantification of field of views taken of cells. Distance was represented as percentage value towards membrane, with 0% representing the cell midpoint and 100% representing membrane peak intensity. Red line shows median. BJN17 (lacO4, lacI-mNG, WALP23-mCherry).*

To confirm that translation inhibits foci shift and not due to an off target of chloramphenicol, another antibiotic that inhibits translation was used as a control: tetracycline. Tetracycline's mechanism of action is by binding the 30S ribosome and blocking aminoacyl-tRNA binding to the complex (Chopra & Roberts, 2001;Chukwudi, 2016). Also, as with chloramphenicol, tetracycline also condenses the nucleoid morphology (Chai et al., 2014). To test this, tetracycline was used in the same experiment as described above, where cells were treated with tetracycline before incubation at 30°C and 15°C. Cells were imaged with HiLO fluorescent microscopy (Figure 5.5A) and analysed by macro, with data plotted on a scatter plot (Figure 5.5B).

At 30°C for tetracycline treated cells, foci are found located throughout the cell with a median of 45 NDM. This matches previous data collected at 30°C with treatment with chloramphenicol. At 15°C, foci do not substantially shift, decreasing to 43 NDM. Tetracycline treated cell foci at both 30°C and 15°C do not shift in any direction, suggesting further that translation in essential for gene movement towards the membrane.

If translation is indeed involved in gene induction dependant gene locus movements, then does inhibiting translation after induction have an effect on gene locus location? In this question, foci already moved towards the membrane in cells are then subjected to inhibition of translation by chloramphenicol. In a transertion event, prevention of translation would result in loss of insertion into the membrane. However, the question should be asked as to whether loss of translation after the start of peptide insertion into membrane would result in either loss of gene loci localisation at the membrane or would foci remain trapped at the membrane. Additionally, if the gene locus is indeed trapped at the membrane, would shutting down expression (recovery) bring foci back to the nucleoid interior. To test this, cells were grown at 30°C and incubated further at either 15°C or 30°C for 15 minutes. Cells were then immobilised vertically in micro-holes in agarose containing chloramphenicol. Immobilised cells were kept at their respective temperatures before imaging via HiLO fluorescent microscopy (Figure 5.6A). Recovery cells were treated with chloramphenicol after 15°C cold shock and then allowed to recover at 30°C for 15 minutes. Foci were then quantified by macro for data point which are represented below in scatter plots (Figure 5.6B).

Foci at 30°C had a median of 51 NDM, similar to untreated cells in figure 5.4B. Inducing cells at 15°C for 15 minutes then treating with chloramphenicol resulted in a median increase by 20-points to 71 NDM. The increase is substantial, similar to what is seen before in untreated cells at 15°C (Figure 5.4B). Recovery from 15°C to 30°C alternatively showed a decrease in percentage value towards the membrane, decreasing by a smaller 10-points. Recovery had a median value of 61 NDM, a less substantial shift from 15°C than seen previously (Figure 5.4B). The difference between 30°C to recovery is small but mostly negligible.

Such a shift from 30°C to 15°C matches the untreated pattern (Figure 5.4B), supporting the notion that foci remain at the membrane even when translation is inhibited.

Shutting off expression (recovery) from 15°C results in a decrease of normalised distance towards the membrane, where foci shift towards the midcell (0). The degree to which this recovery occurs is less than previously seen in cells untreated by chloramphenicol, by ~10-points. Partial recovery in this case implies that inhibition of translation does not affect *des* locus shift back towards the cell centre.

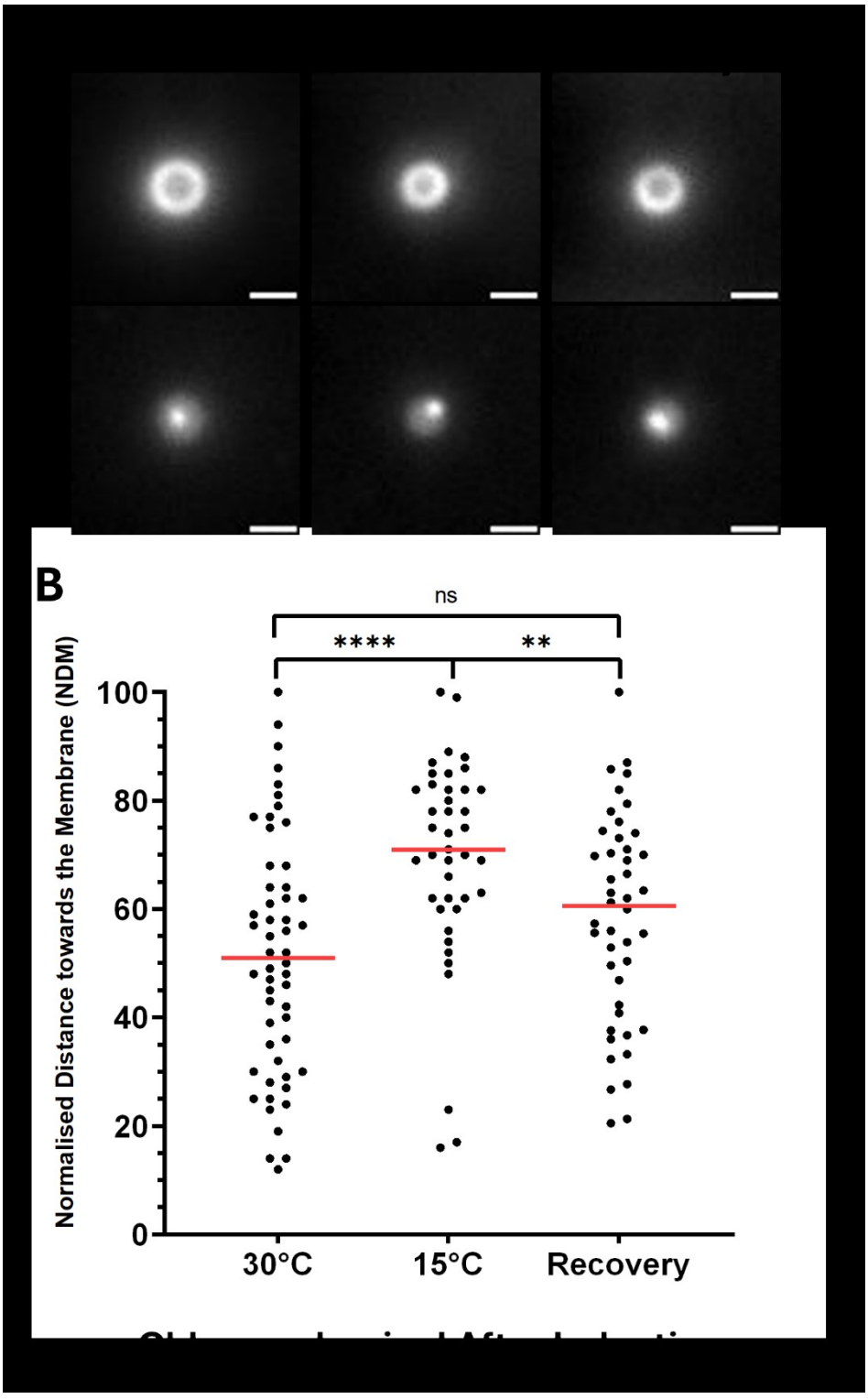

Figure 5.6: Treatment with chloramphenicol after induction A.) *Phase contrast and HiLO fluorescent images of B. subtilis with lacO4 array. Cells were constitutively expressing lacI-mNG and WALP23-mCherry. Cells were grown at 30°C to* OD_{600} *0.3, undergoing induction for 15 minutes at 15°C, before undergoing VerCINI prep as per 2.3.5, maintained at 15°C. Chloramphenicol was added to agarose in slide at 100µg/ml. Scale bar 1µm.* ***B.)*** *Quantification of field of views taken of cells. Distance was represented as percentage value towards membrane, with 0% representing the cell midpoint and 100% representing membrane peak intensity. Red line shows median. BJN17 (lacO4, lacI-mNG, WALP23-mCherry).*

5.2.4 Rifampicin abolishes foci shift to membrane

Transertion is also affected by transcription, where RNAP transcribing the gene produces mRNA which is linked to translation and insertion. By inhibiting transcription, both translation and insertion are no longer functional in the cell either, including transertion theoretically. Previous work with rifampicin was done to inhibit transcription and for experiments related to decondensing the nucleoid.

Previously rifampicin was used for decondensation of the nucleoid to analyse lac array localisation. Rifampicin is now used to observe if transcription is necessary for foci movement. Cells were grown at 30°C before incubation with rifampicin, immobilised in vertical micro-holes and induced at 15°C or kept at 30°C for 15 minutes. Foci were then imaged by HiLO fluorescent microscopy to observe membrane and foci (Figure 5.7A). Foci location was quantified by macro and represented on scatter plots (Figure 5.7B).

Cells treated with rifampicin at 30°C had foci at a median value of 62 NDM, an increase of 11-poinst from cells not treated with rifampicin also at 30°C. Lower median value in untreated cells is consistent with loci confined within the nucleoid interior, where with rifampicin the foci are more disperse after nucleoid decondensation, as expected. Induced cells at 15°C had a median of 61 NDM, showing no meaningful difference between rifampicin treated cells at 30°C and 15°C. Therefore, transcription inhibition results in loss of foci shift generation, thus transcription is required. Transcription inhibition also would inhibit ribosomal activity, by loss of mRNA transcript product, which has already been shown to be responsible for foci migration.

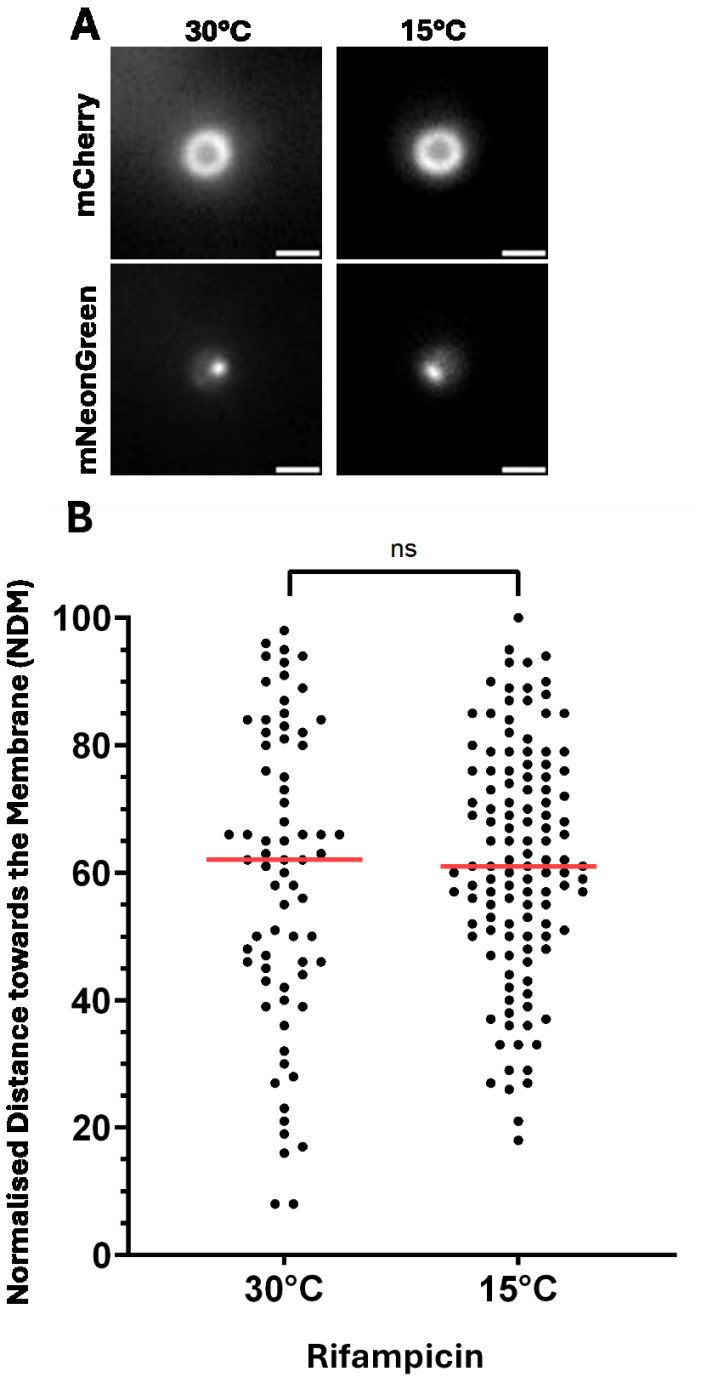

Figure 5.7: Effect of rifampicin on des locus positioning in vertical cells A.) *Phase contrast and HiLO fluorescent images of B. subtilis with lacO4 array. Cells were grown at 30°C to OD_{600} 0.3, then incubated with 100µg/ml Rifampicin before undergoing VerCINI prep as per 2.3.5. Cells were induced at 15°C for 15 minutes on slide. Scale bar 1µm* ***B.)*** *Quantification of field of views taken of cells. Distance was represented as percentage value towards membrane, with 0% representing the cell midpoint and 100% representing membrane peak intensity. Red line shows median. Strains: BJN17 (lacO4, lacI-mNG, WALP23-mCherry).*

5.2.5 Cold shock but not steady state growth in cold results in peripheral des localisation

Des expression is signalled by sudden temperature drops, as it is sensed by DesK in the membrane. DesK senses membrane fluidity through thickness, which changes upon cold shock conditions (Cybulski et al., 2004). Thus, Des expression can only be induced from cold shock conditions. Cells can grow in lower temperatures, although at a significantly reduced rate. Cells grown steadily at 15°C are not subjected to sudden drops in temperature and Des expression to alter the membrane is not required. To confirm the observations of induced gene loci shifts to the membrane are indeed triggered by Des expression and not by other effects at colder temperatures unrelated to Des induction, cells were grown at 15°C. Upon reaching OD_{600} 0.3, cells were kept at 15°C whilst immobilised in vertical agarose micro-holes before imaging (Figure 5.8A). Foci were then quantified and represented in scatter plots (Figure 5.8B). A parallel control of cells grown at 30°C was also carried out following the same procedure.

The population of foci at 30°C, as previously seen, were spread throughout the cell, with a median of 50 NDM. Foci did not appear towards the lower 10% of the normalised distance towards the membrane. In comparison, foci population at 15°C showed a median of 45 NDM. Foci not shifting in cells adapted to cell growth at 15°C confirms that temperature alone is not responsible for the *des* locus shift upon incubation in the colder temperature. Instead, cold shock, and specifically the cold shock induction on Des expression is responsible for initiation of foci shifting. The only time *des* is induced during 15°C growth should be upon inoculation of cells from 30°C overnight cultures into 15°C in fresh medium, immediately rescuing the cytoplasmic membrane.

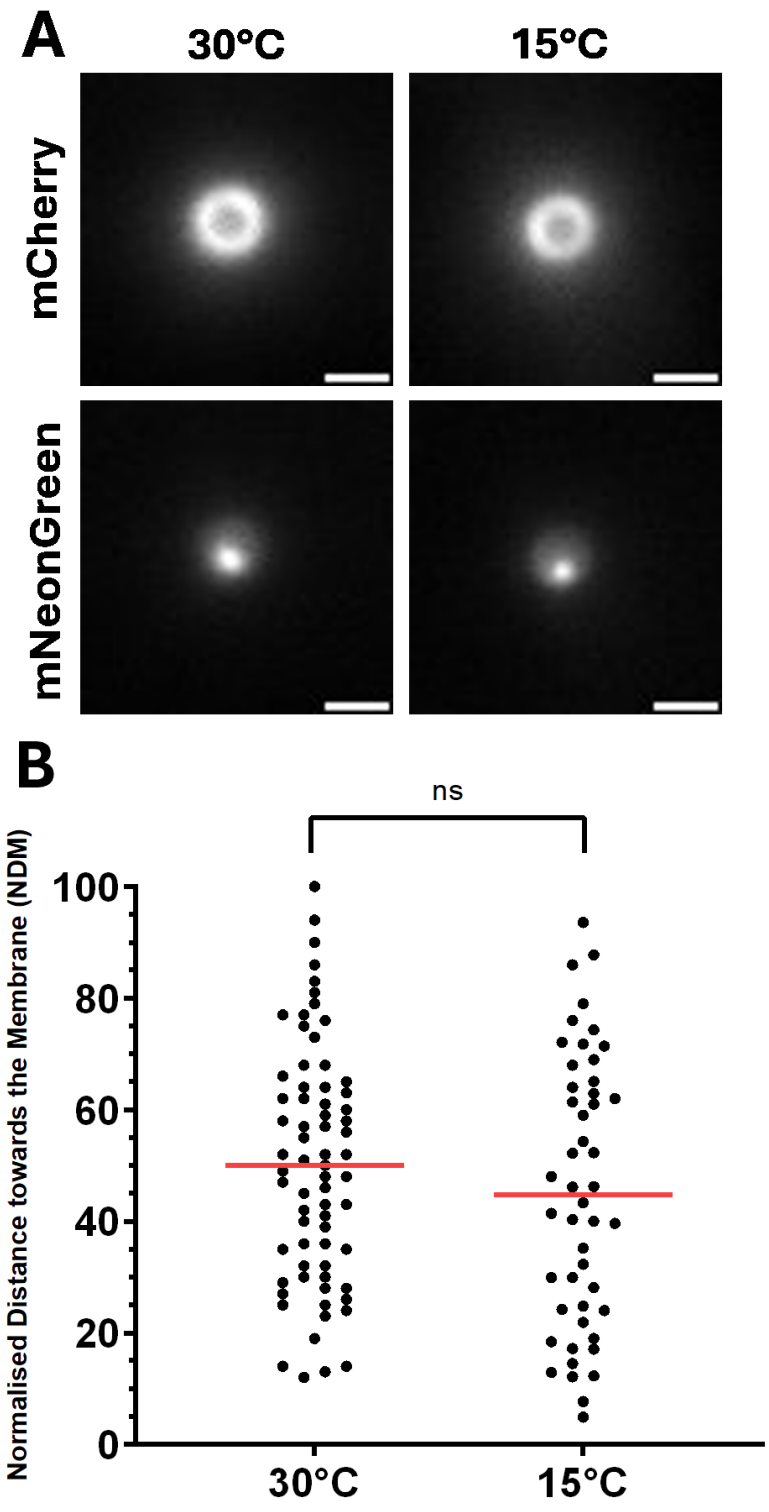

Figure 5.8: Comparing 15°C grown cells to 30°C grown cells for foci positioning ***A.)*** *Phase contrast and HiLO fluorescent images of B. subtilis with lacO4 array. Cells were constitutively expressing lacI-mNG and WALP23-mCherry. Cells were grown 30°C or 15°C to* OD_{600} *0.3, before undergoing VerCINI prep as per 2.3.5. Scale bar 1µm.* ***B.)*** *Quantification of field of views taken of cells. Distance was represented as percentage value towards membrane, with 0% representing the cell midpoint and 100% representing membrane peak intensity. Red line shows median. BJN17 (lacO4, lacI-mNG, WALP23-mCherry).*

5.2.6 Foci repositioning is dependent on translation

Previous work above on determining the involvement of either transcription or translation uses inhibition of transcription or translation by rifampicin and chloramphenicol, respectively. The limitation with this approach is that they do so for all transcription or translation events within the cell. Alternative off targets of rifampicin or chloramphenicol could be affecting gene loci positioning within the cell. One notable such effect being the decondensation of the nucleoid with rifampicin, or the condensation of the nucleoid with chloramphenicol. Experiments above (Chapter 5.2.3 and 4) show that foci movement requires both transcription and translation. To rule out lack of side effects by antibiotics on other genes, is to specifically abolish *des* translation through mutagenesis.

To observe *des* gene dynamics, a strain was developed whereby the Des start codon ATG site was mutated to AAA, to prevent recognition and translation by ribosome. The ATG→AAA mutant strain, with lacO4 upstream of *des* promoter and lacI-mNG, was grown at 30°C and immobilised in vertical agarose micro-holes. Cells were incubated at either 30°C or 15°C for 15 minutes before imaging (Figure 5.9A). The cellular position of foci was quantified from images and represented on a scatter plot (Figure 5.9B).

Strain lacking the start codon, ATG→AAA mutant strain, were found at a median of 44 NDM at 30°C. Induction at 15°C saw the foci population at median of 41 NDM. Such a value decrease is negligible. The wild-type start codon strain previously observed above (Figure 5.4) at 15°C has a median of 74 NDM, a 30-point increase towards the membrane from the ATG→AAA mutant strain. The foci found in both populations are found spread throughout the cell, with less foci found at the cell midline (0 NDM). According to nucleoid spread calculated in Chapter 5.2.1, roughly ~60% of the percentage value towards the membrane is taken up by nucleoid. 30°C and 15°C mutant ATG→AAA foci populations have a majority of their foci located within this nucleoid interior.

Crucially no shift takes place between 30°C and 15°C for des locus in absence of Des start codon, indicating that specific translation of Des is need for *des* locus shift upon induction. This also supports the chloramphenicol experiment above as it is consistent with the start codon mutation.

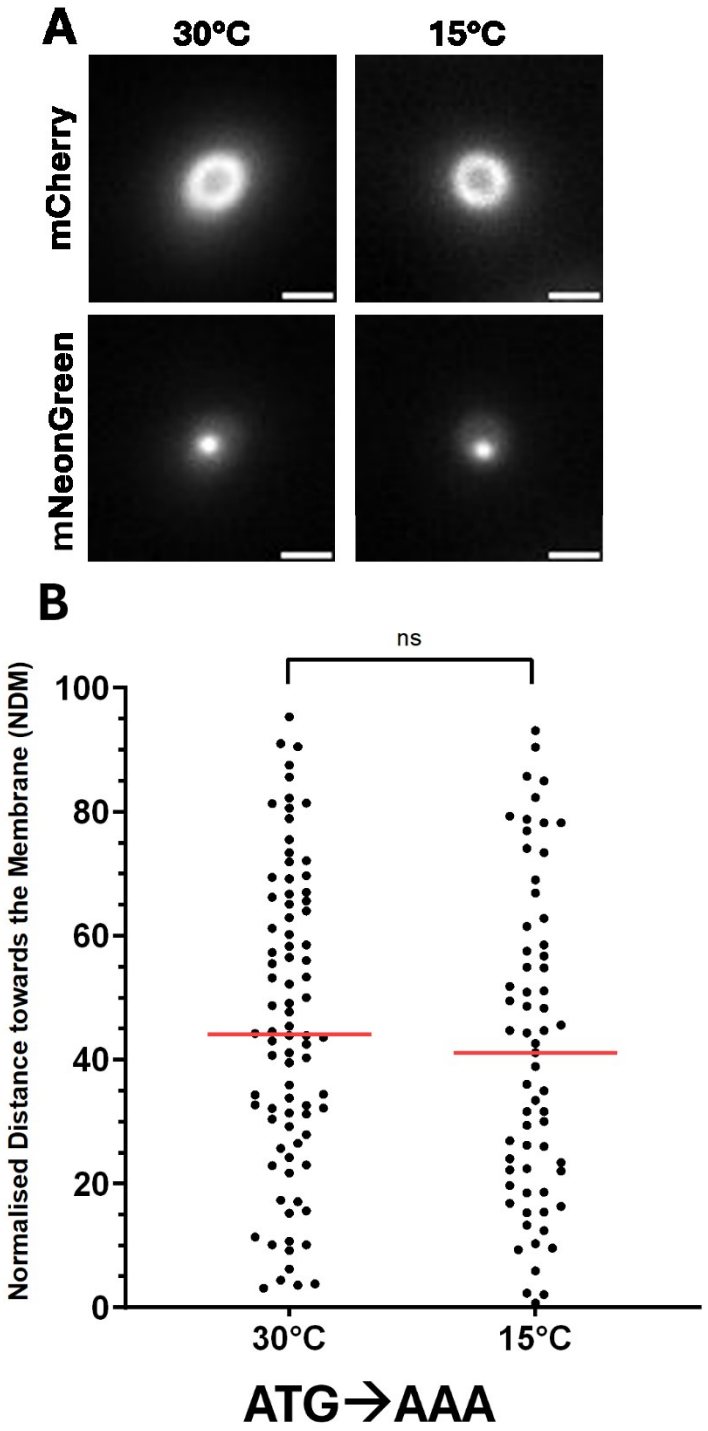

Figure 5.9: Induction of des foci without start codon A.) *Phase contrast and HiLO fluorescent images of B. subtilis with lacO4 array. Cells were constitutively expressing lacI-mNG and WALP23-mCherry. Cells were grown at 30°C to* OD_{600} *0.3, before undergoing VerCINI prep as per 2.3.5. Induction by 15°C was done for 15 minutes on the prepared slide. Scale bar 1µm.* ***B.)*** *Quantification of field of views taken of cells. Distance was represented as percentage value towards membrane, with 0% representing the cell midpoint and 100% representing membrane peak intensity. Red line shows median. Strains: BJN55 (desATG→AAA, lacO4, lacI-mNG, WALP23-mCherry)*

5.3 Discussion

In this chapter, the mechanism by which loci of *des* gene reposition towards the membrane upon induction was explored, using the tool of VerCINI and HiLO fluorescent microscopy.

As shown in chapter 4, *des* locus shifts towards the cell membrane upon induction by cold shock at 15°C. Critically it is also known that changes in Des expression result in abolishment of this shift (Figure 5.8). By analysing the location of the nucleoid and calculating its percentage value towards the membrane, a majority of foci are found to be within the nucleoid before induction. Upon induction by cold shock, *des* locus shifts outside of the nucleoid interior. This shift from nucleoid to membrane heavily implies transertion. In previous reports of transertion in *E. coli (Libby et al., 2012),* transertion was shown by foci proximity to the membrane. My experiments confirm a similar phenomenon where the foci shift to the membrane in *B. subtilis* upon induction of a membrane protein. Further testing this by secretion independent approaches would be ideal, where action by SRP and SecYEG could be depleted.

Loss of induction results in foci returning back towards the nucleoid, as seen in Figure 5.4. This can be explained by understanding Des expression, which is controlled by a two-step signalling system. DesK sits in the membrane as a sensor of membrane thickness. Upon cold shock the lipid bilayer's fluidity is altered and reduced. Sensing this, DesK phosphorylates DesR dimer, which allows DesR to interact with the binding region upstream of *des* promoter. Binding of DesR to the DNA binding site promotes RNAP binding and activates *des* transcription. Upon insertion of Des into the membrane, phospholipid membrane fluidity is increased by Des's enzymatic activity, which stops expression of Des (Cybulski et al., 2004). Due to this, it confirms that *des* locus shifts are due to Des transcription changes rather than cell changes.

Crucially, to pinpoint transertion as the responsible mechanism, both transcription and translation were inhibited by rifampicin and chloramphenicol respectively. Inhibition of translation by chloramphenicol resulted in elimination of foci movement. However, as previously discussed, both antibiotics had pleiotropic effects on cell function. Switching to the ATG→AAA *des* mutant, foci also were immune to repositioning upon induction, thus a similar observation was made that can be confidently attributed to only translation abolishment of *des*. Removal of the start

codon results in the ribosome failing to recognise the *des* mRNA transcript. In both cases of mutant or antibiotic, ribosomes fail to produce the signal anchor required by signal recognition particle (SRP) for the protein to be recognised. This results in SRP not recruiting Des translation to the membrane, thus integration of the polypeptide chain into the membrane would not commence. Either way, for these reasons, expression dependent shift is likely requiring both ribosomes and SRP systems. Future work in this area can help answer what force is responsible for membrane localisation and by what mechanism does it operate?

Treating cells with chloramphenicol after cold shock results in foci remaining at the membrane (Figure 5.6). As induction and foci shifting to the membrane have already occurred and are ongoing, addition of chloramphenicol seems to only pause the transertion complex at the membrane. Chloramphenicol binds to 50S ribosomal subunit, whereby it prevents peptide bond formation (Nagar & Siddiqui, 2020). Due to this, addition of chloramphenicol to ribosomes already at the membrane can be expected to have no further effect on *des* locus location. Upon return to 30°C however, this changes, as foci appear to move back towards the cell centre. This makes sense, as foci appear to partially move back towards the cell centre. Foci are *lacO4*/*lacI-mNG* interactions at the DNA. Loss of induction results in loss of transcription, so RNAP would finish, and no new transcription events would occur. This would result in DNA returning to the nucleoid as no new RNAP-ribosome interactions would be occurring. However, the foci repositioning back towards cell centre is not as exaggerated as previously seen. Perhaps inhibited ribosomes are stalled at the membrane, where the interaction between RNAP and trapped ribosome with SecYEG is all that is keeping the foci at the membrane, as secretion cannot continue in absence of ribosomes. (Figure 5.10). In this case, it could be hypothesized that RNAP-mRNA-Ribosome links only remain as long as the RNAP is transcribing, where it falls off the transertion complex upon finishes the transcript. In this case, foci at longer recovery timepoints might be further decreased. Additionally, work with fluorescence *in situ* hybridisation (FISH) could be utilised, whereby fluorescently labelled *des* mRNA and fluorescently tagged ribosomes could be observed for co-localisation. Further work into this should be looked at, including further repeats of this current experiment.

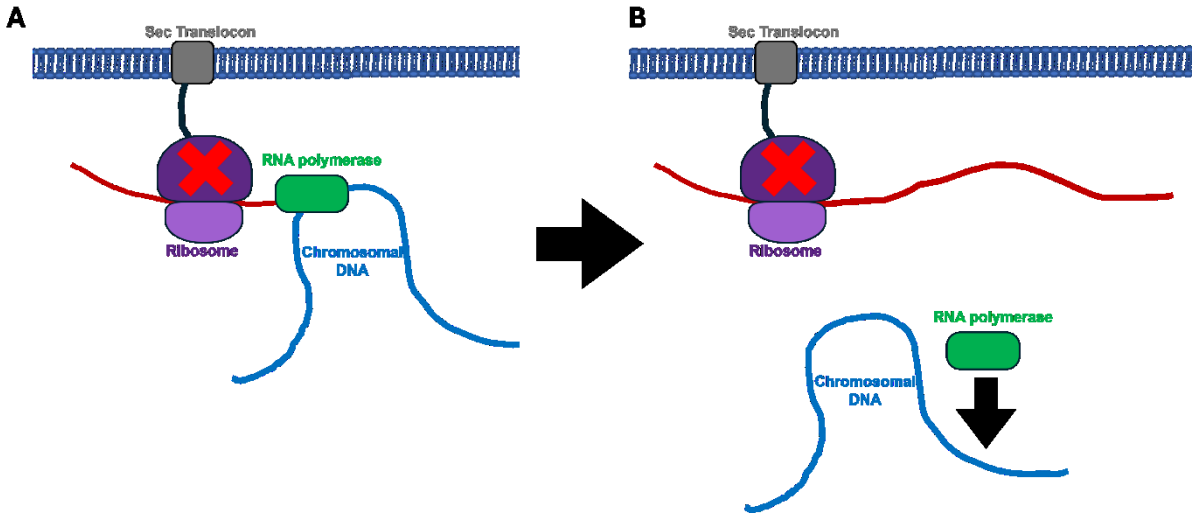

Figure 5.10: inhibition of translation after transertion has been induced A.) *Inhibiting ribosomes after transertion induction does not affect gene locus positioning, whereby ribosomes inserting a peptide into the membrane are trapped.* ***B.)*** *RNAP will finish transcribing des gene, however ribosomes will be stalled. Thus, with time, RNAP will dissociate from the transertion complex along with the chromosomal DNA. Additionally, loss of expression would result in no new RNAP transcripts of des occurring, thus chromosomal DNA will also return to the nucleoid interior.*

Rifampicin was also used to similar effect, whereby RNAP was inhibited and prevented transcription of *des.* Rifampicin was observed to also prevent gene repositioning to the membrane upon cold shock induction. Rifampicin however will shut down transcription for every gene, as well as affect the nucleoid decompaction. To fully confirm that transcription has a role in foci repositioning towards the membrane, another mutant strain where the transcription start site is mutated should be constructed. Additionally, a strain whereby DesR binding is abolished, by deletion of DesR binding site, is currently constructed and ready to analyse. It cannot be ruled out that when transcription start site or DesR binding site is deleted, that the Des gene moves still, not seen currently due the broad range of effects provided by rifampicin within the cell. This is highly unlikely however, as transcription inhibition will also always directly inhibit translation of the gene effected, due in absence of transcription no mRNA is available for translation. As translation is confirmed to be required for gene locus movement, inhibition of transcription may be simply preventing movement by translation. This in transertion is true regardless, so far it can only be said that rifampicin treatment also prevents foci movement.

One hypothesis for *B. subtilis* was that transcription and translation are functionally uncoupled (Johnson et al., 2020). Here they conclude that due to the observation that RNAP has a higher rate of transcription than is comparable to the ribosomes rate of translation, the two are unlikely to interact. As based on my experiments,

transertion a real phenomenon in *B. subtilis*. This implies that transcription and translation can be physically coupled, in the least in terms of expression of integral membrane proteins. Further work into this is needed, perhaps by structural work on *B. subtilis* RNAP and ribosome.

One other observation that has continuously been made throughout this thesis is the noticeable depletion of foci located at the very centre of the cell and the nucleoid. Foci in principle can be expected to be distributed homogeneously throughout the nucleoid in a population, however we observe clear depletion of foci in the very midcell. Interestingly this was seen for with horizontal cells and now with vertical cells. With vertical cells the effect is most evident. One potential explanation is the very centre of the nucleoid is hollow and contains cytoplasm. Such a gap would prevent foci from reaching the midpoint of the cell. Additionally super resolution microscopy achieved recently has resulted in the discovery of *B. subtilis'* nucleoid possessing a crescent shape (Tišma et al., 2024). Such a shape would be consistent with cytoplasm in the hollow nucleoid centre. To provide further evidence for this new cellular feature a nucleoid stain in combination with fluorescently labelled proteins should be carried out.

Despite attempts to contextualize the location of foci to either the membrane or the nucleoid, it can be said that gene loci with arrays will likely never reach the membrane peak at 100 NDM, as highlighted in figure 5.3. Partially this is due to *lacO4* not being able to be at the transertion complex. However, there is also a maximum value. *lacO4* is directly upstream of *des* promoter, which itself is upstream of *des* by 50bp. The start of the array is therefore 112bp from the start codon of *des.* For transertion to occur, the signal anchor/ first transmembrane domain must emerge from the ribosome, to allow SRP to recognise, bind and pause translation. The first transmembrane domain in Des is completed after 53aa (159bp). Therefore, if I assume that the first transmembrane domain is what is exactly required for transertion, the RNAP must at least be 158bp through the *des* gene. Thus, the *lacO4* is at minimum 270bp away from the transertion site. Each base pair on average is 0.34 nm. Without including size of the ribosome and RNAP complex, the *lacO4* could be up to 91.8 nm away from the membrane. For context, a *B. subtilis* cell's width on average is 1 μm or 1000 nm. Thus, the foci could be ~10% of the cell away from the membrane. If at the maximum distance from array to end of *des* gene is considered,

foci could be up to ~30% of the cell away. This won't always be the case, as DNA can fold up and be angled close to the membrane.

Additionally, whether the gene locus is at the membrane or at the nucleoid remains an important question. To test this, analysis of *lacO4* at *des* promoter but replacement of gene *des* with a non-membrane encoding gene allow analysis of cytoplasmic localised genes comparatively, whilst retaining chromosomal context and surroundings found at *des*. These results also provide evidence for co-translation translocation of ribosomes to the membrane, although further work can be done to highlight the involvement of SRP. A protein with no signal anchor to be recognised by SRP, in theory, would also result in no localisation to the membrane. Deletion of *des*' transmembrane domains might result in loss of foci movement. Currently, insertion of stop codons at 10aa, 20aa, 53aa and 80aa into Des are being constructed. Such mutations may shine a light on SRP interactions such how it handles shortened proteins (10aa and 20aa) and reduction in transmembrane domains (53aa and 80aa).

Analysis of the dynamics of foci by using time lapse microscopy could also be performed. Preliminary results of *lacO4* and VerCINI saw brief motion of foci, however photo bleaching of the short array quickly occurred (Appendix Figure 2). Further optimisation with time lapse should be looked into, such as utilising lacI-HaloTag for brighter and more stable fluorescent signal. Additionally, use of microfluidics with VerCINI has been developed previously, whereby use of an inducible promoter could become activated and analysed overtime.

In this chapter I set out to use VerCINI to analyse transertion more accurately than previously in chapter 4. I identified the effect of gene movement upon induction to the membrane, which itself is regulated by transcription and translation, followed by the observation of the return of a gene back to cell centre after induction. This provides the first direct experimental evidence for transertion in *B. subtilis* or any Gram-positive in general, as well as first evidence for the coupling of transcription and translation.

Chapter 6: Conclusion and future directions

The research question of this thesis was to directly observe *B. subtilis* via fluorescent microscopy to detect the effect of transcription on *des* locus' cellular positioning. I aimed to gain insight into this by analysing the movement of *des* locus within live cells with *lacO* arrays and lacI fusion partner. I wanted to see whether gene expression could affect gene location. The transertion hypothesis is the coupling of transcription, translation, and insertion of an integral membrane protein directly into the membrane. This thesis as a result has been focused primarily on observation of gene locus movement and whether it depends on transcription or translation to directly test the transertion hypothesis.

Large arrays have been known to cause replication issues in the past (Webb et al., 1998;Bernard et al., 2010) which led to the construction of intermediate sized operator arrays of *lacO48*, which were shown not to have artifacts (Wang et al., 2014b). In this thesis it is shown that these intermediate sized arrays also have artifacts, where the gene locus with *lacO48* do not respond to induction. Initially *lacO48* showed to be located at the nucleoid periphery, not shifting in location for treatment with chloramphenicol, treatment with rifampicin or induction of *des* locus at varying time points. Only upon construction of short array *lacO4* could *lacO48* be shown as insensitive to induction and most likely excluded to the nucleoid periphery. *lacO4* arrays are less disruptive and have shown to be the closest to native locus that is currently possible, to my knowledge, making *lacO4* the only currently available array to not cause artifacts within live cells.

In this thesis a lacO4 was developed, a 12 times shorter array than *lacO48*, which is no longer excluded from the nucleoid interior, therefore making a better candidate for this project. However, the *lacO4* short array has a weaker fluorescent signal of foci. Use of *mNeonGreen* in this project counteracted the loss of brightness from shorter arrays to some degree, however advances in fluorescent proteins have led to brighter and higher sensitivity proteins such as HaloTag (used in conjunction with fluorophores). More stable fluorescent proteins also exist now such as mChartreuse (Fraikin et al., 2024). Initially we thought that *lacO4* may still be interfering with expression and gene locus positioning, however controls have ruled out this possibility. Determining whether the positioning was affected by neighbouring genes, such as DesK or the kanamycin resistance cassette, was another concern. Upon induction of Des, foci reposition to the membrane, which implies that it is Des

expression that is responsible. Upon treatment with chloramphenicol or rifampicin, this foci shift is lost, however this cannot rule out a role of the kanamycin resistance cassette in repositioning the foci. This is due to the significant pleiotropic effects of both rifampicin and chloramphenicol on the cell, which would also affect the expression of the kanamycin resistance cassette. Only through direct inhibition of *des* through mutation could the kanamycin resistance cassette be ruled out. To this end, the start codon mutant provides the same pattern of results as the antibiotics, giving confidence that the local environment is not responsible for foci shifting. This combined with gene locus shifting being sensitive to induction gives confidence in the use of *lacO4*.

Induction of *des* expression by cold shock shifts the gene foci from the nucleoid towards the cell periphery. Previous observations of DNA movement upon induction in *E. coli* showed a similar effect (Libby et al., 2012) of shifting towards the membrane, with *tetO* array in lacY proximity. Upon analysis of horizontally orientated cells in *B. subtilis*, substantial shifts of foci towards the membrane make clear that this effect can also be seen.

Such a substantial increase implies expression affects foci movement that is expression dependent, however the question of whether foci move to the nucleoid periphery or to the membrane became an important part of this thesis. To analyse expression dependent foci shifts with better precision, the choice to analyse cells immobilised vertically was made. VerCINI in conjunction with HiLO microscopy allowed for greater resolution of foci and membrane, thus resulting in more precise data measured from images. Cells imaged by VerCINI and HiLO fluorescent microscopy revealed the same shifting pattern as the horizontally oriented cell foci. The limitation of horizontally oriented cells of lower resolution and the awkward cell geometry was rectified with use of VerCINI. The position of a gene locus in the Z-plane in VerCINI mattered significantly less than compared to horizontally orientated cells; gene loci in horizontal cells could shift towards the membrane in the Z-plane and skew measurement whilst vertical cells make no difference to measurements. Figures 3.1A and 5.1B highlight these differences.

Induction of *des* by cold shock in VerCINI confirms the shift of foci from the nucleoid interior to the membrane. It should be noted that physical interaction with the membrane has not been confirmed in this study, only the overlap of membrane fluorescent signals with the foci fluorescent signal. Experiments in horizontal cells

cannot resolve the difference between the nucleoid surface and membrane surface, however work in VerCINI can, but not confirm physical interaction. The distance between the array and *des* could not allow this observation with this current experimental setup. Gene loci shift towards the membrane as highlighted in this thesis heavily implies transertion, though it also implies coupled transcription-translation at the least.

Induction of expression of Des is responsible for initiation of gene shifts. Cold shock from 30°C to 15°C results in the above observed foci shift from midcell towards the membrane, which correlates with Des expression, not temperature. Cells grown in steady state cold temperatures have gene loci that are not shifted towards the membrane. Thus, only cold shock and Des expression is responsible for gene locus shifts.

Inhibition of translation by chloramphenicol and tetracycline both eliminate the foci shift generated by cold shock induction of *des*. The loss of foci shift upon antibiotic treatment implies that translation is required for foci movement, however both chloramphenicol and tetracycline will affect all cellular ribosomal activity, having various knock-on effects throughout the cell. Thus, it can only be said that the foci shift is lost upon treatment with chloramphenicol or tetracycline treatment. Start codon mutation of *des* also eliminates *des* locus movement upon induction, thus specifically local translation of *des* is required for foci movement. This argues that translation is required both globally and specifically for a gene locus to shift upon induction. This hints further at coupled transcription-translation and/or transertion being involved in gene locus movement.

Findings throughout this thesis also implicates the involvement of the SRP and co-translational translocation in a Gram-positive bacteria, an area currently not well understood. As foci are seen at the membrane, interaction can be implied to be between SRP/Ffh and FtsY. In the case of mutant start codon, the ribosome fails to translate the *des* transcript. As such, no signal anchor is produced. Thus, SRP and Ffh have nothing to recognise on the ribosome and will not bind to it. This results in the loss of shift to the membrane. When no start codon mutation is present however, the signal anchor is produced, allowing the SRP/Ffh complex to bind the ribosome/RNAP/DNA complex, pause translation and rapidly shift the complex to FtsY and SecYEG. The co-translation and translocation of Des into the membrane occurs where foci are seen upon induction at 15°C. Although rifampicin has global

cellular effects, a similar conclusion can be drawn about transcriptions relationship to foci shifting and the SRP. In this case the inhibition of RNAP results in no mRNA, thus no translation, thus no translocation. Interestingly treating with chloramphenicol after co-translation-translocation has resulted in DNA foci shifting back into the nucleoid. Chloramphenicol treatment would pause translation of already translocated complexes and prevent further co-translational-translocation events occurring. Further work into SRP and translocation in tangent with transertion would highlight greater the importance of SRP signal anchor recognition and translation arrest, both independently and in terms of transertion. To this end, working with *E. coli* SRP RNA in *B. subtilis* may enlighten the importance of translational arrest, as the *E. coli* SRP RNA lacks the required Alu domain. There is potential worth in also exploring the effects from other secretory systems, specifically looking at foci location of genes encoded for proteins destined outside the cell.

Thus far, translation is at least partially responsible for gene locus movement. Additionally, treatment with rifampicin disrupts global transcription in the cell, which has the effect of inhibiting gene locus movement. As both transcription and translation have an effect on gene locus positioning, it can be determined that transcription and translation can be coupled in *B. subtilis.* However, questions on how the two can couple is still under review. Transcription by itself does not shift genes to the nucleoid edge, as seen when the start codon mutation results in no shift upon induction. In *B. subtilis* then, it cannot be said from this investigation that RNAP and ribosomes interactions are facilitated by transcription itself.

Gene loci are found depleted around the cell centre throughout the project, though most prominently seen in vertically orientated cells. I speculate the effect is due to a cytoplasmic space found in the centre of the nucleoid. *B. subtilis* nucleoid shape has been found to be a crescent (Tišma et al., 2024). This shape would be consistent with the cytoplasmic space in the centre of the nucleoid at the midcell.

Further work on this hollow nucleoid should be studied by use of Structure Illumination Microscopy (SIM) with Hbu fluorescent fusion to analyse the structure of the nucleoid, aswell as analysing fluorescent cytoplasmic protein fusions in parallel. Other future research focusing on this topic of gene locus positioning can further studied. As discussed previously in chapter 5, the deletion of DesR binding site and deletion of transcription start site would both offer insight into specific transcription inhibition for *des* locus only. Additionally, further analysis of transertion could be

observed via attempts at looking into SRP based insertion. Indeed, no inhibitor exists to disrupt SRP based interactions and insertion into the membrane, however degradation of a component of the Sec translocon or SRP itself could offer insight, by using CrispR or degron protein tagging.

Another array-based observation system in *tetO* has great potential for simultaneous observation with *lacO* arrays within the cell. One such array, *tetO10*, has been constructed during this project for future work, whereby local chromosomal organisation of genes could be observed via the unfolding of the gene. Here a *tetO10* array integrated at the terminator of *des* would allow simultaneous imaging with *lacO*, with arrays at either end of *des.* The question of if the gene is unpacked can then be asked. Such is relevant to this project as it can help understand how one gene can reach the membrane by length of the gene, via unpacking. An array such as *tetO10* effect on localisation has not been compared as of yet, however.

Work has commenced on using an alternative inducible promoter alongside the ability to integrate at different genomic localisations. In addition to this, work is ongoing for analysis of various genes that are membrane bound, secreted and cytoplasmic. Such genes are being inserted into *des* locus, to be screened and analysed in the near future. Such work will confirm that membrane encoding gene loci shift to the membrane in comparison to where cytoplasmic encoding gene loci shift to within the cell upon induction. From this the analysis into transcription-translation coupling could be further studied, as cytoplasmic proteins may not shift in the same way as membrane integrated ones.

In summary, a novel short *lacO4* array was developed that allows observation of gene loci and their movement upon induction. Both translation and transcription are directly needed for gene loci shifting, further suggesting transertion. By observing loci shifting, evidence is also provided for co-translational translocation within *B. subtilis* and Gram-positive bacteria and highlighted the importance of SRP for transertion. By focusing on *des,* strong support for transertion in *B. subtilis* is provided. Such observations suggest that functional coupling of transcription and translation can occur in *B. subtilis.* Furthermore, for the first time, I have shown direct observational evidence for transertion, for the first time in *B. subtilis* and in any Gram-positive bacteria.

Appendix

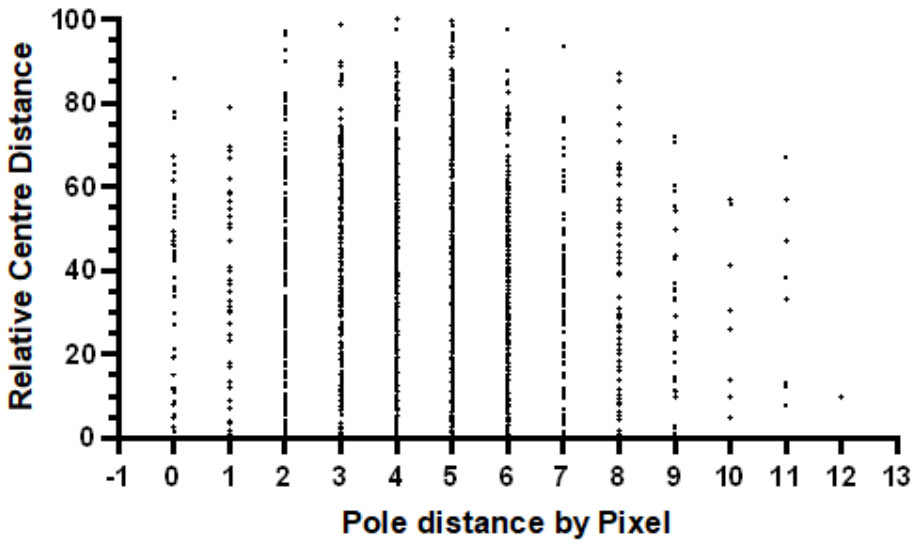

Figure Appendix 1: Determination of effect of foci at poles on the cell population. *Plot of distance from pole in pixels by the relative distance from the centre (0) to the membrane (100). Each spot represents a foci and both its measurement in cell width and to the membrane. Distance to pole was always determined to be the shortest distance. Average cells are ~30 pixels in length. Strains: BJN017 (lacO4, lacI-mNG).*

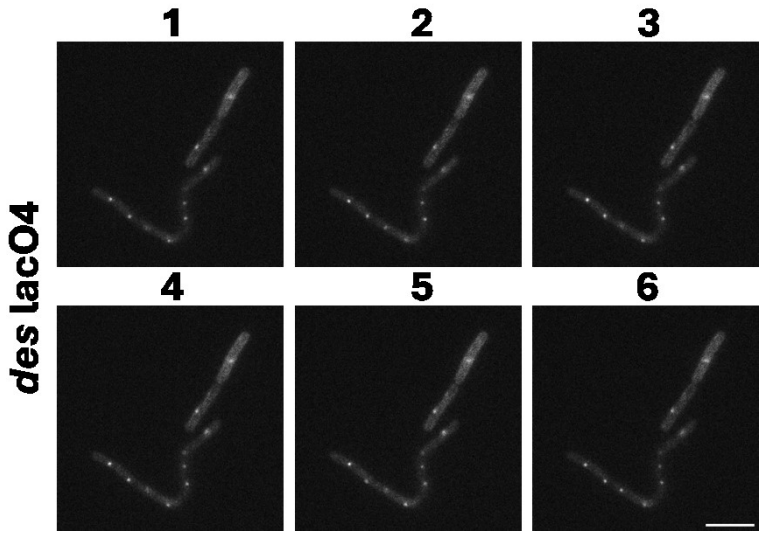

Figure Appendix 2: Observation of dynamics of gene locus by time lapse microscopy. *The first 6 frames of fluorescent time lapse images of lacO4 located at des. Cells constitutively express WALP23-mCherryy and lacI-mNG. Cells were grown at 30°C to OD_{600} 0.3. Each frame was taken every second for 5 seconds. Scale bar 5 µm. Strains: BJN017 (lacO4, lacI-mNG).*

References

Adams, D. W., Wu, L. J., & Errington, J. (2015). Nucleoid occlusion protein <scp>N</scp> oc recruits <scp>DNA</scp> to the bacterial cell membrane. *The EMBO Journal*, *34*(4), 491–501. https://doi.org/10.15252/embj.201490177

Aguilar, P. S., Lopez, P., & de Mendoza, D. (1999). Transcriptional Control of the Low-Temperature-Inducible *des* Gene, Encoding the Δ5 Desaturase of *Bacillus subtilis*. *Journal of Bacteriology*, *181*(22), 7028–7033. https://doi.org/10.1128/JB.181.22.7028-7033.1999

Albano, M., Smits, W. K., Ho, L. T. Y., Kraigher, B., Mandic-Mulec, I., Kuipers, O. P., & Dubnau, D. (2005). The Rok Protein of *Bacillus subtilis* Represses Genes for Cell Surface and Extracellular Functions. *Journal of Bacteriology*, *187*(6), 2010–2019. https://doi.org/10.1128/JB.187.6.2010-2019.2005

Amemiya, H. M., Schroeder, J., & Freddolino, P. L. (2021). Nucleoid-associated proteins shape chromatin structure and transcriptional regulation across the bacterial kingdom. *Transcription*, *12*(4), 182–218. https://doi.org/10.1080/21541264.2021.1973865

Badrinarayanan, A., Le, T. B. K., & Laub, M. T. (2015a). Bacterial Chromosome Organization and Segregation. *Annual Review of Cell and Developmental Biology*, *31*, 171–199. https://doi.org/10.1146/annurev-cellbio-100814-125211

Badrinarayanan, A., Le, T. B. K., & Laub, M. T. (2015b). Bacterial Chromosome Organization and Segregation. *Annual Review of Cell and Developmental Biology*, *31*(1), 171–199. https://doi.org/10.1146/annurev-cellbio-100814-125211

Bakshi, S., Choi, H., Mondal, J., & Weisshaar, J. C. (2014). Time-dependent effects of transcription- and translation-halting drugs on the spatial distributions of the <scp> *E* </scp> *scherichia coli* chromosome and ribosomes. *Molecular Microbiology*, *94*(4), 871–887. https://doi.org/10.1111/mmi.12805

Bakshi, S., Siryaporn, A., Goulian, M., & Weisshaar, J. C. (2012). Superresolution imaging of ribosomes and RNA polymerase in live *Escherichia coli* cells. *Molecular Microbiology*, *85*(1), 21–38. https://doi.org/10.1111/j.1365-2958.2012.08081.x

Beckert, B., Kedrov, A., Sohmen, D., Kempf, G., Wild, K., Sinning, I., Stahlberg, H., Wilson, D. N., & Beckmann, R. (2015). Translational arrest by a prokaryotic signal recognition particle is mediated by RNA interactions. *Nature Structural & Molecular Biology*, *22*(10), 767–773. https://doi.org/10.1038/nsmb.3086

Berlatzky, I. A., Rouvinski, A., & Ben-Yehuda, S. (2008). Spatial organization of a replicating bacterial chromosome. *Proceedings of the National Academy of Sciences*, *105*(37), 14136–14140. https://doi.org/10.1073/pnas.0804982105

Bernard, R., Marquis, K. A., & Rudner, D. Z. (2010). Nucleoid occlusion prevents cell division during replication fork arrest in Bacillus subtilis. *Molecular Microbiology*, *78*(4), 866–882. https://doi.org/10.1111/j.1365-2958.2010.07369.x

Bernsel, A., & Daley, D. O. (2009). Exploring the inner membrane proteome of Escherichia coli: which proteins are eluding detection and why? *Trends in Microbiology*, *17*(10), 444–449. https://doi.org/10.1016/j.tim.2009.07.005

Bettridge, K., Verma, S., Weng, X., Adhya, S., & Xiao, J. (2021). Single-molecule tracking reveals that the nucleoid-associated protein HU plays a dual role in maintaining proper nucleoid volume through differential interactions with chromosomal DNA. *Molecular Microbiology*, *115*(1), 12–27. https://doi.org/10.1111/mmi.14572

Bock, F. P., Anchimiuk, A., Diebold-Durand, M.-L., & Gruber, S. (2021). The ParB clamp docks onto Smc for DNA loading via a joint-ParB interface. *BioRxiv*, 2021.12.15.472096. https://doi.org/10.1101/2021.12.15.472096

Brandão, H. B., Paul, P., van den Berg, A. A., Rudner, D. Z., Wang, X., & Mirny, L. A. (2019a). RNA polymerases as moving barriers to condensin loop extrusion. *Proceedings of the National Academy of Sciences*, *116*(41), 20489–20499. https://doi.org/10.1073/pnas.1907009116

Brandão, H. B., Paul, P., van den Berg, A. A., Rudner, D. Z., Wang, X., & Mirny, L. A. (2019b). RNA polymerases as moving barriers to condensin loop extrusion. *Proceedings of the National Academy of Sciences*, *116*(41), 20489–20499. https://doi.org/10.1073/pnas.1907009116

Britton, R. A., Lin, D. C.-H., & Grossman, A. D. (1998). Characterization of a prokaryotic SMC protein involved in chromosome partitioning. *Genes & Development*, *12*(9), 1254–1259. https://doi.org/10.1101/gad.12.9.1254

Cabrera, J. E., Cagliero, C., Quan, S., Squires, C. L., & Jin, D. J. (2009). Active Transcription of rRNA Operons Condenses the Nucleoid in *Escherichia coli* : Examining the Effect of Transcription on Nucleoid Structure in the Absence of Transertion. *Journal of Bacteriology*, *191*(13), 4180–4185. https://doi.org/10.1128/JB.01707-08

Cabrera, J. E., & Jin, D. J. (2003). The distribution of RNA polymerase in *Escherichia coli* is dynamic and sensitive to environmental cues. *Molecular Microbiology*, *50*(5), 1493–1505. https://doi.org/10.1046/j.1365-2958.2003.03805.x

Chai, Q., Singh, B., Peisker, K., Metzendorf, N., Ge, X., Dasgupta, S., & Sanyal, S. (2014). Organization of Ribosomes and Nucleoids in Escherichia coli Cells during Growth and in Quiescence. *Journal of Biological Chemistry*, *289*(16), 11342–11352. https://doi.org/10.1074/jbc.M114.557348

Chen, M., & Fredrick, K. (2018). Measures of single- versus multiple-round translation argue against a mechanism to ensure coupling of transcription and translation. *Proceedings of the National Academy of Sciences*, *115*(42), 10774–10779. https://doi.org/10.1073/pnas.1812940115

Chopra, I., & Roberts, M. (2001). Tetracycline Antibiotics: Mode of Action, Applications, Molecular Biology, and Epidemiology of Bacterial Resistance. *Microbiology and Molecular Biology Reviews*, *65*(2), 232–260. https://doi.org/10.1128/MMBR.65.2.232-260.2001

Chukwudi, C. U. (2016). rRNA Binding Sites and the Molecular Mechanism of Action of the Tetracyclines. *Antimicrobial Agents and Chemotherapy*, *60*(8), 4433–4441. https://doi.org/10.1128/AAC.00594-16

Cybulski, L. E., del Solar, G., Craig, P. O., Espinosa, M., & de Mendoza, D. (2004). Bacillus subtilis DesR Functions as a Phosphorylation-activated Switch to Control Membrane Lipid Fluidity. *Journal of Biological Chemistry*, *279*(38), 39340–39347. https://doi.org/10.1074/jbc.M405150200

Cybulski, L. E., Martín, M., Mansilla, M. C., Fernández, A., & de Mendoza, D. (2010). Membrane Thickness Cue for Cold Sensing in a Bacterium. *Current Biology*, *20*(17), 1539–1544. https://doi.org/https://doi.org/10.1016/j.cub.2010.06.074

Dame, R. T. (2005). The role of nucleoid-associated proteins in the organization and compaction of bacterial chromatin. *Molecular Microbiology*, *56*(4), 858–870. https://doi.org/10.1111/j.1365-2958.2005.04598.x

Dame, R. T., Rashid, F.-Z. M., & Grainger, D. C. (2020). Chromosome organization in bacteria: mechanistic insights into genome structure and function. *Nature Reviews Genetics*, *21*(4), 227–242. https://doi.org/10.1038/s41576-019-0185-4

Daniela, A., Cecilia, M. M., & Diego, de M. (2004). The Membrane Fluidity Sensor DesK of Bacillus subtilis Controls the Signal Decay of Its Cognate Response Regulator. *Journal of Bacteriology*, *186*(9), 2655–2663. https://doi.org/10.1128/jb.186.9.2655-2663.2004

Deana, A., & Belasco, J. G. (2005). Lost in translation: the influence of ribosomes on bacterial mRNA decay: Figure 1. *Genes & Development*, *19*(21), 2526–2533. https://doi.org/10.1101/gad.1348805

Deneke, C., Lipowsky, R., & Valleriani, A. (2013). Effect of ribosome shielding on mRNA stability. *Physical Biology*, *10*(4), 046008. https://doi.org/10.1088/1478-3975/10/4/046008

Dillon, S. C., & Dorman, C. J. (2010). Bacterial nucleoid-associated proteins, nucleoid structure and gene expression. *Nature Reviews Microbiology*, *8*(3), 185–195. https://doi.org/10.1038/nrmicro2261

Dorman, C. J. (2014). Function of Nucleoid-Associated Proteins in Chromosome Structuring and Transcriptional Regulation. *Microbial Physiology*, *24*(5–6), 316–331. https://doi.org/10.1159/000368850

Dorman, C. J., Schumacher, M. A., Bush, M. J., Brennan, R. G., & Buttner, M. J. (2020). When is a transcription factor a NAP? *Current Opinion in Microbiology*, *55*, 26–33. https://doi.org/10.1016/j.mib.2020.01.019

Dworkin, J., & Losick, R. (2002). Does RNA polymerase help drive chromosome segregation in bacteria? *Proceedings of the National Academy of Sciences*, *99*(22), 14089–14094. https://doi.org/10.1073/pnas.182539899

Dworsky, P., & Schaechter, M. (1973). Effect of Rifampin on the Structure and Membrane Attachment of the Nucleoid of *Escherichia coli*. *Journal of*

Bacteriology, *116*(3), 1364–1374. https://doi.org/10.1128/jb.116.3.1364-1374.1973

Fiedler, S. M., & Graumann, P. L. (2024). B. subtilis Sec and Srp Systems Show Dynamic Adaptations to Different Conditions of Protein Secretion. *Cells*, *13*(5), 377. https://doi.org/10.3390/cells13050377

Fogg, J. M., Judge, A. K., Stricker, E., Chan, H. L., & Zechiedrich, L. (2021). Supercoiling and looping promote DNA base accessibility and coordination among distant sites. *Nature Communications*, *12*(1), 5683. https://doi.org/10.1038/s41467-021-25936-2

Forth, S., Sheinin, M. Y., Inman, J., & Wang, M. D. (2013). Torque Measurement at the Single-Molecule Level. *Annual Review of Biophysics*, *42*(1), 583–604. https://doi.org/10.1146/annurev-biophys-083012-130412

Fraikin, N., Couturier, A., & Lesterlin, C. (2024). A palette of bright and photostable monomeric fluorescent proteins for bacterial time-lapse imaging. *BioRxiv*. https://doi.org/10.1101/2024.03.28.587235

Gohrbandt, M., Lipski, A., Grimshaw, J. W., Buttress, J. A., Baig, Z., Herkenhoff, B., Walter, S., Kurre, R., Deckers-Hebestreit, G., & Strahl, H. (2022). Low membrane fluidity triggers lipid phase separation and protein segregation in living bacteria. *The EMBO Journal*, *41*(5). https://doi.org/10.15252/embj.2021109800

Gottesman, S., & Storz, G. (2011). Bacterial Small RNA Regulators: Versatile Roles and Rapidly Evolving Variations. *Cold Spring Harbor Perspectives in Biology*, *3*(12), a003798–a003798. https://doi.org/10.1101/cshperspect.a003798

Gowrishankar, J., & Harinarayanan, R. (2004). Why is transcription coupled to translation in bacteria? *Molecular Microbiology*, *54*(3), 598–603. https://doi.org/10.1111/j.1365-2958.2004.04289.x

Green, E. R., & Mecsas, J. (2016). Bacterial Secretion Systems: An Overview. *Microbiology Spectrum*, *4*(1). https://doi.org/10.1128/microbiolspec.VMBF-0012-2015

Grimshaw, J. W. D. L. (2022). *Cellular localisation and stress induced clustering of RNase Y* [Newcastle University]. https://libsearch.ncl.ac.uk/permalink/f/1jraif3/NCL_ALMA51241112220002411

Gualerzi, C. O., & Pon, C. L. (2015). Initiation of mRNA translation in bacteria: structural and dynamic aspects. *Cellular and Molecular Life Sciences*, *72*(22), 4341–4367. https://doi.org/10.1007/s00018-015-2010-3

Guo, J. (2014). Transcription: the epicenter of gene expression. *Journal of Zhejiang University SCIENCE B*, *15*(5), 409–411. https://doi.org/10.1631/jzus.B1400113

Gupta, A., Joshi, A., Arora, K., Mukhopadhyay, S., & Guptasarma, P. (2023). The bacterial nucleoid-associated proteins, HU and Dps, condense DNA into context-dependent biphasic or multiphasic complex coacervates. *Journal of Biological Chemistry*, *299*(5). https://doi.org/10.1016/j.jbc.2023.104637

Helmann, J. D. (2009). RNA polymerase: A nexus of gene regulation. *Methods*, *47*(1), 1–5. https://doi.org/10.1016/j.ymeth.2008.12.001

Hoencamp, C., & Rowland, B. D. (2023). Genome control by SMC complexes. *Nature Reviews Molecular Cell Biology*, *24*(9), 633–650. https://doi.org/10.1038/s41580-023-00609-8

Hołówka, J., & Zakrzewska-Czerwińska, J. (2020). Nucleoid Associated Proteins: The Small Organizers That Help to Cope With Stress. In *Frontiers in Microbiology* (Vol. 11, p. 590). Frontiers Media S.A. https://doi.org/10.3389/fmicb.2020.00590

Irastortza-Olaziregi, M., & Amster-Choder, O. (2021). Coupled Transcription-Translation in Prokaryotes: An Old Couple With New Surprises. In *Frontiers in Microbiology* (Vol. 11, p. 3532). Frontiers Media S.A. https://doi.org/10.3389/fmicb.2020.624830

Irastortza-Olaziregi, M., & Amster-Choder, O. (2021). RNA localization in prokaryotes: Where, when, how, and why. *WIREs RNA*, *12*(2). https://doi.org/10.1002/wrna.1615

Johnson, G. E., Lalanne, J.-B., Peters, M. L., & Li, G.-W. (2020). Functionally uncoupled transcription–translation in Bacillus subtilis. *Nature*, *585*(7823), 124–128. https://doi.org/10.1038/s41586-020-2638-5

Joyeux, M. (2016). In vivo compaction dynamics of bacterial DNA: A fingerprint of DNA/RNA demixing? *Current Opinion in Colloid & Interface Science*, *26*, 17–27. https://doi.org/10.1016/j.cocis.2016.08.005

Joyeux, M. (2018). A segregative phase separation scenario of the formation of the bacterial nucleoid. *Soft Matter*, *14*(36), 7368–7381. https://doi.org/10.1039/C8SM01205A

Kahramanoglou, C., Seshasayee, A. S. N., Prieto, A. I., Ibberson, D., Schmidt, S., Zimmermann, J., Benes, V., Fraser, G. M., & Luscombe, N. M. (2011). Direct and indirect effects of H-NS and Fis on global gene expression control in Escherichia coli. *Nucleic Acids Research*, *39*(6), 2073–2091. https://doi.org/10.1093/nar/gkq934

Kamashev, D. (2000). The histone-like protein HU binds specifically to DNA recombination and repair intermediates. *The EMBO Journal*, *19*(23), 6527–6535. https://doi.org/10.1093/emboj/19.23.6527

Kang, Z., Yang, S., Du, G., & Chen, J. (2014). Molecular engineering of secretory machinery components for high-level secretion of proteins in *Bacillus* species. *Journal of Industrial Microbiology and Biotechnology*, *41*(11), 1599–1607. https://doi.org/10.1007/s10295-014-1506-4

Kannaiah, S., Livny, J., & Amster-Choder, O. (2019). Spatiotemporal Organization of the E. coli Transcriptome: Translation Independence and Engagement in Regulation. *Molecular Cell*, *76*(4), 574-589.e7. https://doi.org/10.1016/j.molcel.2019.08.013

Kaval, K. G., Chimalapati, S., Siegel, S. D., Garcia, N., Jaishankar, J., Dalia, A. B., & Orth, K. (2023). Membrane-localized expression, production and assembly of Vibrio parahaemolyticus T3SS2 provides evidence for transertion. *Nature Communications*, *14*(1), 1178. https://doi.org/10.1038/s41467-023-36762-z

Kennell, D., & Riezman, H. (1977). Transcription and translation initiation frequencies of the Escherichia coli lac operon. *Journal of Molecular Biology*, *114*(1), 1–21. https://doi.org/10.1016/0022-2836(77)90279-0

Kleckner, N., Fisher, J. K., Stouf, M., White, M. A., Bates, D., & Witz, G. (2014). The bacterial nucleoid: nature, dynamics and sister segregation. *Current Opinion in Microbiology*, *22*, 127–137. https://doi.org/10.1016/j.mib.2014.10.001

Kleppe, K., Ovrebo, S., & Lossius, I. (1979). The Bacterial Nucleoid. *Journal of General Microbiology*, *112*(1), 1–13. https://doi.org/10.1099/00221287-112-1-1

Kohler, R., Mooney, R. A., Mills, D. J., Landick, R., & Cramer, P. (2017). Architecture of a transcribing-translating expressome. *Science*, *356*(6334), 194–197. https://doi.org/10.1126/science.aal3059

Kouzine, F., Gupta, A., Baranello, L., Wojtowicz, D., Ben-Aissa, K., Liu, J., Przytycka, T. M., & Levens, D. (2013). Transcription-dependent dynamic supercoiling is a short-range genomic force. *Nature Structural & Molecular Biology*, *20*(3), 396–403. https://doi.org/10.1038/nsmb.2517

Kudva, R., Denks, K., Kuhn, P., Vogt, A., Müller, M., & Koch, H.-G. (2013). Protein translocation across the inner membrane of Gram-negative bacteria: the Sec and Tat dependent protein transport pathways. *Research in Microbiology*, *164*(6), 505–534. https://doi.org/10.1016/j.resmic.2013.03.016

Lagomarsino, M. C., Espéli, O., & Junier, I. (2015). From structure to function of bacterial chromosomes: Evolutionary perspectives and ideas for new experiments. In *FEBS Letters* (Vol. 589, Issue 20, pp. 2996–3004). Elsevier B.V. https://doi.org/10.1016/j.febslet.2015.07.002

Lass-Napiorkowska, A., & Heyduk, T. (2016). Real-Time Observation of Backtracking by Bacterial RNA Polymerase. *Biochemistry*, *55*(4), 647–658. https://doi.org/10.1021/acs.biochem.5b01184

Lavelle, C. (2014). Pack, unpack, bend, twist, pull, push: the physical side of gene expression. *Current Opinion in Genetics & Development*, *25*, 74–84. https://doi.org/10.1016/j.gde.2014.01.001

Le, T. B., & Laub, M. T. (2016). Transcription rate and transcript length drive formation of chromosomal interaction domain boundaries. *The EMBO Journal*, *35*(14), 1582–1595. https://doi.org/10.15252/embj.201593561

Lee, P. S., & Grossman, A. D. (2006). The chromosome partitioning proteins Soj (ParA) and Spo0J (ParB) contribute to accurate chromosome partitioning, separation of replicated sister origins, and regulation of replication initiation in *Bacillus subtilis*. *Molecular Microbiology*, *60*(4), 853–869. https://doi.org/10.1111/j.1365-2958.2006.05140.x

Lewis, M., Chang, G., Horton, N. C., Kercher, M. A., Pace, H. C., Schumacher, M. A., Brennan, R. G., & Lu, P. (1996). Crystal Structure of the Lactose Operon Repressor and Its Complexes with DNA and Inducer. *Science*, *271*(5253), 1247–1254. https://doi.org/10.1126/science.271.5253.1247

Lewis, P. J., Thaker, S. D., & Errington, J. (2000). Compartmentalization of transcription and translation in Bacillus subtilis. *The EMBO Journal*, *19*(4), 710–718. https://doi.org/10.1093/emboj/19.4.710

Libby, E. A., Roggiani, M., & Goulian, M. (2012). Membrane protein expression triggers chromosomal locus repositioning in bacteria. *Proceedings of the National Academy of Sciences of the United States of America*, *109*(19), 7445–7450. https://doi.org/10.1073/pnas.1109479109

Lioy, V. S., Cournac, A., Marbouty, M., Duigou, S., Mozziconacci, J., Espéli, O., Boccard, F., & Koszul, R. (2018). Multiscale Structuring of the E. coli Chromosome by Nucleoid-Associated and Condensin Proteins. *Cell*, *172*(4), 771-783.e18. https://doi.org/10.1016/j.cell.2017.12.027

Luirink, J., Heijne, G. von, Houben, E., & Gier, J.-W. de. (2005). BIOGENESIS OF INNER MEMBRANE PROTEINS IN *ESCHERICHIA COLI*. *Annual Review of Microbiology*, *59*(1), 329–355. https://doi.org/10.1146/annurev.micro.59.030804.121246

Ma, J., & Wang, M. D. (2016). DNA supercoiling during transcription. *Biophysical Reviews*, *8*(S1), 75–87. https://doi.org/10.1007/s12551-016-0215-9

Mäkelä, J., & Sherratt, D. (2020). SMC complexes organize the bacterial chromosome by lengthwise compaction. *Current Genetics*, *66*(5), 895–899. https://doi.org/10.1007/s00294-020-01076-w

Martínez-Antonio, A., Medina-Rivera, A., & Collado-Vides, J. (2009). Structural and functional map of a bacterial nucleoid. In *Genome Biology* (Vol. 10, Issue 12, pp. 1–4). BioMed Central Ltd. https://doi.org/10.1186/gb-2009-10-12-247

Martis B., S., Forquet, R., Reverchon, S., Nasser, W., & Meyer, S. (2019). DNA Supercoiling: an Ancestral Regulator of Gene Expression in Pathogenic Bacteria? *Computational and Structural Biotechnology Journal*, *17*, 1047–1055. https://doi.org/10.1016/j.csbj.2019.07.013

Matalon, E., Kaminker, I., Zimmermann, H., Eisenstein, M., Shai, Y., & Goldfarb, D. (2013). Topology of the Trans-Membrane Peptide WALP23 in Model Membranes under Negative Mismatch Conditions. *The Journal of Physical Chemistry B*, *117*(8), 2280–2293. https://doi.org/10.1021/jp310056h

Matsumoto, K., Hara, H., Fishov, I., Mileykovskaya, E., & Norris, V. (2015a). The membrane: transertion as an organizing principle in membrane heterogeneity. *Frontiers in Microbiology*, *6*. https://doi.org/10.3389/fmicb.2015.00572

Matsumoto, K., Hara, H., Fishov, I., Mileykovskaya, E., & Norris, V. (2015b). The membrane: transertion as an organizing principle in membrane heterogeneity. *Frontiers in Microbiology*, *6*. https://doi.org/10.3389/fmicb.2015.00572

Mayer, B., Schwan, M., Oviedo-Bocanegra, L. M., Bange, G., Thormann, K. M., & Graumann, P. L. (2021). Dynamics of Bacterial Signal Recognition Particle at a Single Molecule Level. *Frontiers in Microbiology*, *12*. https://doi.org/10.3389/fmicb.2021.663747

McAdams, N. M., & Gollnick, P. (2014). The Bacillus subtilis TRAP Protein Can Induce Transcription Termination in the Leader Region of the Tryptophan Biosynthetic (trp) Operon Independent of the trp Attenuator RNA. *PLoS ONE*, *9*(2), e88097. https://doi.org/10.1371/journal.pone.0088097

McLeod, B. N., Allison-Gamble, G. E., Barge, M. T., Tonthat, N. K., Schumacher, M. A., Hayes, F., & Barillà, D. (2016). A three-dimensional ParF meshwork assembles through the nucleoid to mediate plasmid segregation. *Nucleic Acids Research*, gkw1302. https://doi.org/10.1093/nar/gkw1302

Middlemiss, S., Blandenet, M., Roberts, D. M., McMahon, A., Grimshaw, J., Edwards, J. M., Sun, Z., Whitley, K. D., Blu, T., Strahl, H., & Holden, S. (2024). Molecular motor tug-of-war regulates elongasome cell wall synthesis dynamics in Bacillus subtilis. *Nature Communications*, *15*(1), 5411. https://doi.org/10.1038/s41467-024-49785-x

Miller, V. L., Taylor, R. K., & Mekalanos, J. J. (1987). Cholera toxin transcriptional activator ToxR is a transmembrane DNA binding protein. *Cell*, *48*(2), 271–279. https://doi.org/10.1016/0092-8674(87)90430-2

Minakhin, L., Bhagat, S., Brunning, A., Campbell, E. A., Darst, S. A., Ebright, R. H., & Severinov, K. (2001). Bacterial RNA polymerase subunit ω and eukaryotic RNA

polymerase subunit RPB6 are sequence, structural, and functional homologs and promote RNA polymerase assembly. *Proceedings of the National Academy of Sciences*, *98*(3), 892–897. https://doi.org/10.1073/pnas.98.3.892

Mondal, J., Bratton, B. P., Li, Y., Yethiraj, A., & Weisshaar, J. C. (2011). Entropy-Based Mechanism of Ribosome-Nucleoid Segregation in E. coli Cells. *Biophysical Journal*, *100*(11), 2605–2613. https://doi.org/10.1016/j.bpj.2011.04.030

Montero Llopis, P., Jackson, A. F., Sliusarenko, O., Surovtsev, I., Heinritz, J., Emonet, T., & Jacobs-Wagner, C. (2010). Spatial organization of the flow of genetic information in bacteria. *Nature*, *466*(7302), 77–81. https://doi.org/10.1038/nature09152

Moser, C., Mol, O., Goody, R. S., & Sinning, I. (1997). The signal recognition particle receptor of *Escherichia coli* (FtsY) has a nucleotide exchange factor built into the GTPase domain. *Proceedings of the National Academy of Sciences*, *94*(21), 11339–11344. https://doi.org/10.1073/pnas.94.21.11339

Murakami, K. S., & Darst, S. A. (2003). Bacterial RNA polymerases: the wholo story. *Current Opinion in Structural Biology*, *13*(1), 31–39. https://doi.org/https://doi.org/10.1016/S0959-440X(02)00005-2

Murakami, K. S., Masuda, S., Campbell, E. A., Muzzin, O., & Darst, S. A. (2002). Structural Basis of Transcription Initiation: An RNA Polymerase Holoenzyme-DNA Complex. *Science*, *296*(5571), 1285–1290. https://doi.org/10.1126/science.1069595

Nagar, J., & Siddiqui, M. (2020). *Asian Journal of Pharmaceutical Research and Development An Updated Review on Pharmacology and Toxicities Related to Chloramphenicol*. *8*, 104–109. https://doi.org/10.22270/ajprd.v8i4.671

Nandana, V., & Schrader, J. M. (2021). Roles of liquid–liquid phase separation in bacterial RNA metabolism. *Current Opinion in Microbiology*, *61*, 91–98. https://doi.org/10.1016/j.mib.2021.03.005

Nguyen, H. H., De La Tour, C. B., Toueille, M., Vannier, F., Sommer, S., & Servant, P. (2009). The essential histone-like protein HU plays a major role in *Deinococcus radiodurans* nucleoid compaction. *Molecular Microbiology*, *73*(2), 240–252. https://doi.org/10.1111/j.1365-2958.2009.06766.x

Nielsen, H. J., Ottesen, J. R., Youngren, B., Austin, S. J., & Hansen, F. G. (2006). The *Escherichia coli* chromosome is organized with the left and right chromosome arms in separate cell halves. *Molecular Microbiology*, *62*(2), 331–338. https://doi.org/10.1111/j.1365-2958.2006.05346.x

Nishiguchi, M., Honda, K., Amikura, R., Nakamura, K., & Yamane, K. (1994). Structural requirements of Bacillus subtilis small cytoplasmic RNA for cell growth, sporulation, and extracellular enzyme production. *Journal of Bacteriology*, *176*(1), 157–165. https://doi.org/10.1128/jb.176.1.157-165.1994

Norris, V. (1995). Hypothesis: chromosome separation in *Escherichia coli* involves autocatalytic gene expression, transertion and membrane-domain formation. *Molecular Microbiology*, *16*(6), 1051–1057. https://doi.org/10.1111/j.1365-2958.1995.tb02330.x

Ptacin, J. L., Gahlmann, A., Bowman, G. R., Perez, A. M., von Diezmann, L., Eckart, M. R., Moerner, W. E., & Shapiro, L. (2014). Bacterial scaffold directs pole-specific centromere segregation. *Proceedings of the National Academy of Sciences*, *111*(19). https://doi.org/10.1073/pnas.1405188111

Reilman, E., Mars, R. A. T., van Dijl, J. M., & Denham, E. L. (2014). The multidrug ABC transporter BmrC/BmrD of Bacillus subtilis is regulated via a ribosome-mediated transcriptional attenuation mechanism. *Nucleic Acids Research*, *42*(18), 11393–11407. https://doi.org/10.1093/nar/gku832

Roberts, J. W. (2019). Mechanisms of Bacterial Transcription Termination. *Journal of Molecular Biology*, *431*(20), 4030–4039. https://doi.org/10.1016/j.jmb.2019.04.003

Roggiani, M., & Goulian, M. (2015). Chromosome-Membrane Interactions in Bacteria. *Annual Review of Genetics*, *49*(1), 115–129. https://doi.org/10.1146/annurev-genet-112414-054958

Ryan, V. T., Grimwade, J. E., Nievera, C. J., & Leonard, A. C. (2002). IHF and HU stimulate assembly of pre-replication complexes at *Escherichia coli oriC* by two different mechanisms. *Molecular Microbiology*, *46*(1), 113–124. https://doi.org/10.1046/j.1365-2958.2002.03129.x

Said, N., Hilal, T., Sunday, N. D., Khatri, A., Bürger, J., Mielke, T., Belogurov, G. A., Loll, B., Sen, R., Artsimovitch, I., & Wahl, M. C. (2021). Steps toward

translocation-independent RNA polymerase inactivation by terminator ATPase ρ. *Science*, *371*(6524). https://doi.org/10.1126/science.abd1673

Sanamrad, A., Persson, F., Lundius, E. G., Fange, D., Gynnå, A. H., & Elf, J. (2014). Single-particle tracking reveals that free ribosomal subunits are not excluded from the *Escherichia coli* nucleoid. *Proceedings of the National Academy of Sciences*, *111*(31), 11413–11418. https://doi.org/10.1073/pnas.1411558111

Saxena, S., Myka, K. K., Washburn, R., Costantino, N., Court, D. L., & Gottesman, M. E. (2018). *Escherichia coli* transcription factor NusG binds to 70S ribosomes. *Molecular Microbiology*, *108*(5), 495–504. https://doi.org/10.1111/mmi.13953

Scholz, S. A., Diao, R., Wolfe, M. B., Fivenson, E. M., Lin, X. N., & Freddolino, P. L. (2019). High-Resolution Mapping of the Escherichia coli Chromosome Reveals Positions of High and Low Transcription. *Cell Systems*, *8*(3), 212-225.e9. https://doi.org/10.1016/j.cels.2019.02.004

Serna-Rico, A., Salas, M., & Meijer, W. J. J. (2002). The Bacillus subtilis Phage φ29 Protein p16.7, Involved in φ29 DNA Replication, Is a Membrane-localized Single-stranded DNA-binding Protein. *Journal of Biological Chemistry*, *277*(8), 6733–6742. https://doi.org/10.1074/jbc.M109312200

Shaner, N. C., Lambert, G. G., Chammas, A., Ni, Y., Cranfill, P. J., Baird, M. A., Sell, B. R., Allen, J. R., Day, R. N., Israelsson, M., Davidson, M. W., & Wang, J. (2013). A bright monomeric green fluorescent protein derived from Branchiostoma lanceolatum. *Nature Methods*, *10*(5), 407–409. https://doi.org/10.1038/nmeth.2413

Silhavy, T. J., Kahne, D., & Walker, S. (2010). The Bacterial Cell Envelope. *Cold Spring Harbor Perspectives in Biology*, *2*(5), a000414–a000414. https://doi.org/10.1101/cshperspect.a000414

Somalinga, B. R., & Roy, R. P. (2002). Volume Exclusion Effect as a Driving Force for Reverse Proteolysis. *Journal of Biological Chemistry*, *277*(45), 43253–43261. https://doi.org/10.1074/jbc.M207974200

Song, E., Uhm, H., Munasingha, P. R., Hwang, S., Seo, Y.-S., Kang, J. Y., Kang, C., & Hohng, S. (2022). Rho-dependent transcription termination proceeds via three routes. *Nature Communications*, *13*(1), 1663. https://doi.org/10.1038/s41467-022-29321-5

Spahn, C., Middlemiss, S., Gómez-de-Mariscal, E., Henriques, R., Bode, H. B., Holden, S., & Heilemann, M. (2023). Transertion and cell geometry organize the Escherichia coli nucleoid during rapid growth. *BioRxiv*. https://doi.org/10.1101/2023.10.16.562172

Stent, G. S. (1964). The Operon: On Its Third Anniversary. *Science*, *144*(3620), 816–820. https://doi.org/10.1126/science.144.3620.816

Stevenson-Jones, F., Woodgate, J., Castro-Roa, D., & Zenkin, N. (2020). Ribosome reactivates transcription by physically pushing RNA polymerase out of transcription arrest. *Proceedings of the National Academy of Sciences*, *117*(15), 8462–8467. https://doi.org/10.1073/pnas.1919985117

Stojkova, P., Spidlova, P., & Stulik, J. (2019). Nucleoid-Associated Protein HU: A Lilliputian in Gene Regulation of Bacterial Virulence. *Frontiers in Cellular and Infection Microbiology*, *9*. https://doi.org/10.3389/fcimb.2019.00159

Stuger, R., Woldringh, C. L., van der Weijden, C. C., Vischer, N. O. E., Bakker, B. M., van Spanning, R. J. M., Snoep, J. L., & Weterhoff, H. V. (2002). DNA supercoiling by gyrase is linked to nucleoid compaction. *Molecular Biology Reports*, *29*(1/2), 79–82. https://doi.org/10.1023/A:1020318705894

Taylor, R. G., Walker, D. C., & Mclnnes, R. R. (1993). *E.coli* host strains significantly affect the quality of small scale plasmid DNA preparations used for sequencing. *Nucleic Acids Research*, *21*(7), 1677–1678. https://doi.org/10.1093/nar/21.7.1677

te Winkel, J. D., Gray, D. A., Seistrup, K. H., Hamoen, L. W., & Strahl, H. (2016). Analysis of Antimicrobial-Triggered Membrane Depolarization Using Voltage Sensitive Dyes. *Frontiers in Cell and Developmental Biology*, *4*. https://doi.org/10.3389/fcell.2016.00029

Tetsch, L., Koller, C., Haneburger, I., & Jung, K. (2008). The membrane-integrated transcriptional activator CadC of *Escherichia coli* senses lysine indirectly via the interaction with the lysine permease LysP. *Molecular Microbiology*, *67*(3), 570–583. https://doi.org/10.1111/j.1365-2958.2007.06070.x

Tišma, M., Bock, F. P., Kerssemakers, J., Antar, H., Japaridze, A., Gruber, S., & Dekker, C. (2024). Direct observation of a crescent-shape chromosome in

expanded Bacillus subtilis cells. *Nature Communications*, *15*(1), 2737. https://doi.org/10.1038/s41467-024-47094-x

Tokunaga, M., Imamoto, N., & Sakata-Sogawa, K. (2008a). Highly inclined thin illumination enables clear single-molecule imaging in cells. *Nature Methods*, *5*(2), 159–161. https://doi.org/10.1038/nmeth1171

Tokunaga, M., Imamoto, N., & Sakata-Sogawa, K. (2008b). Highly inclined thin illumination enables clear single-molecule imaging in cells. *Nature Methods*, *5*(2), 159–161. https://doi.org/10.1038/nmeth1171

Toro, E., & Shapiro, L. (2010). Bacterial chromosome organization and segregation. In *Cold Spring Harbor perspectives in biology* (Vol. 2, Issue 2, p. a000349). Cold Spring Harbor Laboratory Press. https://doi.org/10.1101/cshperspect.a000349

Tsirigotaki, A., De Geyter, J., Šoštaric´, N., Economou, A., & Karamanou, S. (2017). Protein export through the bacterial Sec pathway. *Nature Reviews Microbiology*, *15*(1), 21–36. https://doi.org/10.1038/nrmicro.2016.161

Valent, Q. A., De Gier, J. L., Heijne, G. von, Kendall, D. A., Ten Hagen-Jongman, C. M., Oudega, B., & Luirink, J. (1997). Nascent membrane and presecretory proteins synthesized in *Escherichia coli* associate with signal recognition particle and trigger factor. *Molecular Microbiology*, *25*(1), 53–64. https://doi.org/10.1046/j.1365-2958.1997.4431808.x

Verma, S. C., Qian, Z., & Adhya, S. L. (2019). Architecture of the Escherichia coli nucleoid. *PLOS Genetics*, *15*(12), e1008456. https://doi.org/10.1371/journal.pgen.1008456

Viollier, P. H., Thanbichler, M., McGrath, P. T., West, L., Meewan, M., McAdams, H. H., & Shapiro, L. (2004). Rapid and sequential movement of individual chromosomal loci to specific subcellular locations during bacterial DNA replication. *Proceedings of the National Academy of Sciences*, *101*(25), 9257–9262. https://doi.org/10.1073/pnas.0402606101

Vogel, U., & Jensen, K. F. (1994). The RNA chain elongation rate in Escherichia coli depends on the growth rate. *Journal of Bacteriology*, *176*(10), 2807–2813. https://doi.org/10.1128/jb.176.10.2807-2813.1994

Vos, S. M., Stewart, N. K., Oakley, M. G., & Berger, J. M. (2013). Structural basis for the MukB-topoisomerase IV interaction and its functional implications *in vivo*. *The EMBO Journal*, *32*(22), 2950–2962. https://doi.org/10.1038/emboj.2013.218

Wang, C., Molodtsov, V., Firlar, E., Kaelber, J. T., Blaha, G., Su, M., & Ebright, R. H. (2020). Structural basis of transcription-translation coupling. *Science*, *369*(6509), 1359–1365. https://doi.org/10.1126/science.abb5317

Wang, X., Brandão, H. B., Le, T. B. K., Laub, M. T., & Rudner, D. Z. (2017). *Bacillus subtilis* SMC complexes juxtapose chromosome arms as they travel from origin to terminus. *Science*, *355*(6324), 524–527. https://doi.org/10.1126/science.aai8982

Wang, X., Liu, X., Possoz, C., & Sherratt, D. J. (2006). The two *Escherichia coli* chromosome arms locate to separate cell halves. *Genes & Development*, *20*(13), 1727–1731. https://doi.org/10.1101/gad.388406

Wang, X., Montero Llopis, P., & Rudner, D. Z. (2014a). *Bacillus subtilis* chromosome organization oscillates between two distinct patterns. *Proceedings of the National Academy of Sciences*, *111*(35), 12877–12882. https://doi.org/10.1073/pnas.1407461111

Wang, X., Montero Llopis, P., & Rudner, D. Z. (2014b). *Bacillus subtilis* chromosome organization oscillates between two distinct patterns. *Proceedings of the National Academy of Sciences*, *111*(35), 12877–12882. https://doi.org/10.1073/pnas.1407461111

Wang, X., & Rudner, D. Z. (2014a). Spatial organization of bacterial chromosomes. *Current Opinion in Microbiology*, *22*, 66–72. https://doi.org/https://doi.org/10.1016/j.mib.2014.09.016

Wang, X., & Rudner, D. Z. (2014b). Spatial organization of bacterial chromosomes. *Current Opinion in Microbiology*, *22*, 66–72. https://doi.org/10.1016/j.mib.2014.09.016

Webb, C. D., Graumann, P. L., Kahana, J. A., Teleman, A. A., Silver, P. A., & Losick, R. (1998). Use of time-lapse microscopy to visualize rapid movement of the replication origin region of the chromosome during the cell cycle in *Bacillus subtilis*. *Molecular Microbiology*, *28*(5), 883–892. https://doi.org/10.1046/j.1365-2958.1998.00808.x

Weber, M. H. W., Klein, W., Müller, L., Niess, U. M., & Marahiel, M. A. (2001a). Role of the *Bacillus subtilis* fatty acid desaturase in membrane adaptation during cold shock. *Molecular Microbiology*, *39*(5), 1321–1329. https://doi.org/10.1111/j.1365-2958.2001.02322.x

Weber, M. H. W., Klein, W., Müller, L., Niess, U. M., & Marahiel, M. A. (2001b). Role of the *Bacillus subtilis* fatty acid desaturase in membrane adaptation during cold shock. *Molecular Microbiology*, *39*(5), 1321–1329. https://doi.org/10.1111/j.1365-2958.2001.02322.x

Whitley, K. D., Jukes, C., Tregidgo, N., Karinou, E., Almada, P., Cesbron, Y., Henriques, R., Dekker, C., & Holden, S. (2021). FtsZ treadmilling is essential for Z-ring condensation and septal constriction initiation in Bacillus subtilis cell division. *Nature Communications*, *12*(1), 2448. https://doi.org/10.1038/s41467-021-22526-0

Whitley, K. D., Middlemiss, S., Jukes, C., Dekker, C., & Holden, S. (2022). High-resolution imaging of bacterial spatial organization with vertical cell imaging by nanostructured immobilization (VerCINI). *Nature Protocols*, *17*(3), 847–869. https://doi.org/10.1038/s41596-021-00668-1

Woldringh, C. L., Jensen, P. R., & Westerhoff, H. V. (1995). Structure and partitioning of bacterial DNA: determined by a balance of compaction and expansion forces? *FEMS Microbiology Letters*, *131*(3), 235–242. https://doi.org/10.1111/j.1574-6968.1995.tb07782.x

Woodgate, J., & Zenkin, N. (2023). Transcription–translation coupling: Recent advances and future perspectives. *Molecular Microbiology*, *120*(4), 539–546. https://doi.org/10.1111/mmi.15076

Xiang, Y., Surovtsev, I. V, Chang, Y., Govers, S. K., Parry, B. R., Liu, J., & Jacobs-Wagner, C. (2020). Solvent quality and chromosome folding in Escherichia coli. *BioRxiv*. https://doi.org/10.1101/2020.07.09.195560

Yakhnin, A. V., FitzGerald, P. C., McIntosh, C., Yakhnin, H., Kireeva, M., Turek-Herman, J., Mandell, Z. F., Kashlev, M., & Babitzke, P. (2020). NusG controls transcription pausing and RNA polymerase translocation throughout the *Bacillus subtilis* genome. *Proceedings of the National Academy of Sciences*, *117*(35), 21628–21636. https://doi.org/10.1073/pnas.2006873117

Yamaichi, Y., Bruckner, R., Ringgaard, S., Möll, A., Cameron, D. E., Briegel, A., Jensen, G. J., Davis, B. M., & Waldor, M. K. (2012). A multidomain hub anchors the chromosome segregation and chemotactic machinery to the bacterial pole. *Genes & Development*, *26*(20), 2348–2360. https://doi.org/10.1101/gad.199869.112

Yang, S., Kim, S., Kim, D.-K., Jeon An, H., Bae Son, J., Hedén Gynnå, A., & Ki Lee, N. (2019). Transcription and translation contribute to gene locus relocation to the nucleoid periphery in E. coli. *Nature Communications*, *10*(1), 5131. https://doi.org/10.1038/s41467-019-13152-y

Zaritsky, A. (2015). Cell-Shape Homeostasis in Escherichia coli Is Driven by Growth, Division, and Nucleoid Complexity. *Biophysical Journal*, *109*(2), 178–181. https://doi.org/10.1016/j.bpj.2015.06.026

Zhu, M., & Dai, X. (2020). Bacterial stress defense: the crucial role of ribosome speed. *Cellular and Molecular Life Sciences*, *77*(5), 853–858. https://doi.org/10.1007/s00018-019-03304-0

Zhu, M., Dai, X., & Wang, Y.-P. (2016). Real time determination of bacterial *in vivo* ribosome translation elongation speed based on LacZα complementation system. *Nucleic Acids Research*, gkw698. https://doi.org/10.1093/nar/gkw698

Zimmerman, S. B. (2002a). Toroidal nucleoids in Escherichia coli exposed to chloramphenicol. *Journal of Structural Biology*, *138*(3), 199–206. https://doi.org/10.1016/S1047-8477(02)00036-9

Zimmerman, S. B. (2002b). Toroidal nucleoids in Escherichia coli exposed to chloramphenicol. *Journal of Structural Biology*, *138*(3), 199–206. https://doi.org/10.1016/S1047-8477(02)00036-9